

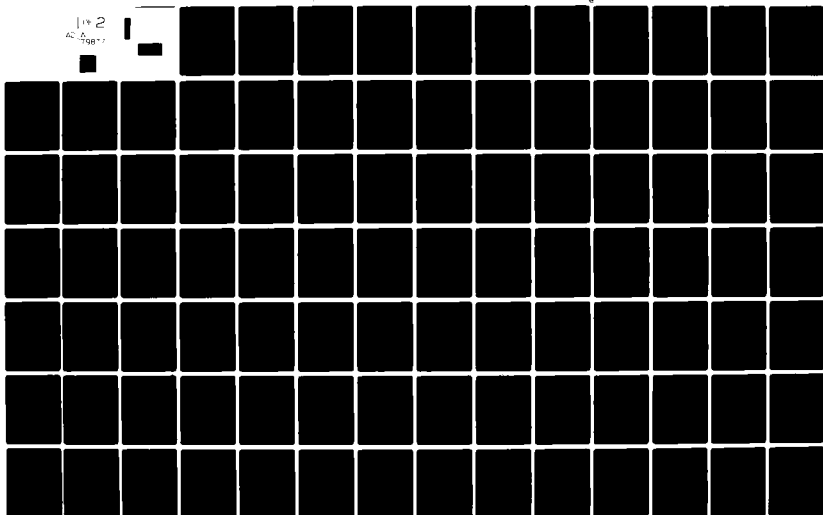
AD-A079 577

AIR FORCE INST OF TECH WRIGHT-PATTERSON AFB OH SCH00--ETC F/G 20/4
GROUND PLANE EFFECTS ON A CONTOURED SURFACE AT LOW SUBSONIC VEL--ETC(U)
DEC 79 J A KRAWTZ
AFIT/GA/AA/80W-3

UNCLASSIFIED

NL

11-2
AC 11-2
1987



(1)

(11) Dec 79

(12) 115

(9) master's thesis

(6) GROUND PLANE EFFECTS ON A
CONTOURED SURFACE AT LOW
SUBSONIC VELOCITIES.

THESIS

(14) AFIT/GA/AA/80M-3

(10) Joseph A. Krawtz
2nd Lt USAF

DDC
RECEIVED
JAN 28 1980
A

012 225

Gu

GROUND PLANE EFFECTS ON A CONTOURED SURFACE
AT LOW SUBSONIC VELOCITIES

THESIS

Presented to the Faculty of the School of Engineering[✓]
of the Air Force Institute of Technology
Air University
in Partial Fulfillment of the
Requirements for the Degree of
Master of Science

by

Joseph A. Krawtz, B.S.E.

2nd Lt

USAF

Graduate Astronautical Engineering

December 1979

Accession For	
NIIS GRA&I	<input checked="checked" type="checkbox"/>
DDC TAB	<input type="checkbox"/>
Unannounced	<input type="checkbox"/>
Justification	
By _____	
Distribution/	
Availability Codes	
Dist	Avail and/or Special
A	

Approved for public release; distribution unlimited.

Preface

This study resulted from the growing interest in the field of wing-in-ground effect vehicles. The performance of these vehicles relies on understanding the stability and control problems associated with intentionally operating within ground effect. The model used to investigate the flow parameters associated with the wing-in-ground effect was suggested by Capt. George D. Catalano, AFFDL/FXM. The model consisted of a contoured upper plate and a flat bottom plate. Velocity measurements were taken in the flow field with various plate separations.

A Laser Velocimeter measurement system was used to gather data. This system was chosen due to the harsh environment of the flow field. Conventional intrusive methods such as hot wire or pressure probes would have presented problems such as the ability to measure velocities close to the surface of the plates and regions of highly turbulent flow.

I wish to thank my thesis advisor, Dr. William C. Elrod, for his support and encouragement. Mr. William Baker and Mr. Harold Cannon provided valuable assistance in the laboratory and equipment installation. The AFIT workshop that provided parts and modifications on the equipment is to be commended for a job well done.

Joseph A. Krawtz

Contents

	Page
Preface	ii
List of Figures	v
List of Tablesviii
List of Symbols	x
Abstract	xii
I. Introduction	1
Background	1
Approach	2
Objectives	2
Scope	2
II. Test Apparatus	4
Nozzle	4
Parallel Plates	4
III. Instrumentation	8
Nozzle	8
Laser Doppler Velocimeter	8
Laser	10
Beamsplitter	10
Telephoto Lens	10
Photomultiplier Tube	11
Digital Correlator	12
Oscilloscope	12
IV. Principle of Operation	14
V. Experimental Procedure	17
Mach Number Calibration	17
Optical Alignment	18
Laser Traverse	19
Pressure Measurements	21
Data Handling Technique	21

	Page
VI. Results and Discussion	24
Velocity Profiles	24
Ground Plate Effects	24
Curved Surface	31
Vertical Measurements	34
Pressure Results	36
Turbulence Intensities	37
VII. Conclusions	43
VIII. Recommendations	46
Bibliography	47
Appendix A: Calculation of the Exit Velocity	48
Appendix B: Pressure Data	50
Appendix C: LV Experimental Results at $M = 0.15$ and $M = 0.2$ for z Axis Profiles	55
Appendix D: LV Experimental Results at $M = 0.15$ and $M = 0.2$ for y Axis Profiles	86
Vita	99

List of Figures

Figure		Page
1	Experimental Apparatus Schematic	5
2	Top Plate Static Pressure Taps	7
3	Laser Velocimeter Measurement System	9
4	Autocorrelation Function	13
5	Schematic of Beam Intersection Point	14
6	Fringe Spacing Parameters	16
7	LV Measurement Points	20
8	Pressure Probe Position in Flow	23
9	Downstream Transition Layer Growth	26
10	Velocity Profile for $M = 0.15$ at $X = 5$ cm for 3 Ground Plate Positions	27
11	Autocorrelation Function Tolerated at High Turbulence Intensities	28
12	Velocity Profile for $M = 0.2$ at $X = 5$ cm for 3 Ground Plate Positions	29
13	Potential Core Decay for $M = 0.15$ and $M = 0.2$ at $X = 15$ cm for 1 cm Separation . . .	30
14	Velocity Increase for $M = 0.15$ at $X = 15$ cm for 3 ground plate positions	32
15	Velocity Profiles for $M = 0.15$ and $M = 0.2$ Along x Axis Centerline	33
16	Schematic of Coanda Effect	34
17	Y Axis Velocity Profiles for $M = 0.15$ and $M = 0.2$ at $X = 5$ cm	35
18	Pressure and LV Similarity Profiles for $M = 0.2$	38
19	Turbulence Intensity for $M = 0.2$ at $X = 5$ cm for 3 Ground Plate Positions . . .	41

Figure		Page
20	Turbulence Intensity Profiles for M = 0.2 at Downstream Stations	42
21	Pressure and LV Velocity Profiles Along x Axis Centerline for M = 0.15	51
22	Pressure and LV Velocity Profiles Along x Axis Centerline for M = 0.2	53
23	Velocity Profiles for M = 0.15 at X = 5 cm . .	56
24	Velocity Profiles for M = 0.15 at X = 10 cm. .	57
25	Velocity Profiles for M = 0.15 at X = 15 cm. .	58
26	Turbulence Intensity Profiles for M = 0.15 at X = 5 cm	59
27	Turbulence Intensity Profiles for M = 0.15 at X = 10 cm	60
28	Turbulence Intensity Profiles for M = 0.15 at X = 15 cm	61
29	Velocity Profiles for M = 0.2 at X = 5 cm . .	62
30	Velocity Profiles for M = 0.2 at X = 10 cm . .	63
31	Velocity Profiles for M = 0.2 at X = 15 cm . .	64
32	Turbulence Intensity Profiles for M = 0.2 at X = 5 cm	65
33	Turbulence Intensity Profiles for M = 0.2 at X = 10 cm	66
34	Turbulence Intensity Profiles for M = 0,2 at X = 15 cm	67
35	Vertical Velocity Profiles for M = 0.15 and M = 0.2 at X = 5 cm	87
36	Vertical Velocity Profiles for M = 0.15 and M = 0.2 at X = 10 cm	88
37	Vertical Velocity Profiles for M = 0.15 and M = 0.2 at X = 15 cm	89
38	Turbulence Intensity Profiles for M = 0.15 and M = 0.2 at X = 5 cm	90

Figure		Page
39	Turbulence Intensity Profiles for $M = 0.15$ and $M = 0.2$ at $X = 10$ cm	90
40	Turbulence Intensity Profiles for $M = 0.15$ and $M = 0.2$ at $X = 15$ cm	92

List of Tables

Table		Page
I	Reynold's Numbers based on Streamwise Direction	36
II	Static Pressure	39
III	Top Plate Pressure Data- Velocities	52
IV	Top Plate Pressure Data	54
V	LV Data for M = 0.15 X = 5, Ground Plate = 5 cm	68
VI	LV Data for M = 0.15 X = 5, Ground Plate = 2 cm	69
VII	LV Data for M = 0.15 X = 5, Ground Plate = 1 cm	70
VIII	LV Data for M = 0.15 X = 10, Ground Plate = 5 cm	71
IX	LV Data for M = 0.15 X = 10, Ground Plate = 2 cm	72
X	LV Data for M = 0.15 X = 10, Ground Plate = 1 cm	73
XI	LV Data for M = 0.15 X = 15, Ground Plate = 5 cm	74
XII	LV Data for M = 0.15 X = 15, Ground Plate = 2 cm	75
XIII	LV Data for M = 0.15 X = 15, Ground Plate = 1 cm	76
XIV	LV Data for M = 0.2 X = 5 Ground Plate = 5 cm	77
XV	LV Data for M = 0.2 X = 5 Ground Plate = 2 cm	78
XVI	LV Data for M = 0.2 X = 5 Ground Plate = 1 cm	79
XVII	LV Data for M = 0.2 X = 10 Ground Plate = 5 cm	80

Table		Page
XVIII	LV Data for M = 0.2 X = 10 Ground Plate = 2 cm	81
XIX	LV Data for M = 0.2 X = 10 Ground Plate = 1 cm	82
XX	LV Data for M = 0.2 X = 15 Ground Plate = 5 cm	83
XXI	LV Data for M = 0.2 X = 15 Ground Plate = 2 cm	84
XXII	LV Data for M = 0.2 X = 15 Ground Plate = 1 cm	85
XXIII	LV Data for Y Axis M = 0.15 X = 5	93
XXIV	LV Data for Y Axis M = 0.2 X = 5	94
XXV	LV Data for Y Axis M = 0.15 X = 10	95
XXVI	LV Data for Y Axis M = 0.2 X = 10	96
XXVII	LV Data for Y Axis M = 0.15 X = 15	97
XXVIII	LV Data for Y Axis M = 0.2 X = 15	98

List of Symbols

<u>Symbol</u>		<u>Units</u>
a	Sonic Velocity	m/sec
D	Beam Separation	cm
g_c	Gravitational Constant	$\frac{\text{Kg} - \text{m}}{\text{N} - \text{sec}^2}$
Δh_m	Height of Meriam Fluid	cm
Δh	Height of Water	cm
L	Length of Beam	cm
M_e	Mach Number at Exit	
M	Mach Number in Flow	
n	Number of Fringes	
P_o	Total Pressure	Kg/m^2
P_a	Atmospheric Pressure	Kg/m^2
ΔP	Measured Pressure	Kg/m^2
R	Dimensionless Value of Autocorrelation Function	
r_o	Radius of Laser Beam	mm
S	Fringe Spacing	μm
T_a	Atmospheric Temperature	$^{\circ}\text{C}$
T_c	Chamber Temperature	$^{\circ}\text{C}$
T_e	Exit Temperature	$^{\circ}\text{C}$
U	Steam Velocity	m/sec
U_e	Exit Velocity	m/sec

<u>Symbol</u>		<u>Units</u>
x	Axial Coordinate in the Direction of Flow	cm
y	Vertical Coordinate	cm
z	Horizontal Coordinate Normal to x y Plane	cm
γ_m	Specific Gravity of Merrian Fluid	
λ_L	Laser Wavelength	m
μ_o	Index of Refraction	
η	Turbulence Intensity	%
ρ	Air Density	Kg/m ³
T	Sample Time	sec

Abstract

The wing-in-ground effect phenomenon was examined by investigating the flow between a flat ground plate and a contoured upper plate. Velocity and turbulence intensity measurements were taken at various points in the flow with a Laser Doppler Velocimeter. Mach numbers studied were Mach 0.15 and Mach 0.2 at the exit plane of a 1 cm by 10 cm two-dimensional nozzle.

Measurements were taken across the width of the jet, 5, 10, and 15 cm downstream with plate separations of 1, 2, and 5 cm and vertically without the ground plate. In addition, measurements were taken near the top plate with conventional pressure measuring techniques and the results compared.

The proximity of the ground plate had the effect of spreading the flow outward across the jet by as much as 20%. The LV showed the turbulence intensity to be constant across the potential core of the jet. Turbulence intensity increased beyond 10% in the boundary layers of the jet and in the plate boundary layer. The pressure measurement data correlated well with the LV results.

GROUND PLANE EFFECTS ON A CONTOURED SURFACE AT LOW SUBSONIC VELOCITIES

I. Introduction

Background

Studies on aerodynamic bodies interacting with a solid boundary have become important after the development of aircraft which are designed to use the wing-in-ground effect (WIG). The concept of the WIG can be applied to surface as well as conventional airborne vehicles. Both can reap the performance and economic advantages of intentionally operating within ground effect. Studies have shown that when WIGs are operated at heights of less than 20% of the span that induced drag is decreased and lift is increased (Ref 11).

With the growing interest of WIGs, problems arise concerning the changes in stability of the wing or vehicle during movement near the ground. Flows in the vicinity of the lifting surfaces become turbulent and create unequal load distributions. Analytical methods fail to give satisfactory results and, at best, can only be applied in some instances. One approach to understanding the stability problem is to map the flow field in the vicinity of the wing and ground. If no definite conclusions are evident from the results, some qualitative trends characteristic of the flow

could be shown.

Approach

The approach included modeling the wing-in-ground effect phenomenon with two plates separated by a region of jet flow. A two-dimensional jet was discharged from a 1 cm by 10 cm nozzle with the plates oriented parallel to the jet flow. The upper plate remained fixed at the top of the nozzle exit while the bottom plate was free to move vertically. The flow field between the plates was investigated at Mach numbers of 0.15 and 0.2 for various ground plate positions.

Velocity distributions were measured at various points in the flow with a Laser Velocimeter operated in the off-axis forward scattering mode. Conventional velocity pressure measurements were taken and results compared to the Laser Velocimeter data.

Objectives

The objectives of this investigation were:

1. to map the flow field with the Laser Velocimeter as a function of ground plate position;
2. to observe the flow in the vicinity of the curved portion of the top plate;
3. to map the flow field vertically; and
4. to map the same flow field with a pressure probe and compare results with those for the laser system.

Scope

Three aspects of jet flow over a curved surface were

investigated with a Laser Velocimeter and with conventional velocity pressure probes. These were chosen to determine the characteristics of a WIG's environment. Mean velocity and turbulence intensity profiles were of interest for:

1. Establishing the mode of development of the profiles on the jet centerline as the flow moves downstream from the nozzle exit plane. Measurements were taken at 5, 10, and 15 cm downstream with the distance between curved plate and ground plane set at 1, 2, and 5 cm.
2. Determining the streamwise profile along the curved surface as near to the surface permitted by the instrumentation.
3. Observing vertical profiles at 5, 10, and 15 cm downstream with the ground plate removed.

II. Test Apparatus

The test apparatus included a nozzle, a contoured upper plate, and a flat lower plate as shown in Figure 1. The plates were mounted on a frame at the nozzle exit. The frame mount allowed the plates to be positioned in various configurations for testing. The placement of the plates at the nozzle exit was chosen to determine the characteristics of a wing-in-ground effect.

Nozzle

The nozzle used was the 1 cm by 10 cm two-dimensional nozzle initially constructed by Shepard (Ref 10). Later internal modifications were made to the system by Cerullo (Ref 3) to attain a lower turbulence and thinner boundary layer at the exit. For this research the model used by Cerullo was not modified as it suited the purpose for the laser velocimeter and pressure measurements. The nozzle test apparatus was located at the Air Force Institute of Technology School of Engineering Laboratory, Wright-Patterson Air Base, Dayton, Ohio.

Parallel Plates

Figure 1 shows the position of the top and bottom plates relative to the nozzle. The top plate or simulated wing in this case was mounted parallel to the flow flush with top of

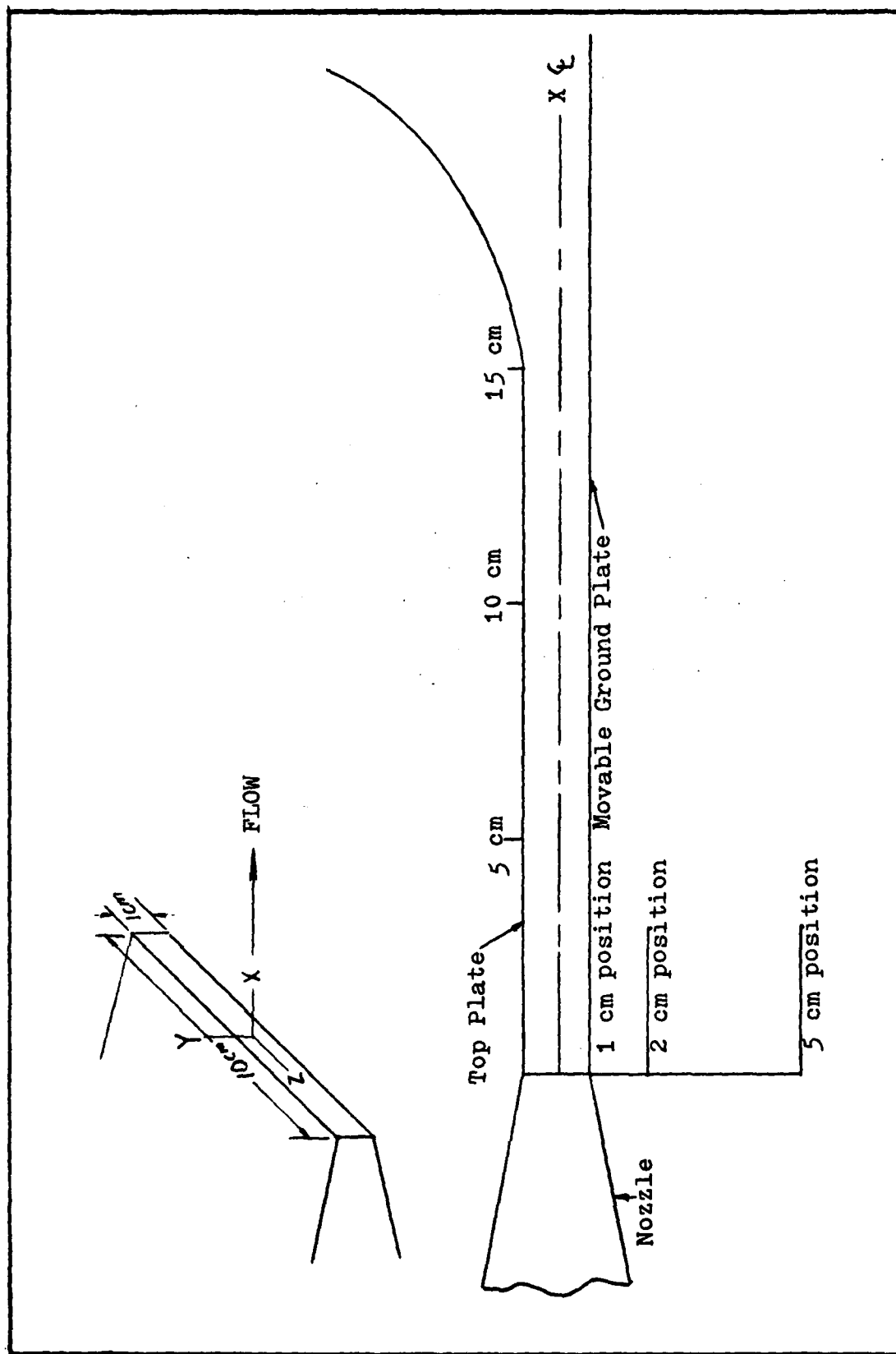


Figure 1. Experimental Apparatus Schematic

the nozzle exit. The top plate had a width of 28 cm with a 15 cm straight section to the curve. The curved surface was bent 65 degrees with a 22 cm radius.

Static pressure taps were placed parallel and perpendicular to the flow at 45 locations corresponding to the LDV test planes. The location of the taps is shown on Figure 2. On the flat portion of the plate taps were placed 1.5 cm apart at the 5, 10, and 15 cm stations perpendicular to the flow. Eight additional ports were located along the center line of the jet 2 cm apart along the curved surface.

The flat bottom plate, or ground plate, was also 28 cm wide and extended 50 cm from the nozzle exit plane. A sliding frame enabled quick and accurate vertical adjustment of the bottom plate without interfering with the flow field or laser beam.

Both plate surfaces adjacent to the flow were painted flat black in order to minimize aberrant light for the optical system. A rigid frame supported both plates from behind the nozzle exit. For the Mach 0.2 run, additional clamp supports were necessary to alleviate the problem of plate vibration due to the turbulent flow field.

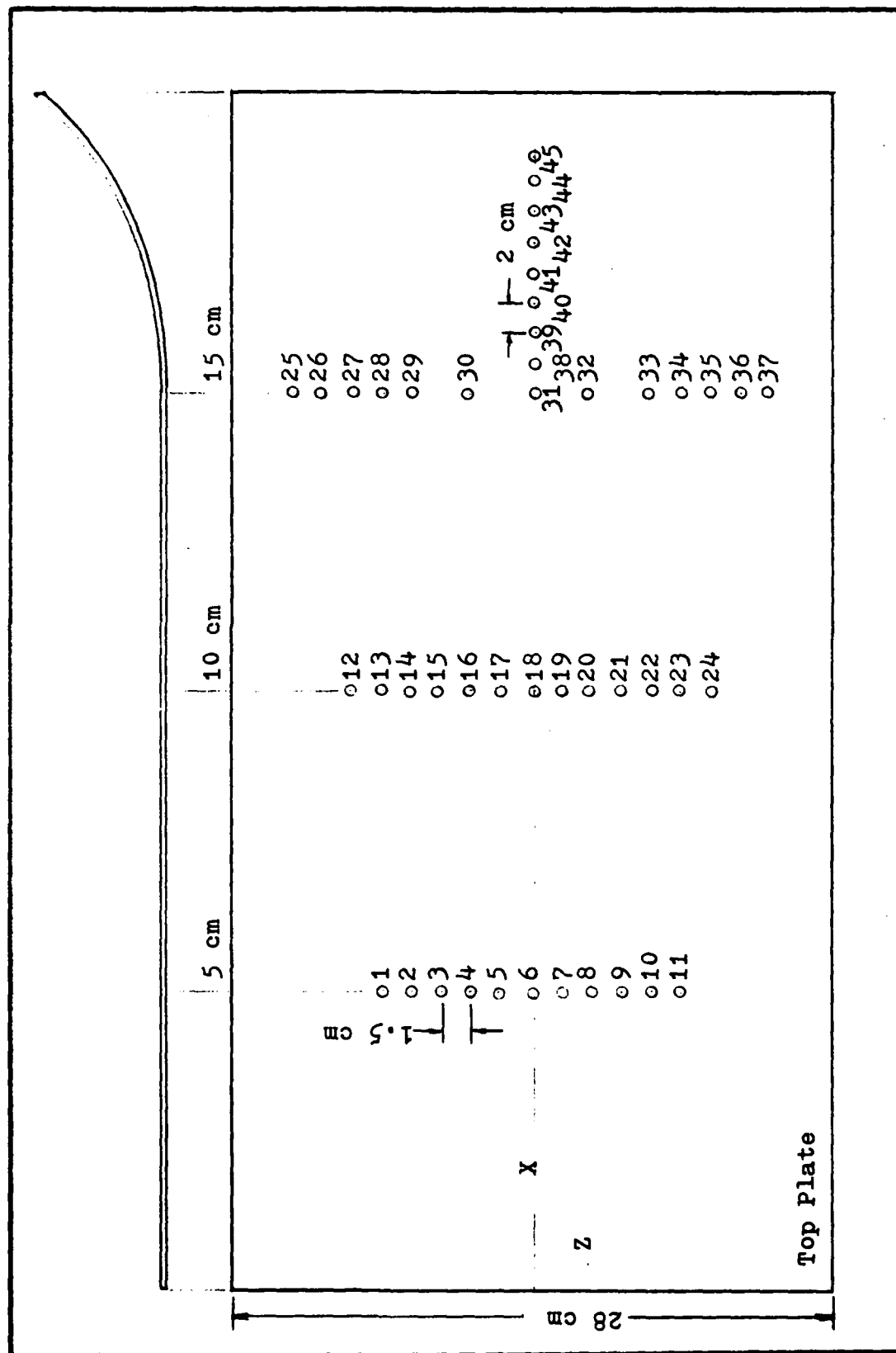


Figure 2. Top Plate Pressure Taps

III. Instrumentation

Instrumentation for data acquisition included Meriam manometers for pressure observations to monitor nozzle exit Mach number, the Laser Velocimeter system mounted on a traversing mechanism and a micromanometer to obtain pressure velocity data. The components of the discharge nozzle and Laser Doppler Velocimeter are discussed in the proceeding section.

Nozzle

Pressures were measured by static pressure taps and Meriam manometers. A 100-inch Meriam manometer was used to measure the pressure in the chamber at the nozzle entrance. A course adjust main valve and a fine adjust bypass valve located at the inlet of the chamber enabled the pressure to be regulated in the chamber. Constant checks on the system for each run were necessary due to fluctuations in the compressed air system. The manometer, in conjunction with a thermometer in the chamber, allowed the system to be adjusted to the desired exit Mach number.

Laser Doppler Velocimeter

A schematic of the LDV system used in the investigation is shown in Figure 3. The LDV and its associated receiving optics were mounted on a three-degree-of-freedom traversing

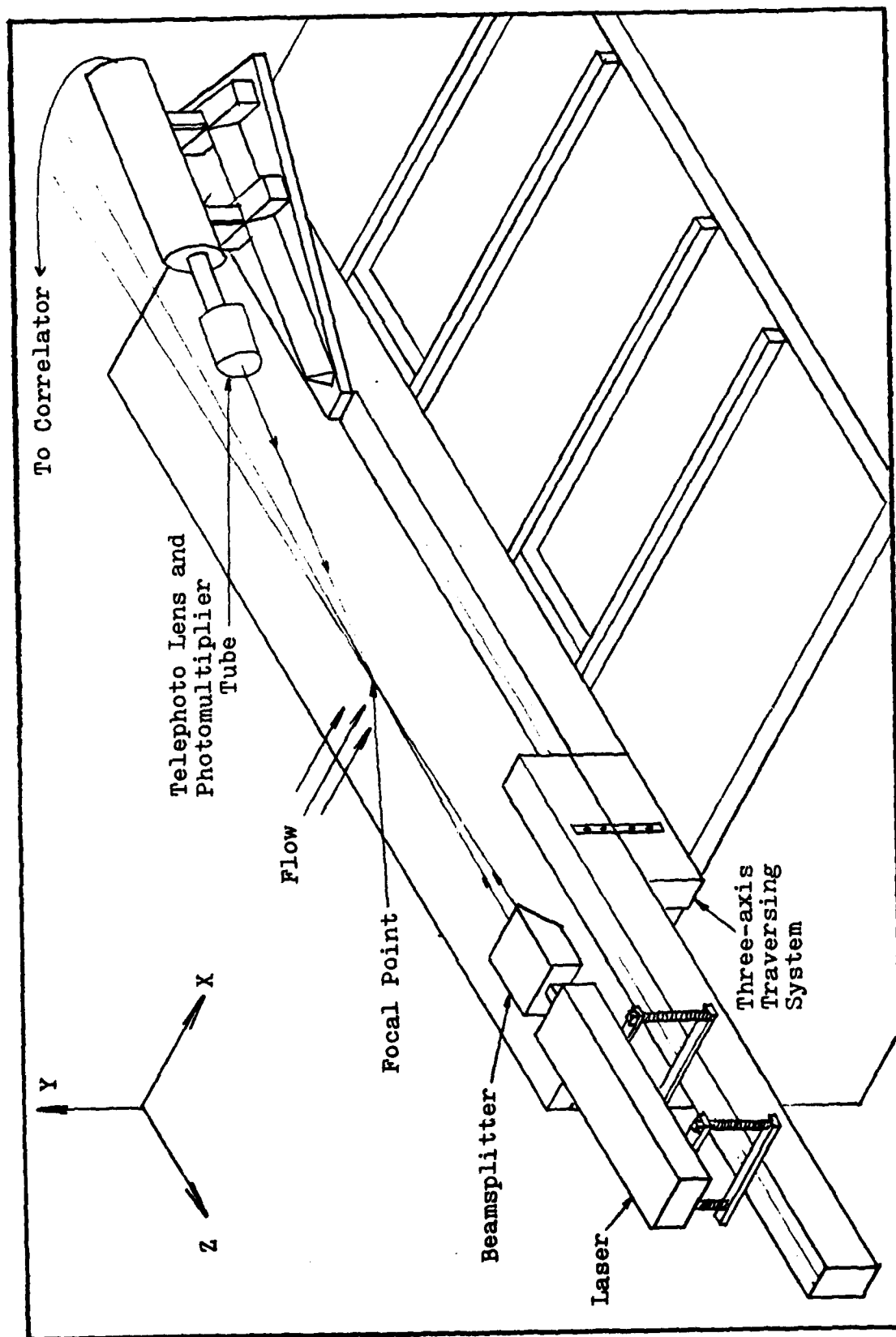


Figure 3. Laser Velocimeter Measurement System

system enabling any point in the flow field to be measured. The instruments used consisted of a helium-neon laser, a beamsplitter, a 200 mm telephoto lens, a photomultiplier tube, a digital correlator, and an oscilloscope. The following is a brief description of the components. A more detailed description of the system can be found in Ref 6.

Laser. A Spectra Physics Model 124A helium-neon laser operating at 6328\AA with a nominal output power of 15 mW was used. The laser produced a beam with a 1.1 mm diameter.

Beamsplitter. The 1.1 mm diameter beam passed through a Malvern RF 307 transmitter beamsplitter mounted directly on the laser body. This unit required a vertically polarized input beam to ensure that the two output beams were of equal intensity. This was easily accomplished with the $\lambda/2$ plate in the beamsplitter to equalize the intensities.

The two output beams intersected downstream to form the focal volume or test control volume. Adjustments were provided to vary the separation of the beams and the point at which the beams intersected (i.e. the cross-over point).

Telephoto Lens. A 200 mm Vivitar telephoto lens installed with a 9.0 cm spacer was used to align the photomultiplier optics. The lens collected the light scattered by the particles as they moved through the focal volume and focused the light onto a pinhole aperture.

The aperture served a dual purpose; first, to regulate the diameter of the control volume, and second, to eliminate any scattered light other than from the observed focal volume.

The instrument was provided with 100, 200, and 400 μm apertures. It was found that the 400 μm aperture gave the best signal-to-noise ratio for this investigation.

The specific lens and spacer combination were chosen to suit the focusing range and size of the control volume that was observed. The focusing range was governed by the amount of traverse needed to obtain the required measurements without interfering with the flow field. The optics used allowed viewing of the control volume at a range of 80 cm.

The size of the control volume was a function of the range, lens-spacer combination, and size of the pinhole. At a range of 80 cm with a 9.0 cm spacer, a 200 mm focal length, and a pinhole of 400 μm the cross-section of the control volume seen by the lens system was 1.2 mm in diameter.

Photomultiplier Tube. The scattered light was detected by a EMI 9863 KB/100 Photomultiplier Tube. A EMI PM 25B power supply regulated a constant 1850 volts to the PM tube. The lens system focused the incident light from the focal volume onto the pinhole aperture and via a narrow band spectral filter on to the PM tube cathode. It was important that the narrow band filter be matched to the wavelength of the helium-neon laser, 6328 \AA . The PM tube circuitry then amplified and sent the signal to the digital correlator.

Care had to be taken with this instrument where accidental exposure to direct laser light would have caused damage to the unprotected circuitry. In addition to the laser's low output and therefore the PM tube's high sensitivity, it was

important to keep room lighting to a minimum. Stray light would have introduced undesired noise to the system.

Digital Correlator. The signal processor of the system was the Malvern digital correlator type K7023. The instrument processed the signal from the PM tube, digitized the signal, and sent it to the oscilloscope as a digital correlation.

Oscilloscope. The autocorrelation function from the digital correlation was displayed on a Tektronix AM/USM-425 (V)1 oscilloscope. The sinusoidal curve shown in Figure 4 represented the characteristic digital correlator display of the incoming signal from the photomultiplier. Velocity and turbulence intensity information was extracted from the curve simply by recording the channel number and content of the first minimum, g_1 , the first maximum or peak, g_2 , and the second minimum, g_3 . The following section describes the operation of the system in detail and how data is extracted.

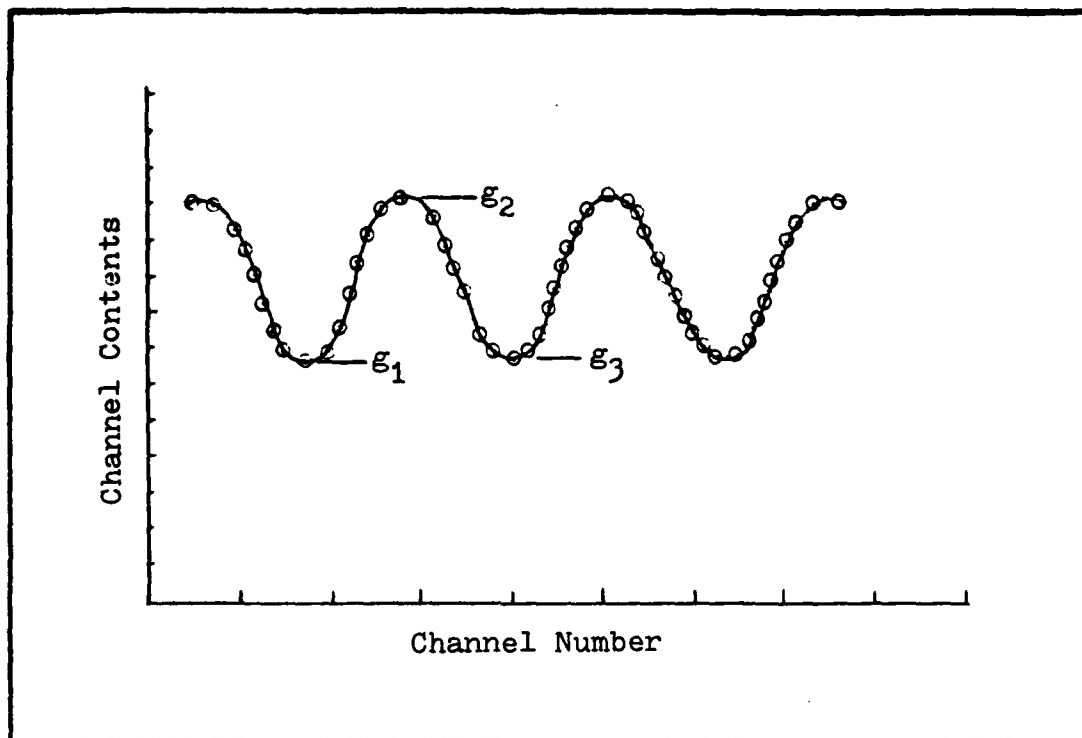


Figure 4. Autocorrelation Function

IV. Principle of Operation

The detailed procedure describing how to install and operate the LDV is contained in the Malvern Manual (Ref 6) and Cerullo's thesis. The principle of operation can be visualized as follows: Two coherent, vertically polarized laser beams are brought to an intersection at a common point in the flow field. Their intersection forms a set of parallel intensity fringes as depicted in Figure 5. As a particle entrained in the flow passes through this field of spatially

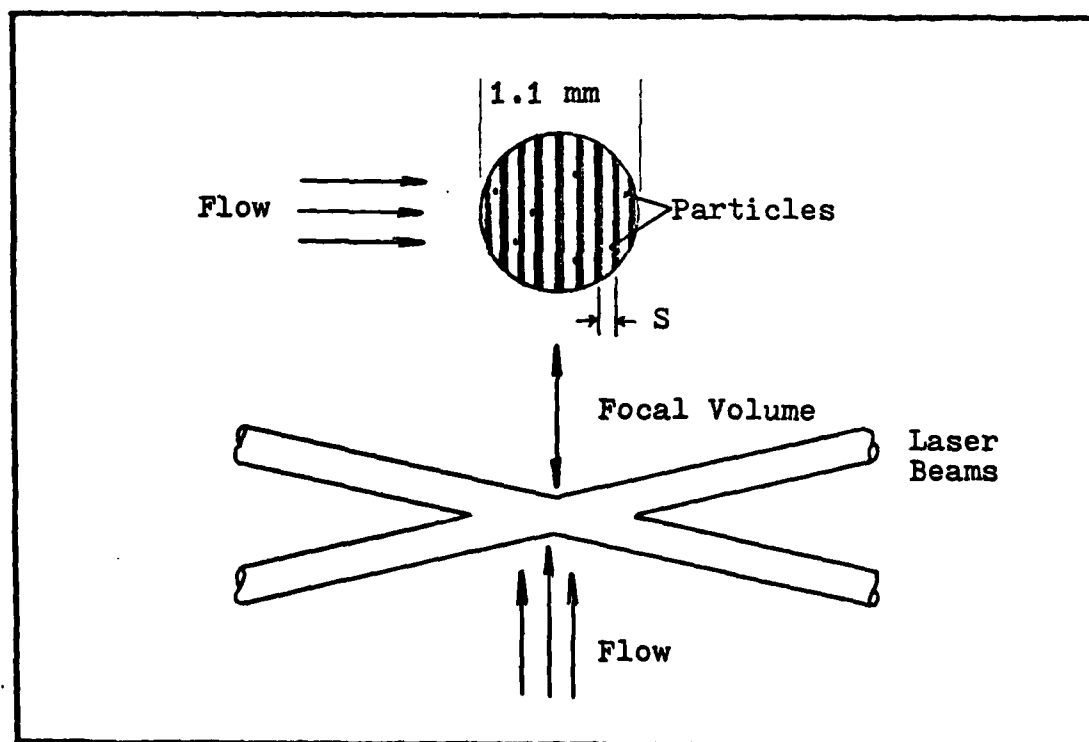


Figure 5. Schematic of Beam Intersection Point

varying light intensity, the amount of light scattered by the particle is detected by the photomultiplier tube. The scattered light that is detected by the photomultiplier allows the photomultiplier to produce an electrical signal that represents the intensity of the fringe pattern in time rather than in space. The signal burst produced at the photomultiplier is sent to the digital correlator, processed, and displayed on the oscilloscope as shown in Figure 4.

The period (T) of this signal was the time required to travel the fringe spacing (S). The period was calculated from the sample time and peak channel number

$$T = (\text{Channel number of peak} - 3) \times \text{sample time}$$

The integer 3 represented the first three monitoring channels of the correlator which contain no useful information. Only the channels from 4 on could be used in calculations; therefore, 3 was subtracted from the peak channel number. Fringe spacing was found from beam geometry and laser wavelength

$$S = \frac{L}{D} \frac{\lambda_L}{\mu_O}$$

where

L = length of beam from the intersection point to a surface normal to a line that bisects the angle between the beams (see Figure 6),

D = beam separation at the surface,

λ_L = 6328 Å, and

μ_O = index of refraction for the medium where the measurement was taken, 1.0 for air.

Figure 6 illustrates these parameters.

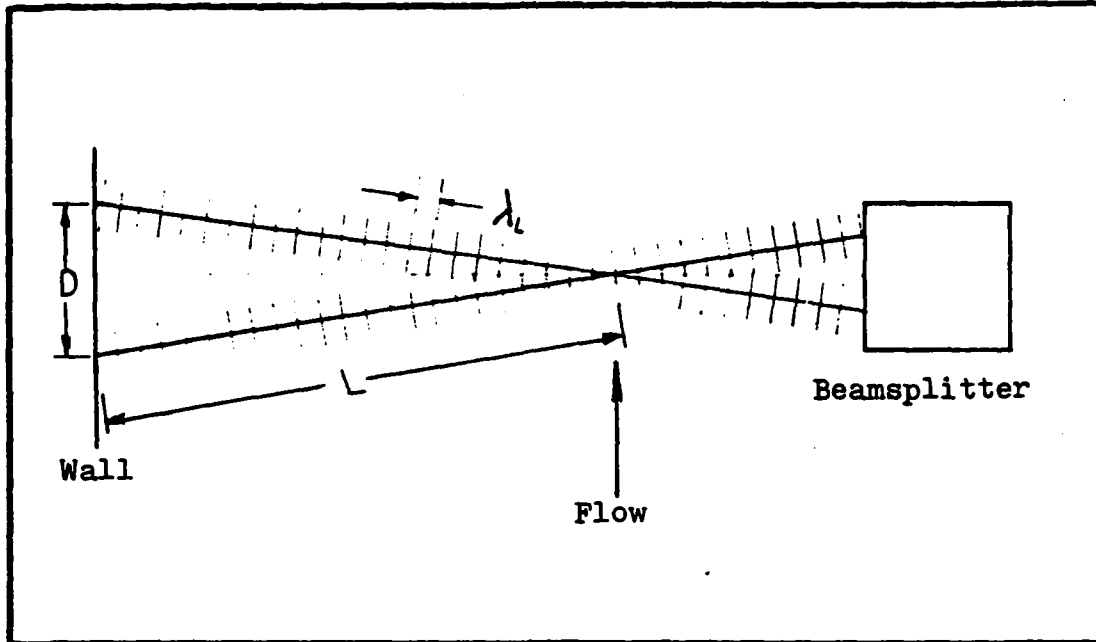


Figure 6. Fringe Spacing Parameters

Since velocity is equal to distance divided by time, the calculation simply is

$$U = \frac{S}{T}$$

The turbulence intensity (η) is calculated by (Ref 6)

$$\eta = \frac{1}{\sqrt{2}\pi} \left[(R-1) + \frac{1}{n^2} \right]^{\frac{1}{2}}$$

where

$$n = \frac{r_0}{S}; r_0 = \text{radius of beam and}$$

$$R = \left(\frac{g_2 - g_1}{g_2 - g_3} \right); g_1, g_2, \text{ and } g_3 \text{ are the channel contents of the autocorrelation function.}$$

V. Experimental Procedure

Mach Number Calibration

The validity of the various measurements depends on precise chamber pressure calibration to obtain and maintain the desired Mach number. For the purpose of calibration incompressible flow conditions were assumed at the nozzle exit.

The procedure followed to set the pressure prior to each test sequence to provide a constant Mach number went as follows:

1. From the chamber temperature (T_c), the velocity was calculated by the definition of Mach number

$$M_e = \frac{U_e}{a}$$

where

$$a = 49 \sqrt{T_c}$$

For the low velocities $T_c = T_e$ was assumed. ($T_c = 1.008 T_e$ @ $M = 0.2$)

2. The calculated U_e was substituted into the following equation to find inches of Merrian fluid required

$$\Delta h_m = \frac{P_a U_e^2}{2g_c R T_a \gamma_m}$$

3. The chamber inlet values were adjusted to give this Δh on the manometer.

4. The Laser Velocimeter was employed to obtain a velocity reading in the center of the jet at the nozzle exit.

5. The experimental velocity compared to the calculated velocity had to agree within 3%. Three percent was found to be the average deviation from the peak correlation channel, g_2 , on the autocorrelation function.

6. This manometer reading was noted and monitored throughout the testing sequence.

Appendix A outlines the equations and assumptions used to calibrate the manometer for the two operating Mach numbers.

Optical Alignment

The procedure detailing the alignment of the beams with respect to the plates and focusing optics was carried out in four steps. The first step encompassed the beam, nozzle, and upper plate orthogonality. To accomplish this, the bisector of the angle between the beams was aligned parallel to both the upper plate and nozzle exit.

Second, the intersection point of the two beams was set at the center-line of the nozzle exit plane at the desired downstream station. The intersection point became the focal volume that the optics observed. A card placed at this point enabled the focal volume cross-section to be observed and aligned by means of the beamsplitter controls.

Once this was accomplished the optics on the photomultiplier tube were aligned and focused by viewing the focal volume image on the card through the polarized eyepiece. The photomultiplier tube stand was then adjusted such that the lens focused the image of the focal volume onto the pinhole aperture.

Finally, a figure or number was selected on the computer card and brought into focus by adjusting the telephoto lens. This allowed the sharpest image of the intersection point to form on the pinhole aperture. This approach prepared the system for a test sequence in a minimum amount of time.

Laser Traverse

The laser and photomultiplier were mounted on a traverse table which could be translated in three perpendicular directions. The traverse position readout system was calibrated so that the position of the beam intersection was known anywhere in the flow field. With this arrangement the flow field could be investigated quickly and easily.

Three traverse sequences were employed to map the flow field and observe the ground plate interaction at $M = .5$ and $M = .2$. Each sequence started at the zero point on the axis to be measured and progressed along the axis in both directions. The traversing table was incremented in 5 mm steps along the y and z axes and 1 cm steps along the x axis.

Velocity profiles were mapped along the z axis on the y axis center-line at the 5, 10, and 15 cm downstream positions (Figure 7). Data was gathered with the ground plate in the 1, 2, and 5 cm positions at the two Mach numbers for a total of 18 profiles.

The Coanda effect was investigated on the curved portion of the top plate. Measurements were made along the x axis in 2 cm increments up the curved surface starting at

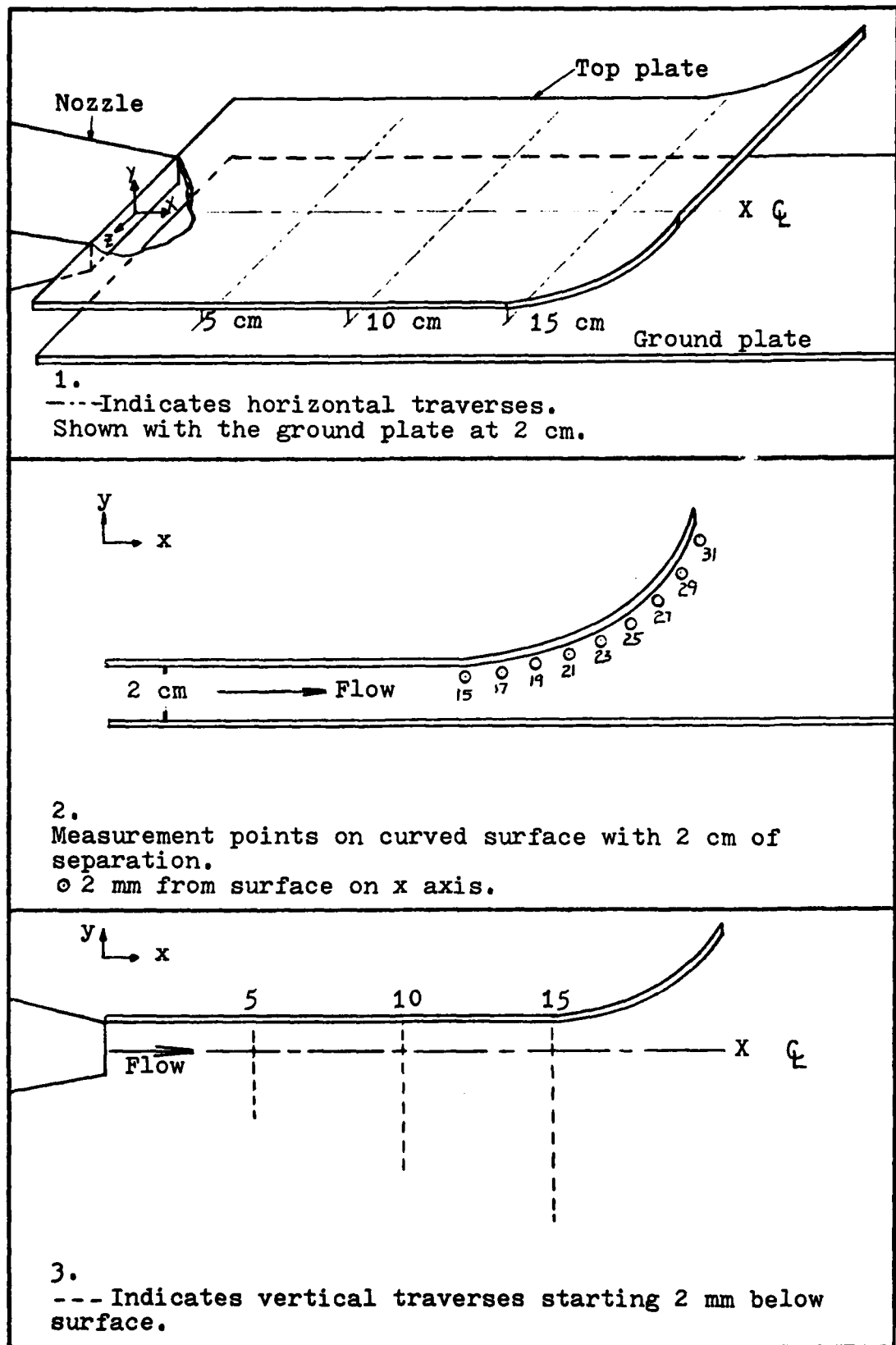


Figure 7. LV Measurement Points

the 15 cm position. The beamsplitter had to be rotated to keep the fringe pattern of the focal volume normal to the surface. Measurements were taken with the ground plane at the 1, 2, and 5 cm positions (Figure 7).

Vertical traverses were made to investigate the flow field with the ground plane removed. Data was observed from the flow as close to the top surface as possible. The planes of interest were along the y axis at the 5, 10, and 15 cm downstream points (Figure 7).

Pressure Measurements

Static pressure readings were taken from all 45 taps with the use of a micromanometer. A pressure probe inserted into the flow measured the total pressure at the tap positions. Figure 8 shows the probe in relation to a tap and the flow. In order to establish valid results without the probe interfering with the tap, measurements were taken independently. Static pressures were taken without the probe in the flow, then total pressures were taken at the edge of the port. Both readings were made with respect to atmospheric pressure.

Data Handling Technique

Prior to each traverse, the values of L and D, the beam length and width measurements, were noted. Beam length was measured from the focal volume to the laboratory wall 420 cm away. The beam length was constant throughout all testing since the measurements were all initiated at the nozzle

center-line on the $x y$ plane. The width, D , measured at the wall, changed slightly from traverse to traverse due to adjusting the beamsplitter after following beam alignment procedures. From Ref 6 the suggested fringe spacing, S , was set to correspond with the velocity range expected. A fringe spacing of $36 \mu\text{m}$ corresponded to a D of 7.4 cm which was typical throughout the sequences. The $36 \mu\text{m}$ spacing was well within tolerances for the low subsonic velocities investigated as found in Ref 6.

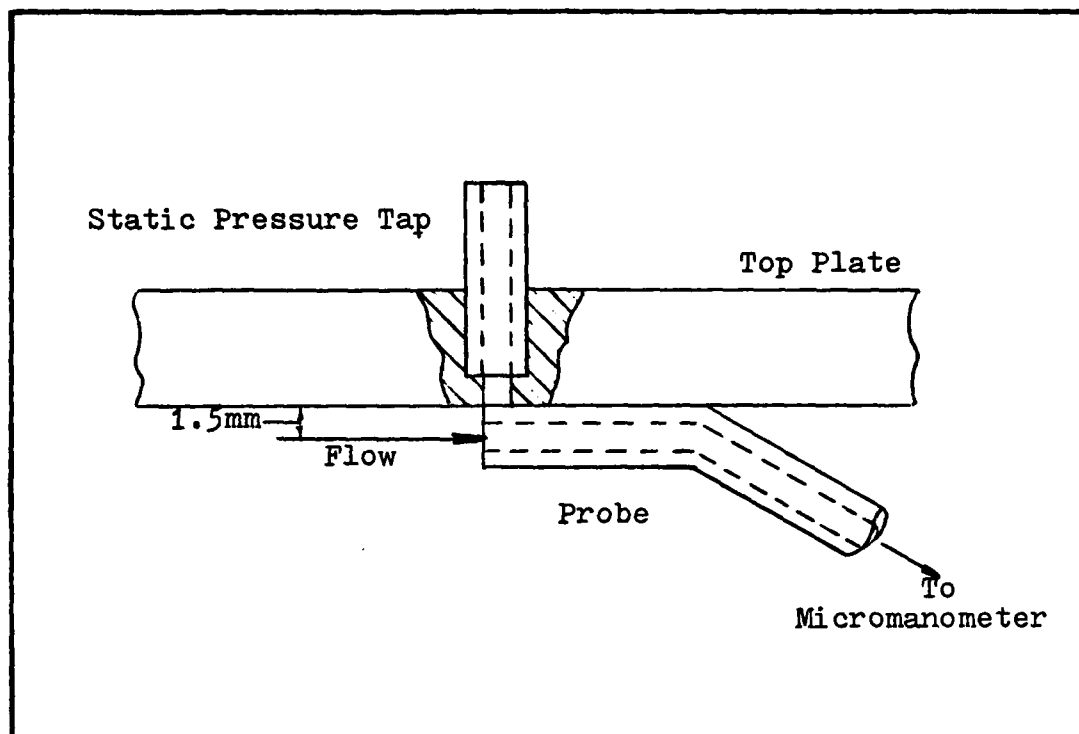


Figure 8. Pressure Probe Position in Flow

VI. Results and Discussion

Emphasis was placed on studying the flow and the effects upon it from ground plate interaction at Mach 0.15 and 0.2. As a secondary interest, measurements were taken at various positions in the flow with the ground plate removed to test the limits of the Laser Velocimeter. Some of the important results of this investigation are discussed in the following pages. The plots presented are representative of the results obtained in that particular flow regime. Appendices B, C, and D contain the remaining plots and data for a detailed comparison.

Velocity Profiles

Ground Plane Effects. Velocity profiles were taken 5 mm below the top plate corresponding to the x axis center-line. The 5, 10, and 15 cm measurement positions were in the mixing region of the jet flow. Analysis of the velocity profiles revealed two parameters which effected the flow field, natural expansion due to mixing with the still air and ground plane position. Natural expansion was completely independent of ground plate position. This was an expected result due to the nature of the jet. The jet became completely turbulent 3 cm from the nozzle exit. Due to shearing interaction with the stationary surrounding air, the emerging jet entrained

and mixed with some of the surrounding air, thus forming a transition layer along the jet boundaries. The jet carried the air entrained in this layer downstream where it expanded inward to the potential core. Figure 9 illustrates the growth of the transition layer as a function of downstream position.

The proximity of the ground plane had the effect of expanding the flow outwards along the z axis. Figure 10 shows the results of the expansion effect for $M = 0.15$ at 5 cm downstream. Velocity appeared uniformly distributed 8 cm across the width of the nozzle. As the ground plane approached the top plate the potential core expanded across the full 10 cm of nozzle width. Including the transition layer, the width of the flow increased 21% from 9.5 cm to 12 cm. The profiles at the two downstream positions indicated similar increases of 20% for the expanding flow. Velocity decay at the 5 cm position was more symmetrical compared to the downstream positions. This resulted from the growth of the transition layer at the downstream position which increased the turbulence level in the flow.

The Laser Velocimeter enabled the flow to be mapped to approximately 1 cm beyond the nozzle width on both sides. Beyond this region the correlation function was virtually flat indicating no measurable flow. This type of curve indicated very high turbulence intensities present in the flow. Data acquisition terminated for a test run when the autocorrelation function attenuated to the point of not building a peak. Figure 11 shows the minimum autocorrelation function from which data could be extracted.

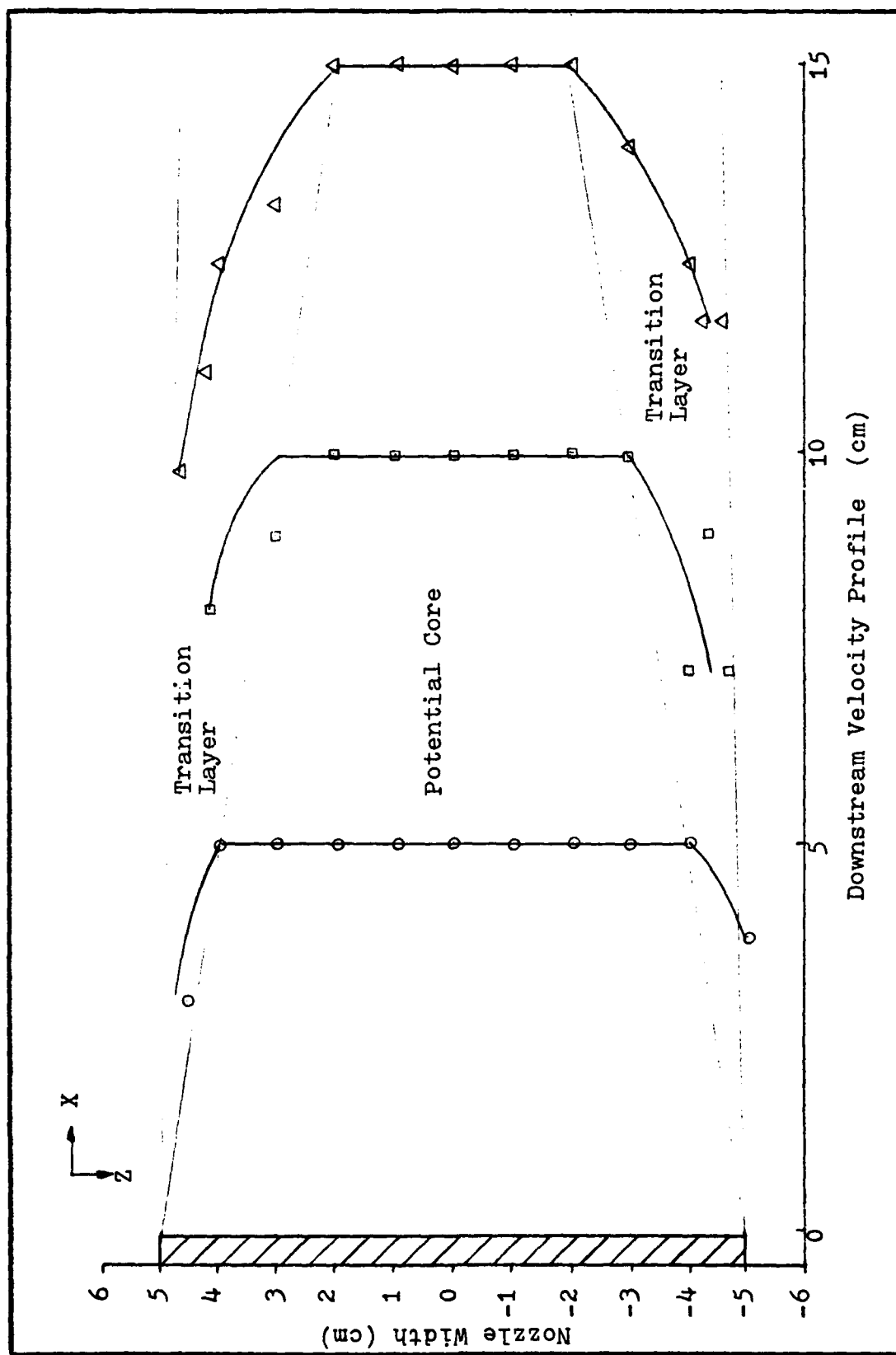


Figure 9. Downstream Transition Layer Growth

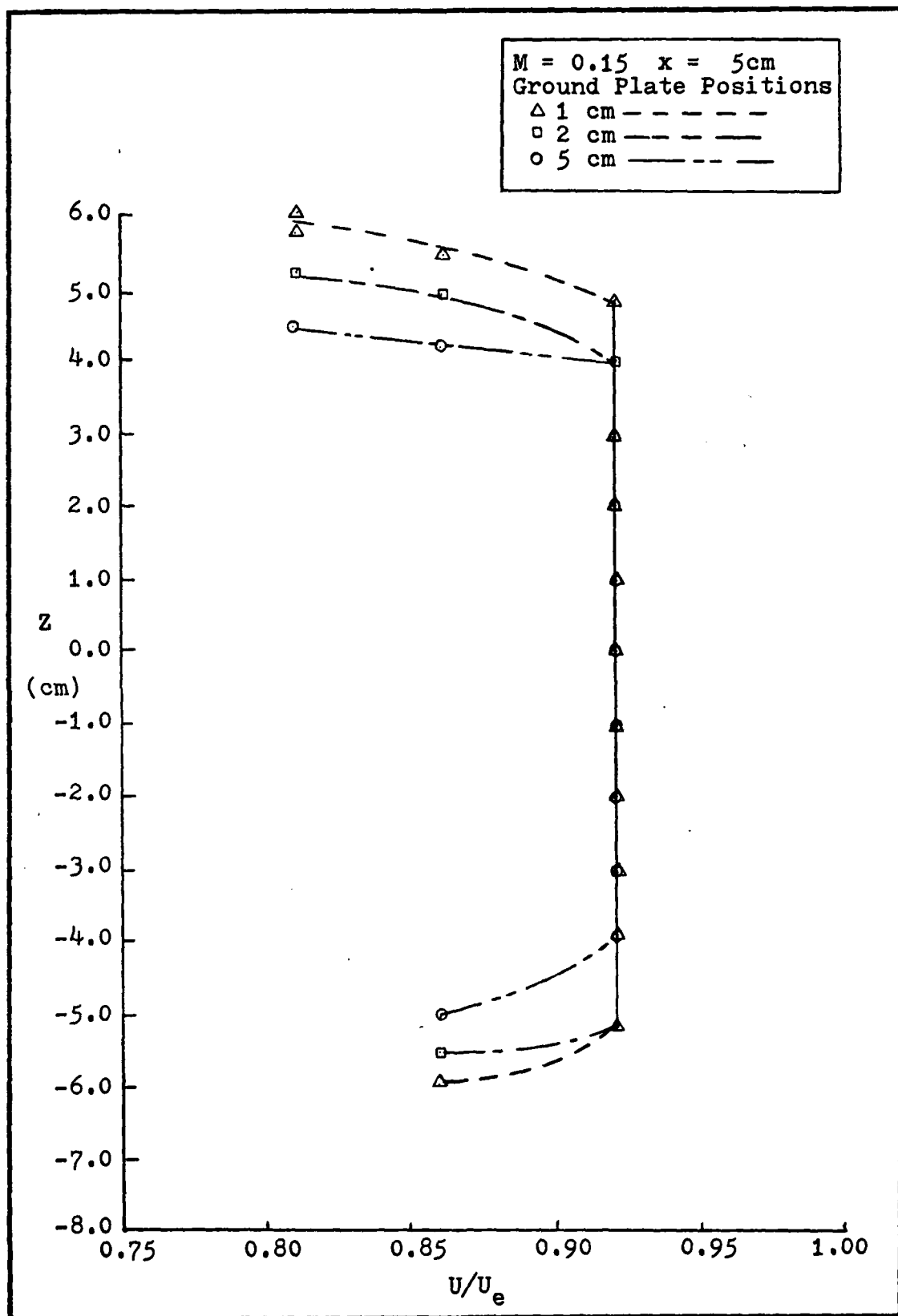


Figure 10. Velocity Profile for $M=0.15$ at $x=5$ cm for 3 Ground Plate Positions

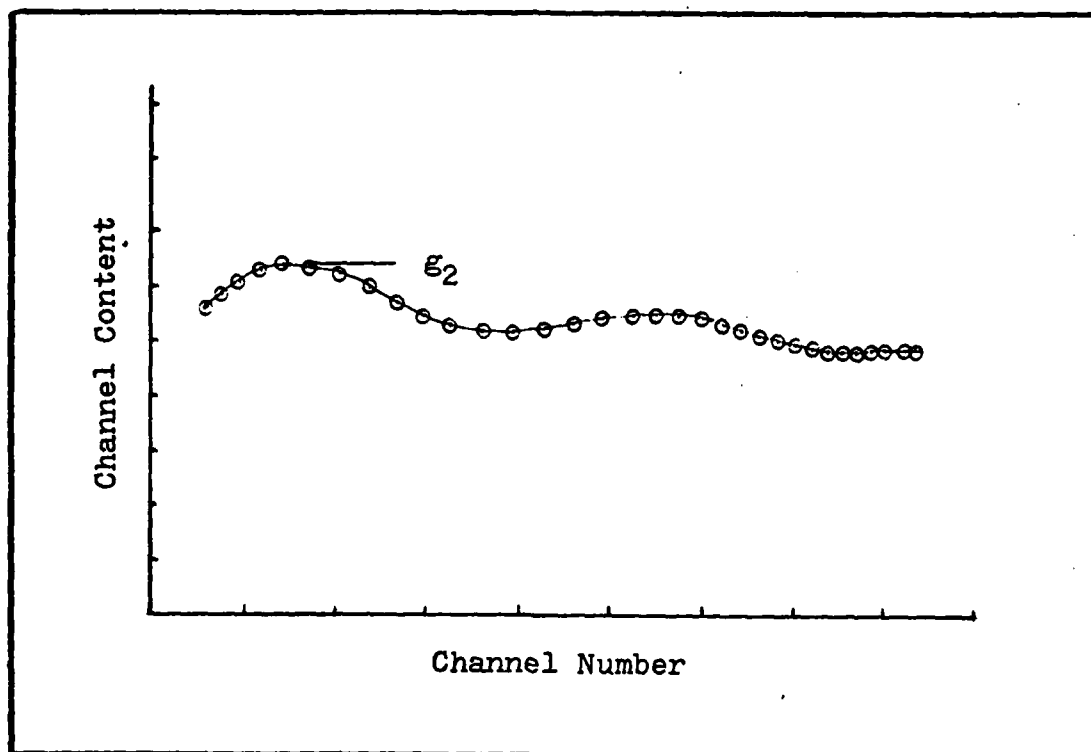


Figure 11. Autocorrelation Function at High Turbulence Intensities

Mach 0.2 profiles indicated a similar trend in flow expansion compared to Mach 0.15 (Figure 12). The difference was the width of the transition layer which was suppressed at the higher velocity. The expansion of the flow due to the ground plane resulted in an increase of only 16% at the 5 cm position. The width of the jet at this point expanded from 9 cm to 11 cm at the boundary. Downstream positions showed similar developments.

The potential core did not exhibit a large decay due to the mixing region compared to the lower Mach number. The width of the potential core for 1 cm of separation of the plates changed from 2 cm at $M = 0.15$ to 6 cm at $M = 0.2$ (Figure 13). The potential core at each station in the

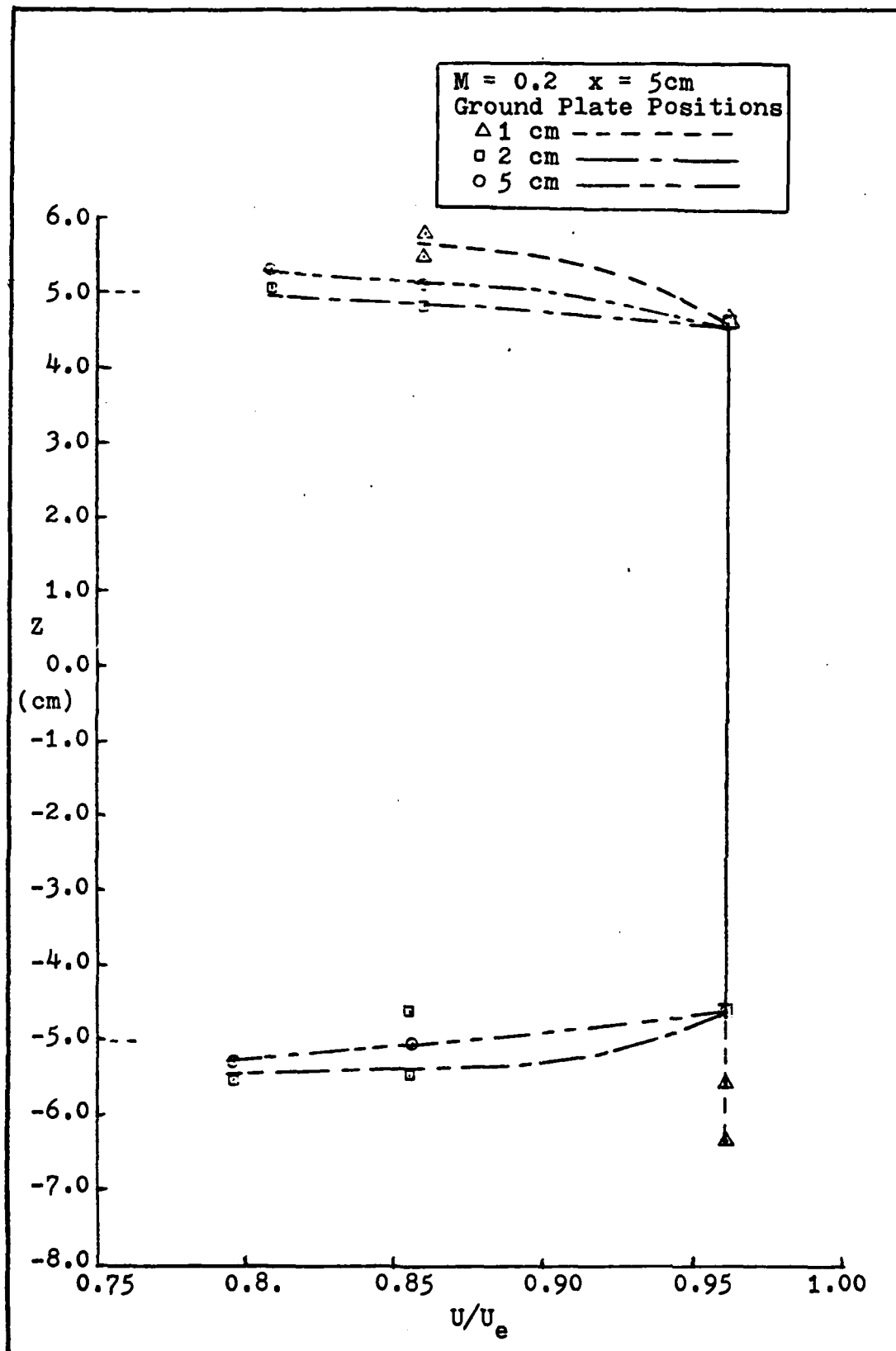


Figure 12. Velocity Profile for $M=0.2$ at $x=5$ cm for 3 Ground Plate Positions

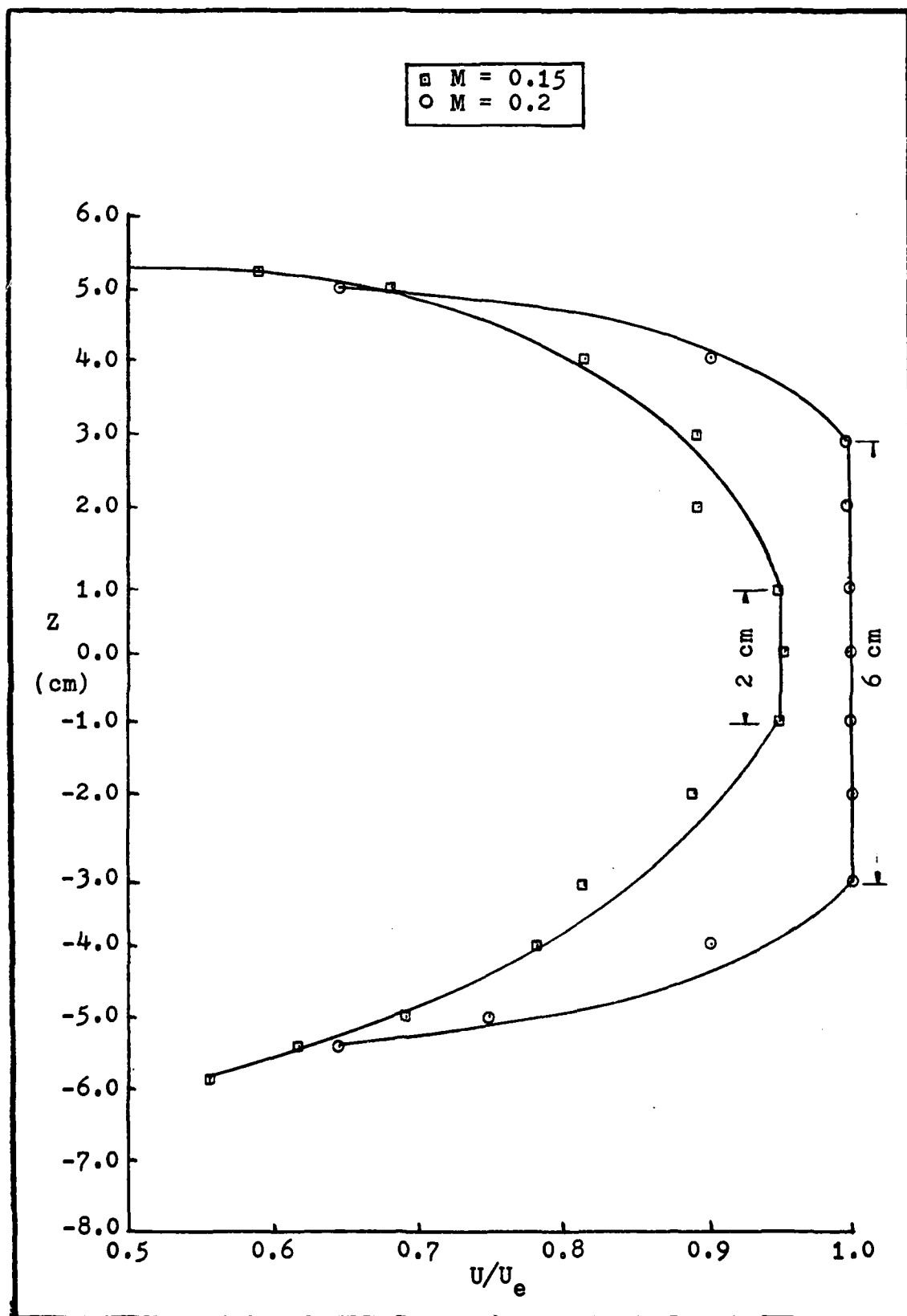


Figure 13. Potential Core Decay for $M=0.15$ and $M=0.2$ at $x=15$ cm for 1 cm Separation

Mach 0.2 flow remained constant as the ground plate approached the top plane.

Also noted was the fact that the velocity profiles were not all symmetrical with respect to the center-line. The result was thought to be due to transients in the flow; however, when the run was repeated, the same effect occurred. Two possible explanations of this asymmetry were that the plate was warped at this station or the transition layer was fully developed from turbulence, friction, and mixing upstream.

The characteristics of the jet at the 15 cm position with the 1 cm separation indicated a velocity increase. Figure 14 shows the increase for Mach 0.15 flow compared to the 2 and 5 cm separations. Since this was only noticeable with the 1 cm separation it was assumed that friction due to the closeness of the plates caused a pressure drop at the curve whereby the flow accelerated.

Curve Surface. The measurements taken along the curve attempted to demonstrate the Coanda effect. This phenomenon was basically the tendency of the jet to attach and follow the solid surface due to a pressure differential near the surface.

Figure 15 shows the Laser Velocimeter results of Mach 0.15 and 0.2 at the jet center-line corresponding to a ground plate position of 5 cm. The flow velocity increased as the flow turned through the first 2 cm, decreased gradually to 24 cm, and finally separated from the plate. Figure 16 shows schematically the Coanda effect near the curved surface.

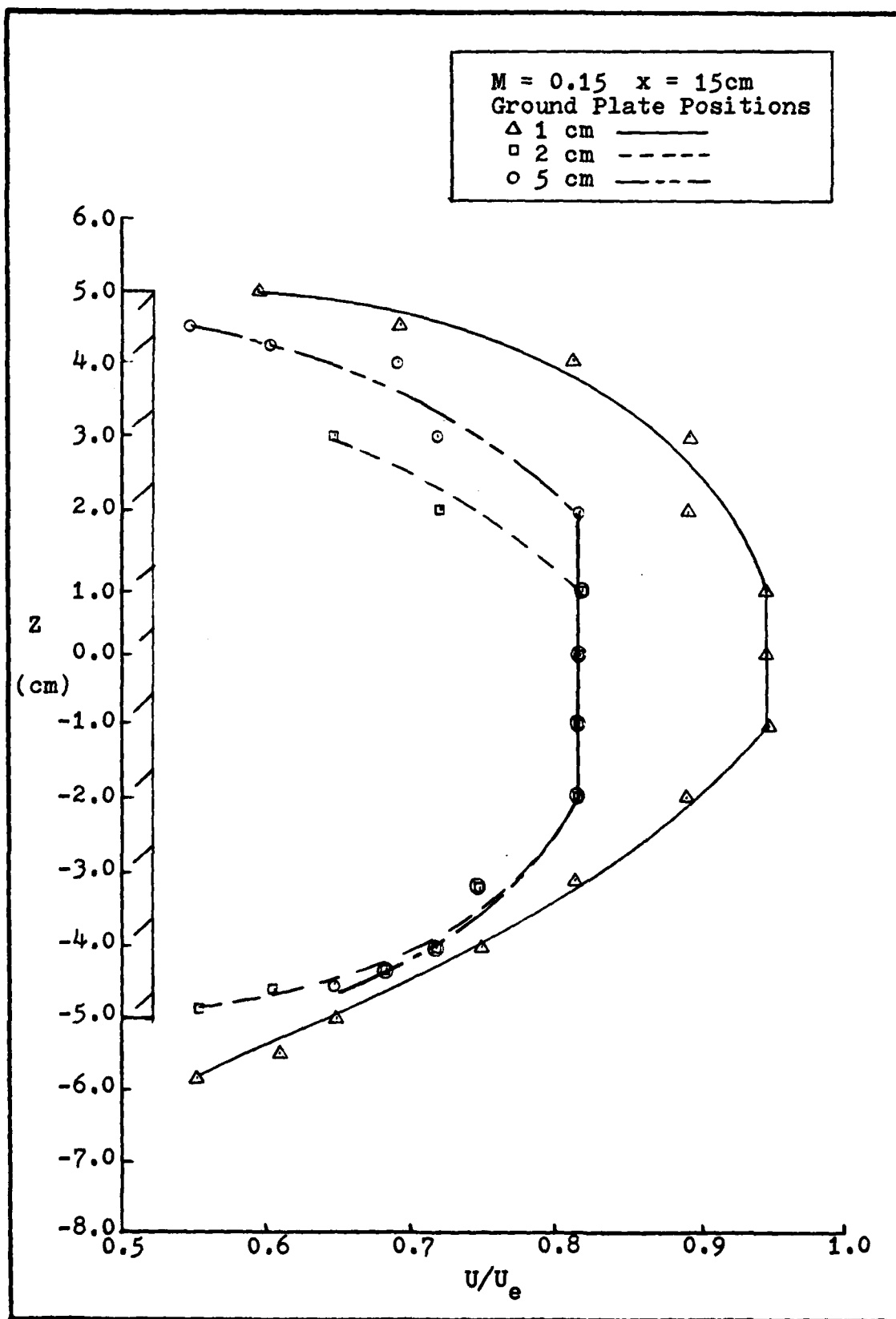


Figure 14. Velocity Increase for $M=0.15$ at $x=15$ cm for 3 Ground Plate Positions

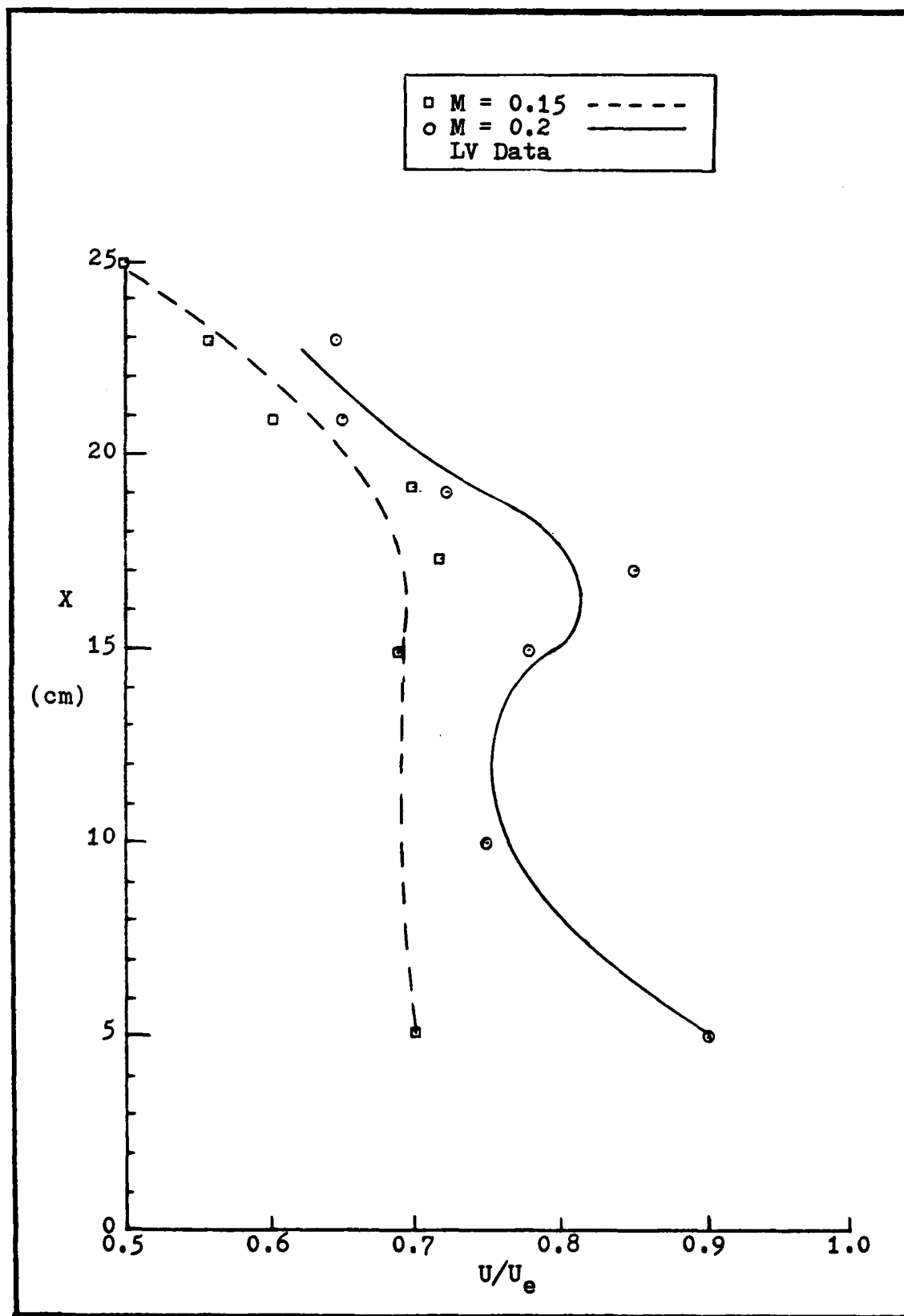


Figure 15. Velocity Profiles for $M=0.15$ and $M=0.2$ Along the x Axis Centerline

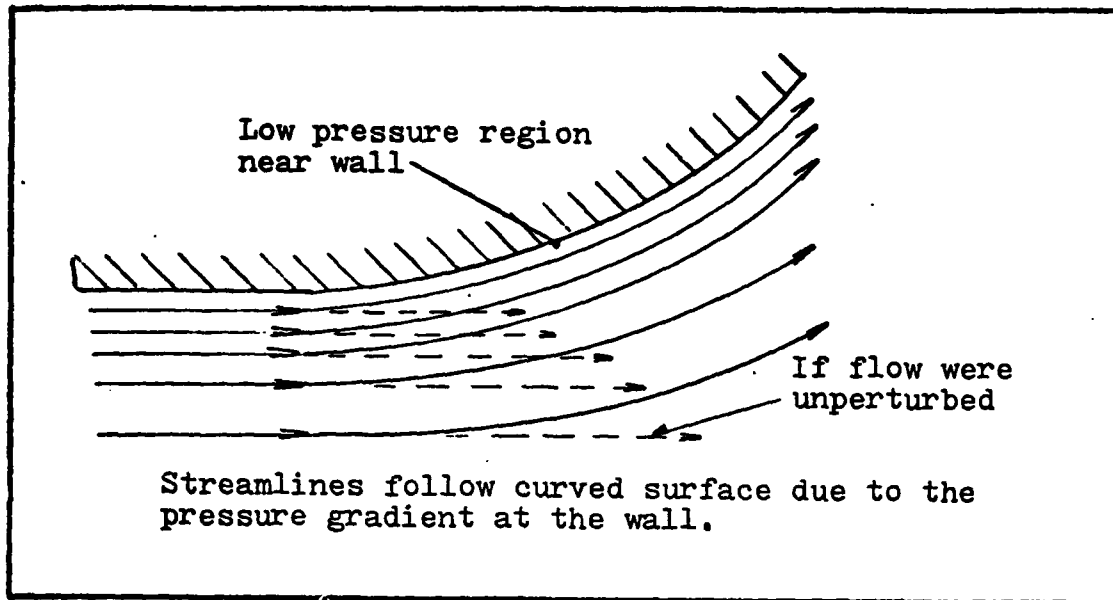


Figure 16. Schematic of Coanda Effect

Vertical Profiles. Vertical traverses were made at the 5, 10, and 15 cm stations from the plate to the lower transition boundary. The 5 mm region from the nozzle center-line to the top plate which included the plate boundary layer was of particular interest. The boundary layer was 3.5 mm thick at the 5 cm station and increased to 5 mm at the 15 cm station. Measurements in this layer confirmed very turbulent flow as a result of the jet flow contacting the plate. Figure 17 compares the vertical profiles at the 5 cm station for the two Mach numbers.

From the geometry of the focal volume and traversing mechanism, the Laser Velocimeter was limited to 2 mm below the surface of the top plate. The electronics were unable to extract any valid data in the high turbulence regime close to the surface. The plate interfered with the beams and optics such that the control volume could not be seen clearly.

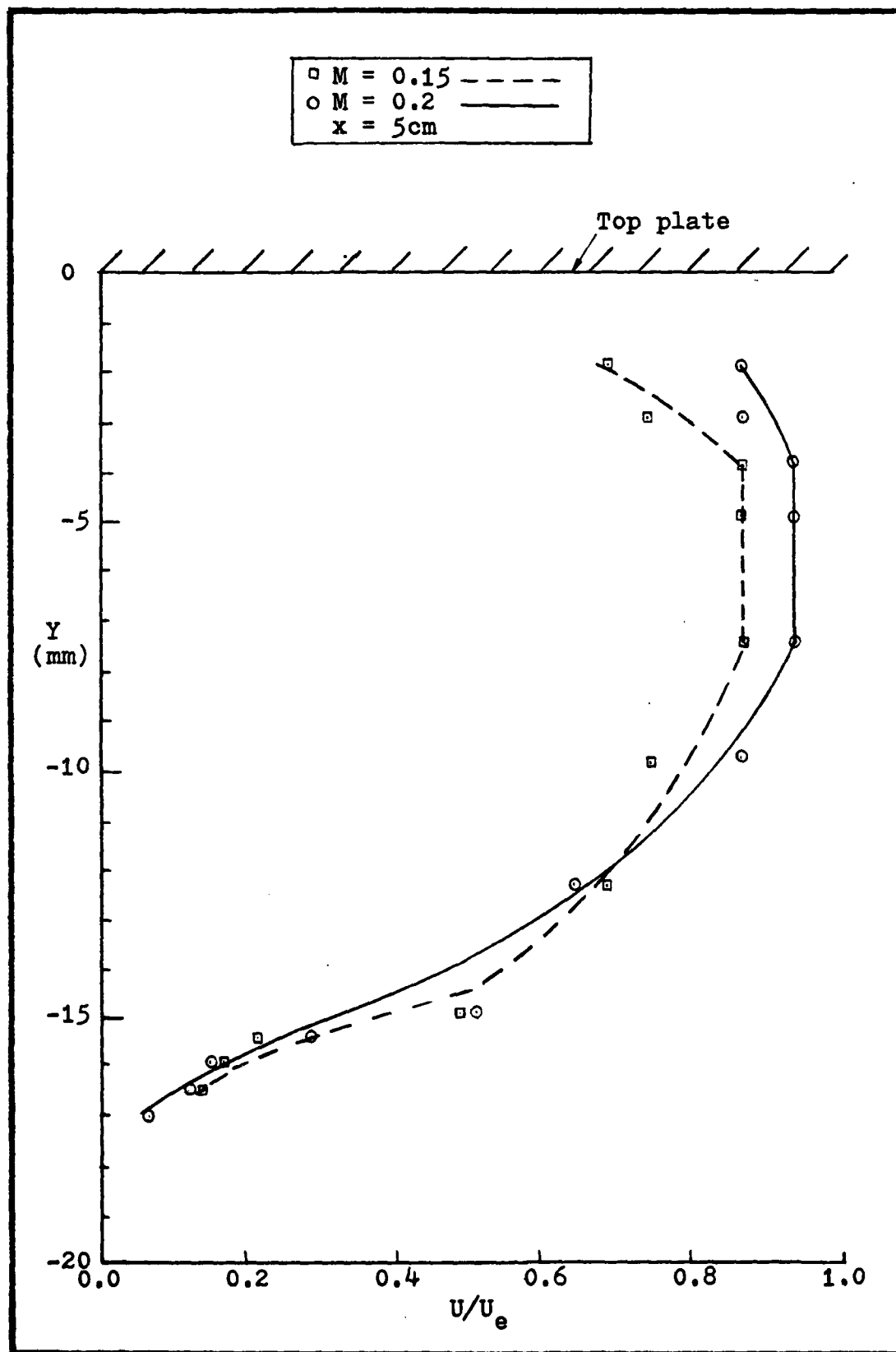


Figure 17. Vertical Velocity Profiles for $M=0.15$ and $M=0.2$ at $x=5\text{cm}$

An analytical approach to calculate the boundary layer was considered; however, results were not consistent with the data (Ref 9). The problem encountered was one of how to categorize this particular boundary layer. Table I lists the Reynold's numbers characteristic of the subsonic flow at the three stations of interest.

TABLE I

Reynold's Numbers Based on Streamwise Direction
Reynold's No. ($\times 10^{-5}$)

X	M = .15	M = .2
5	0.78	1.30
10	1.99	2.68
15	2.25	3.54

The classical approaches only considered one characteristic flow regime. In this investigation the boundary layer was influenced by the jet boundary, plate roughness, unsteady flow near plate, surrounding still air leaking into the jet flow, and plate oscillations. An accurate boundary layer calculation would have encompassed all of parameters and their effects.

Pressure Results. The velocity pressure measurements were taken in the boundary layer at the top plate corresponding to the 11 static pressure taps along the x axis centerline. The pressure probe essentially measured the total pressure corresponding to a streamline 1.5 mm below the top plate. The pressure probe was placed in the flow and

positioned in the xz plane such that the manometer gave the highest reading. This was done so no error would be introduced by incorrect alignment of the probe axis on a streamline. The LV measurements at the same locations were limited to 2 mm below the surface; therefore, the data was presented as a similarity profile in Figure 18. Velocity corrections for probe interference were not included since the corrections were negligible (Ref 7). Evidence of the flow accelerating in the vicinity of the curve was detected by both methods. This effect was more apparent with the Mach 0.2 flow. In the vicinity of the wall and where the flow was not parallel in the xy plane to the probe axis, agreement was not obtained; however the laser data was consistent with the physics of the flow while the pressure data was not.

The static pressures from all taps are shown in Table II. The highest readings were concentrated along the center of the flow. A positive pressure gradient existed along the flat portion of the plate for both Mach numbers. The acceleration effect of the curved surface was evident from the negative pressure readings at the 15 cm position and up along the curve. The flow followed the curved surface until separation which corresponded to tap 42 or 8 cm downstream from the flat plate section.

Turbulence Intensity

Turbulence intensities were indicative of the amount of turbulence in the flow field. The potential core of the jet was typified by measurements of negligible intensities while

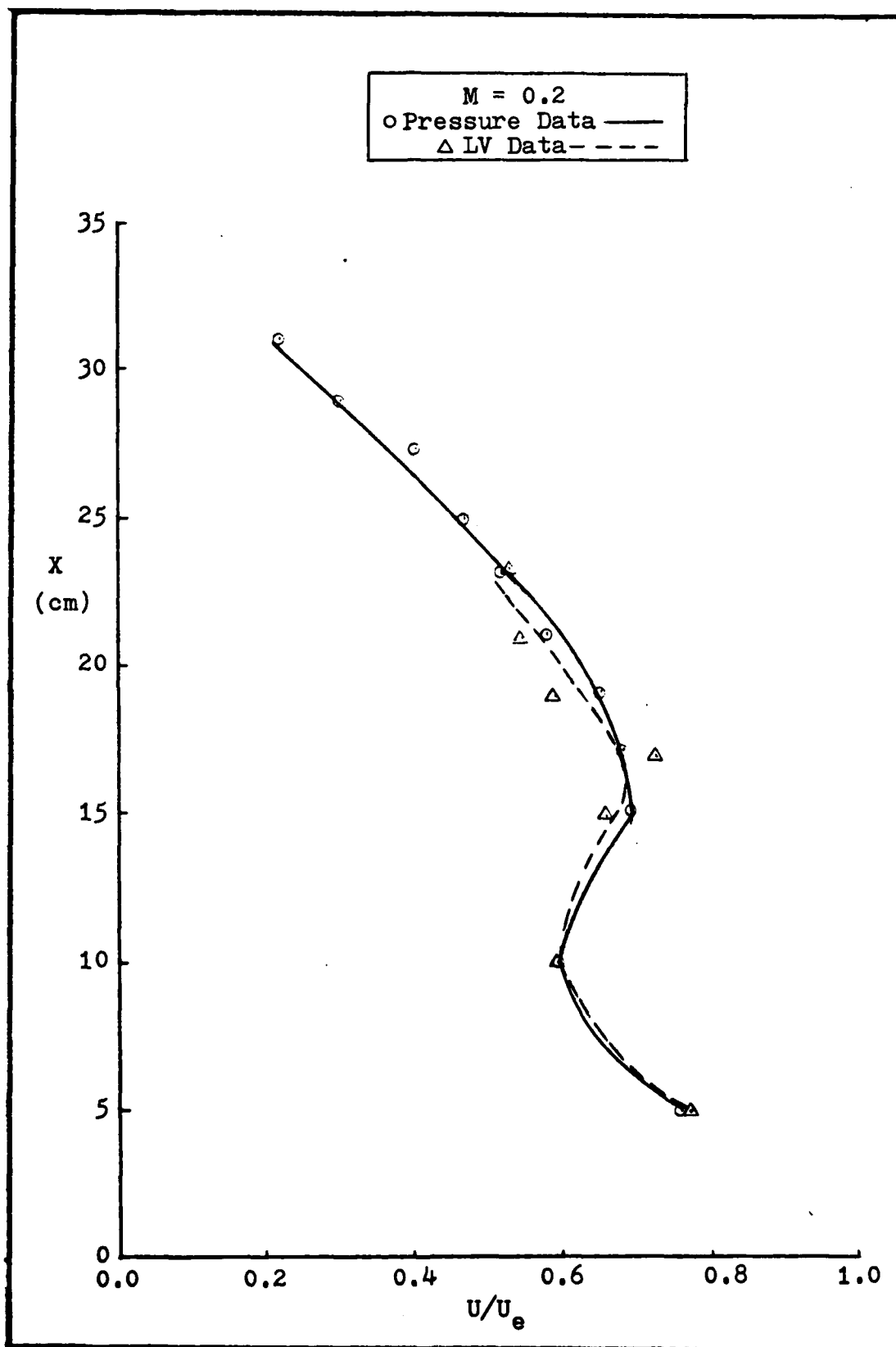


Figure 18. Pressure and LV Similarity Profiles for $M=0.2$

TABLE II

Static Pressures on Top Plate

Station	Δh (inches)		Station	Δh (inches)	
	M=0.15	M=0.2		M=0.15	M=0.2
1	0	0	24	0	0
2	0	.08	25	0	0
3	-.05	-.05	26	0	0
4	0	.08	27	0	0
5	.05	.08	28	0	0
6	.12	.10	29	-.02	-.04
7	.08	.20	30	-.31	-.06
8	.09	.25	21	-.35	-.70
9	.09	.25	32	-.30	-.97
10	0	0	33	-.04	-.70
11	0	0	34	0	-.10
12	0	0	35	0	-.02
13	0	0	36	0	-.02
14	0	0	37	0	0
15	.05	.14	38	-.50	-.88
16	.06	.20	39	-.42	-.82
17	.08	.25	40	-.25	-.55
18	.10	.27	41	-.11	-.25
19	.08	.28	42	-.05	-.10
20	.08	.22	43	-.04	-.10
21	.04	.20	44	-.05	-.09
22	.03	.15	45	-.05	-.09
23	0	.10			

the transition region exhibited intensities of 15% to 30%. Figure 19 illustrates the turbulence intensity profiles for Mach 0.2 flow at 5 cm with the effect of the ground plate. The effect on the potential core indicated small increases of turbulence from 0% at 5 cm of separation to 4.5% at 1 cm of separation. The downstream changes in turbulence intensities are shown in Figure 20 where the turbulence increases from 0% at 5 cm position to maximum of 8% at the 15 cm station.

A problem of computing the turbulence intensity arose when the R value was less than 1.0. The equation for turbulence intensity is

$$\eta = \frac{1}{\sqrt{2} \pi} \left[(R-1) + \frac{1}{n^2} \right]^{\frac{1}{2}}$$

where the term under the radical, when $R < 1$, becomes negative. For this investigation it was assumed that values of R in the range of $R < 1.0$ corresponded to a 0% turbulence intensity.

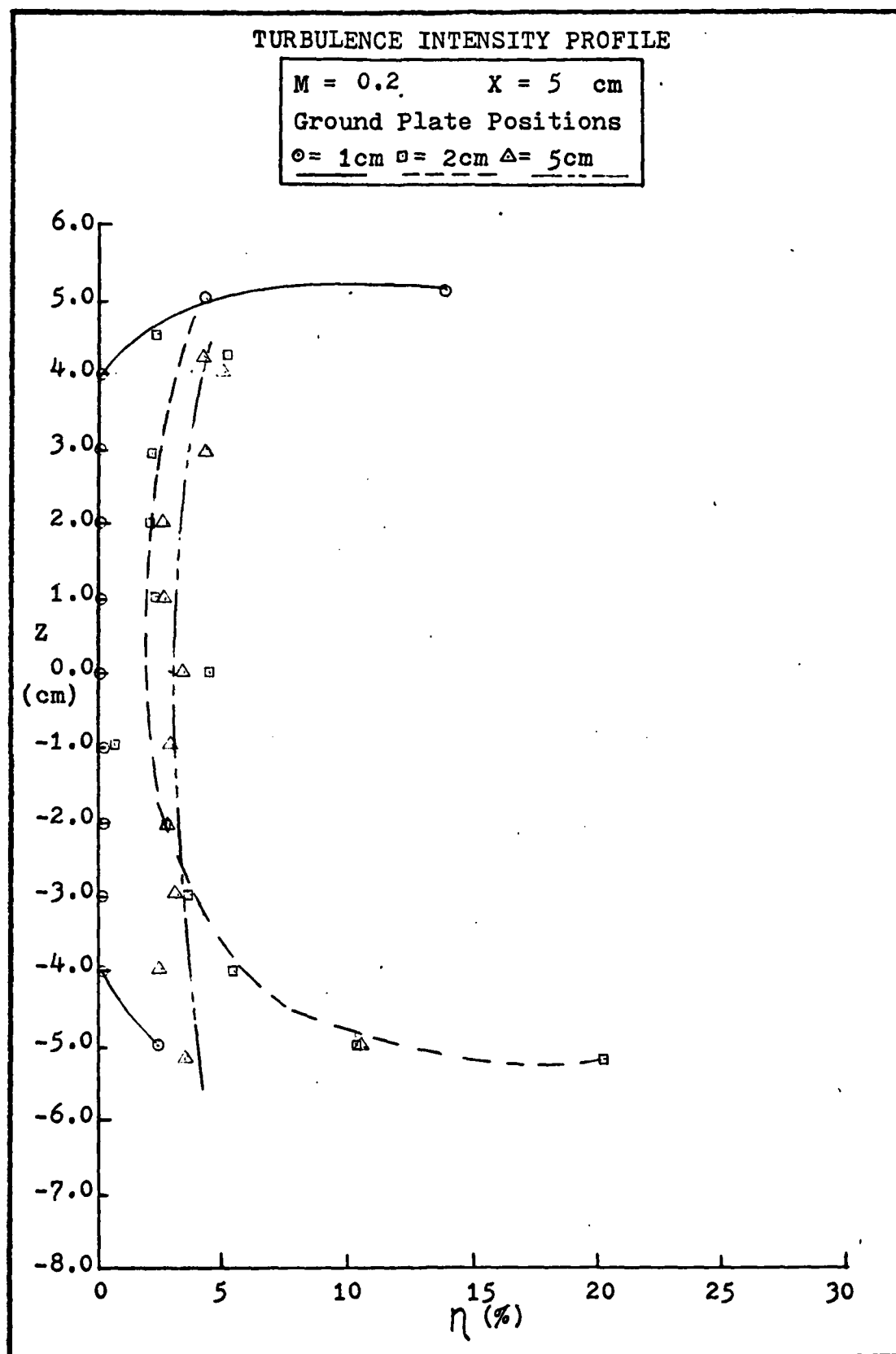


Figure 19. Turbulence Intensity for $M=0.2$ at $x=5\text{cm}$ for 3 Ground Plate Positions

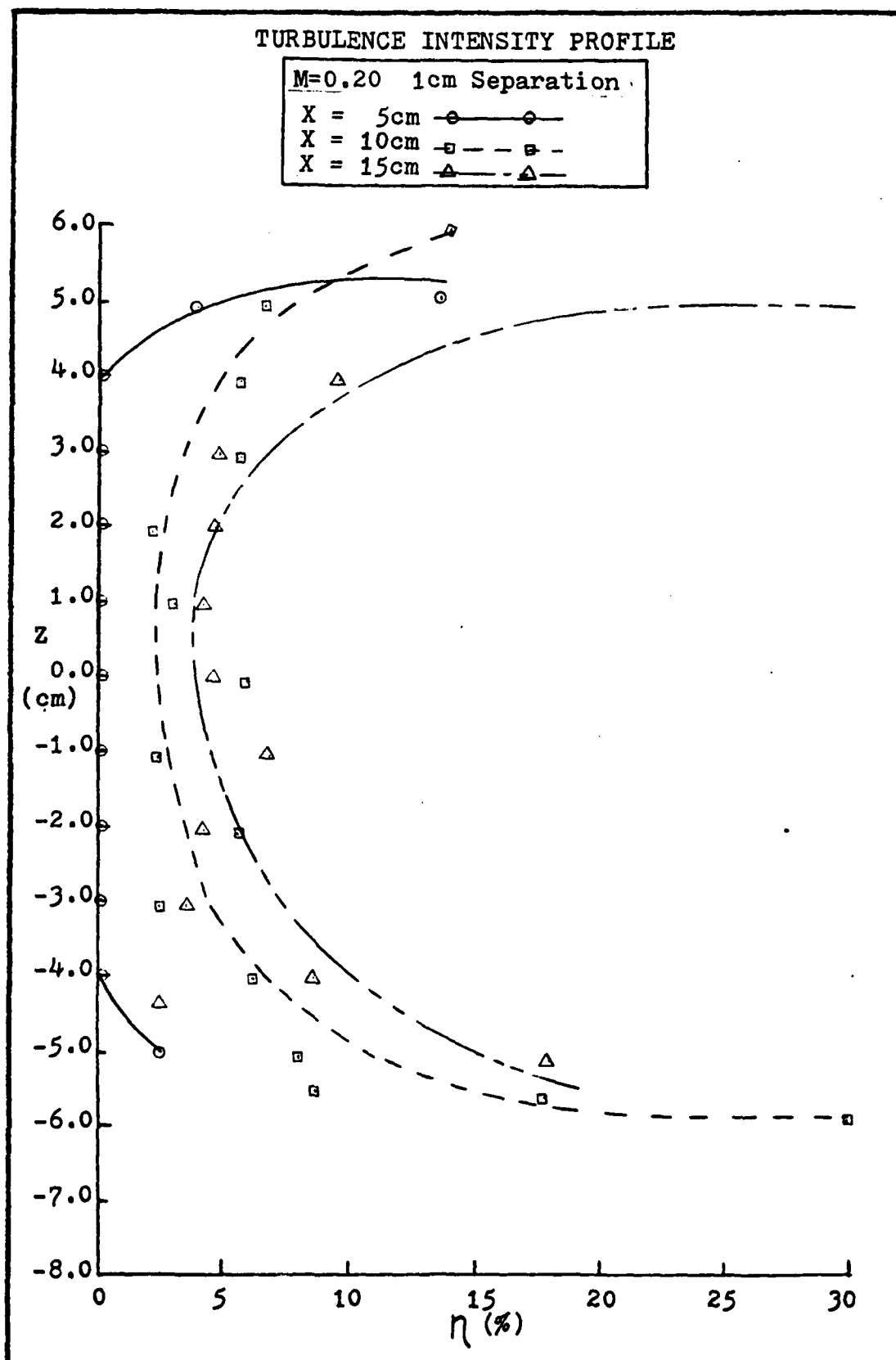


Figure 20. Turbulence Intensity Profiles for M=0.2 at Down stream Stations

VII. Conclusions

The velocity and turbulence intensity parameters for various plate configurations were measured with the Laser Velocimeter. Pressure probe measurements were taken in the jet flow and compared to the LV results. The following are the conclusions from the results:

1. The proximity of the ground plate had the effect of expanding the flow outward. The flow field experienced the onset of expansion with 2 cm of separation from the ground plate. The 5 cm point was considered to be at infinity for all practical purposes since the flow field experienced no plate induced effects. This result can be compared to the result of Staufenbiel (Ref 11) if the flow field width is considered as the effective span of the top plate. The hypothesis then can be stated from this thesis that at separations less than 20% of the span the flow field was influenced by the ground plate.

2. The velocity measurements taken in the vicinity of the curved portion of the top plate did indicate the Coanda effect. However, a more rigorous approach is needed which should include a hot jet discharge much closer to the curve. This arrangement would be better suited to the study of the Coanda effect as applied to high lift devices.

3. The vertical velocity profiles showed the existence

of a fast growing turbulent boundary layer along the top plate. The factors contributing to the growth of this layer included the mixing region of the jet, plate roughness, entrainment of the surrounding air and the ground plate deflecting the flow. A more detailed study of the effect of each of these parameters should be undertaken to understand the influence of each on the boundary layer.

4. The laser velocimeter's capabilities and limits were tested in measurements of the jet flow boundary layers and plate boundary layers. Both of these regions encompassed very high turbulent flow regimes and thin boundary layers. To accurately measure the flow parameters in these regions of high turbulence, the traversing mechanism was moved in smaller increments due to the thin boundary layers. The choice of a smaller time scale from the present 50 nano-seconds for the LV should be considered. The optical receiving equipment should be adapted to enable the portion of the focal volume being viewed to be decreased; therefore, allowing the boundary layers to be studied in more detail. This dictates that the equipment be designed so that the beam does not impinge on a surface very near the probe volume minimizing noise.

5. The turbulence intensities were insignificant in the potential core of the jet near the nozzle exit. Turbulence in the potential core increased to a peak of up to 10% at the 15 cm position. Increases were accredited to natural turbulent mixing in the jet, existence of a shear layer, and

ground plate proximity. Turbulent intensities of 10% and more were found in the extreme velocity gradient regions in the jet transition and plate boundary layers.

VIII. Recommendations

The following recommendations of the present system include modifications of both the test apparatus and LV measurement system. Modifications to the signal processing instruments are not discussed but can be found in Reference 3.

1. The source of air flow was a two dimensional nozzle discharging into still air. The plates and associated hardware could be mounted in a subsonic wind tunnel as an alternate air source. The wind tunnel would simulate the WIG's environment better than the nozzle flow.

2. The present model can be modified to allow flow of secondary air on both sides of the nozzle. With this modification the mixing region of the still air and jet flow can be investigated along with its effect on the two plates.

3. To accurately measure thin boundary layers the control volume in the flow should be decreased. With a smaller control volume smaller increments can be made with the traversing mechanism to measure the boundary. This can be accomplished by reducing the diameter of the intersection point either with smaller laser beam or lenses which focus the beams to a smaller point.

Bibliography

1. Advisory Group for Aerospace Research and Development. Applications of Non-Intrusive Instrumentation in Fluid Flow Research. Papers and Discussion of the Fluid Dynamics Panel Symposium held at the French-German Research Institute (ILR), Saint-Louis, France, May 1976. (AGARD-CP-193)
2. Blakeney, J. H. Exploratory Study of the Turning Characteristics of a Coanda-Operated Jet-Flap. MS Thesis. Monterey, California: Naval Postgraduate School, September 1972. (AD 753 618)
3. Cerullo, N. G. An Experimental Evaluation of a Laser Velocimeter by the Study of Turbulence in a Plane Free Jet at High Subsonic Velocities. MS Thesis. Wright-Patterson Air Force Base, Ohio: Air Force Institute of Technology, June 1979.
4. Keenan, J. M., and Kaye, J. Gas Tables. New York: John Wiley and Sons, Inc., 1945.
5. Kuethe, A. M. and Schetzer, J. D. Foundations of Aerodynamics. 2d ed. New York: Wiley and Sons, Inc., 1959.
6. Malvern Instruments, Ltd. Operating and Installation Manual. Spring Lane Trading Estate, Malvern Link, Worcestershire WR14 1AL, England.
7. Owen, E., and Parkhurst, R. C. The Measurement of Air Flow. 4th ed. Oxford: Pergamon Press, Ltd., 1966.
8. Parker, R. L. Aerodynamic Testing of Wing Sections Using the Laser Doppler Velocimeter. Arnold Engineering Development Center, AFSC, Arnold Air Force Station, Tennessee, November 1971. (AEDL-TR-7-264)
9. Schlichting, H. Boundary Layer Theory. 6th ed. New York: McGraw-Hill Book Company, 1968.
10. Shepard, W. K. Turbulence Measurements in a Plane Free Jet at High Subsonic Velocities. MS Thesis. Wright-Patterson Air Force Base, Ohio: Air Force Institute of Technology, December 1979.
11. Staufenbiel, R. "Some Nonlinear Effects in Stability and Control of Wing-in-Ground Effect Vehicles," Journal of Aircraft, 15:541-544 (August 1978).

Appendix A

Calculation of the Exit Velocity

The validity of the measurements depended on a constant nozzle exit Mach number. The equations and assumptions used are outlined below.

From the temperature in the chamber the exit velocity was found by:

Assume:

$$T_c = T_e \quad A1$$

which agreed with actual measurements. From definition of Mach number

$$M_e = \frac{U_e}{a} \quad A2$$

$$a = \sqrt{\gamma g_c R T_e} \quad A3$$

Eqn A3, with conversion factors, reduced to:

$$a = 14.94 \sqrt{T_e} \quad A4$$

where T_e is in ($^{\circ}R$).

For $M=0.2$ and $T_e=70^{\circ}F$,

$$U_e = M_e a = 67.77 \text{ m/sec}$$

Introducing the incompressible flow equation

$$P_o - P_a = \Delta P = \frac{1}{2} \rho V^2 \quad A5$$

let $V = U_e$

ΔP = measured pressure.

The measure pressure, ΔP , in the 100" Merriam manometer was found by

$$\Delta P = \gamma_m \Delta h_m \quad A6$$

where $\gamma_m = 2.95$.

Substituting Eqn A6 into A5 and solve for

$$\Delta h = \frac{\frac{1}{2} \rho U_e^2}{\gamma_m} \quad A7$$

Again with conversion factors, Δh in inches is

$$\Delta h = U_e^2 (7.15 \times 10^{-4}) \text{ in} \quad A8$$

For $U_e = 67.77 \text{ m/sec}$

$\Delta h = 3.3 \text{ in}$ of Merrian fluid.

This was used to initially set the chamber pressure for finer calibration by the LV. A similar calculation for Mach 0.15 corresponded to an initial setting of 1.7 in of Merrian fluid.

APPENDIX B
Pressure Data

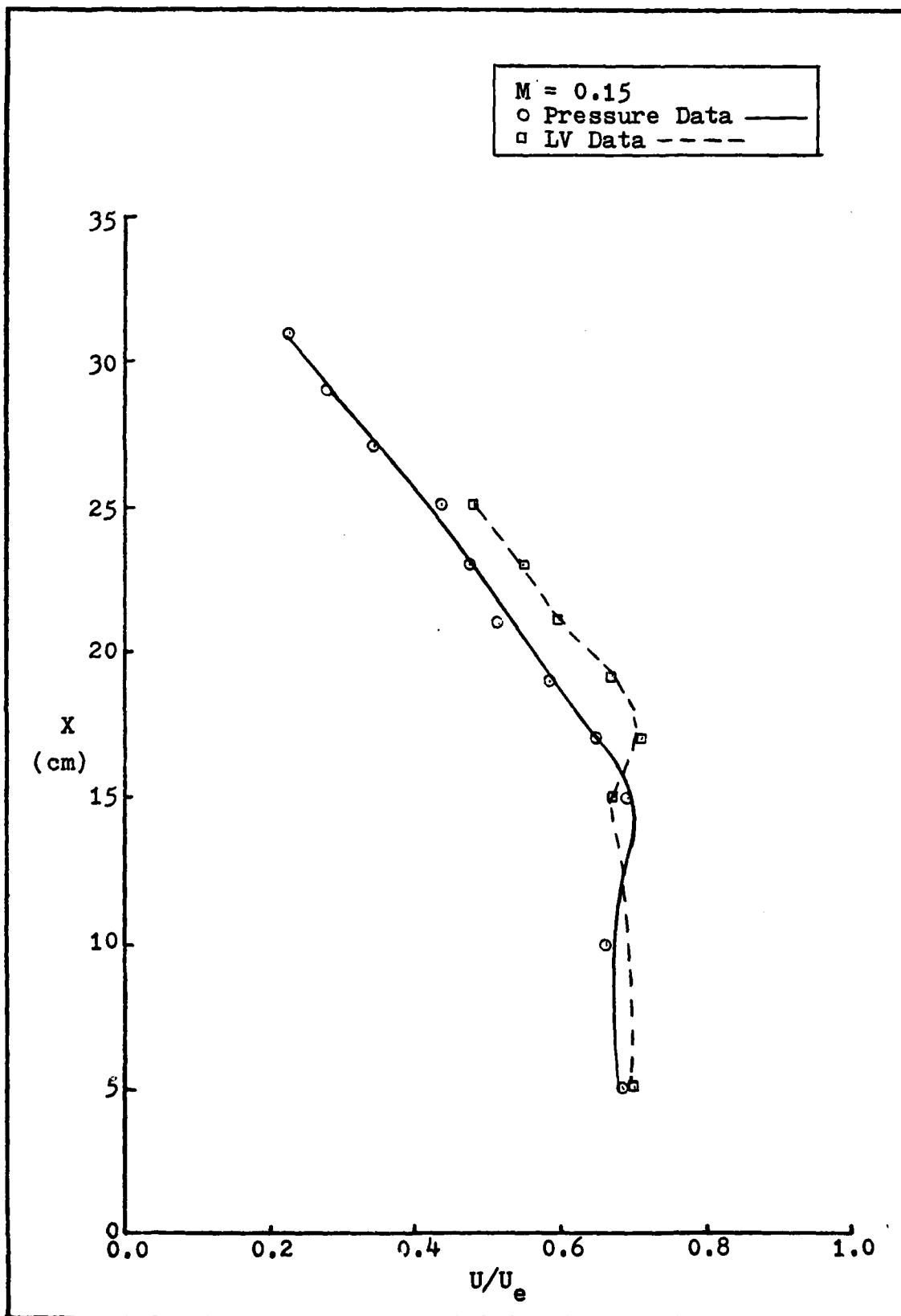


Figure 21. Pressure and LV Velocity Profiles Along the x Axis Centerline for $M=0.15$

Table III

Pressure and LV Velocities					
x (cm)	Tap no.	M = 0.15		M = 0.2	
		Pressure (m/sec)	LV (m/sec)	Pressure (m/sec)	LV (m/sec)
5	6	35.00	35.88	52.20	59.76
10	18	33.10	-	40.30	49.18
15	31	36.40	34.49	47.70	54.19
17	38	32.50	36.30	45.20	57.47
19	39	30.00	34.74	44.00	49.51
21	40	27.30	30.53	39.80	44.81
23	41	24.20	27.77	35.40	44.44
25	42	21.80	24.36	30.20	
27	43	17.50		27.60	
29	44	13.50		20.80	
31	45	11.30		15.30	

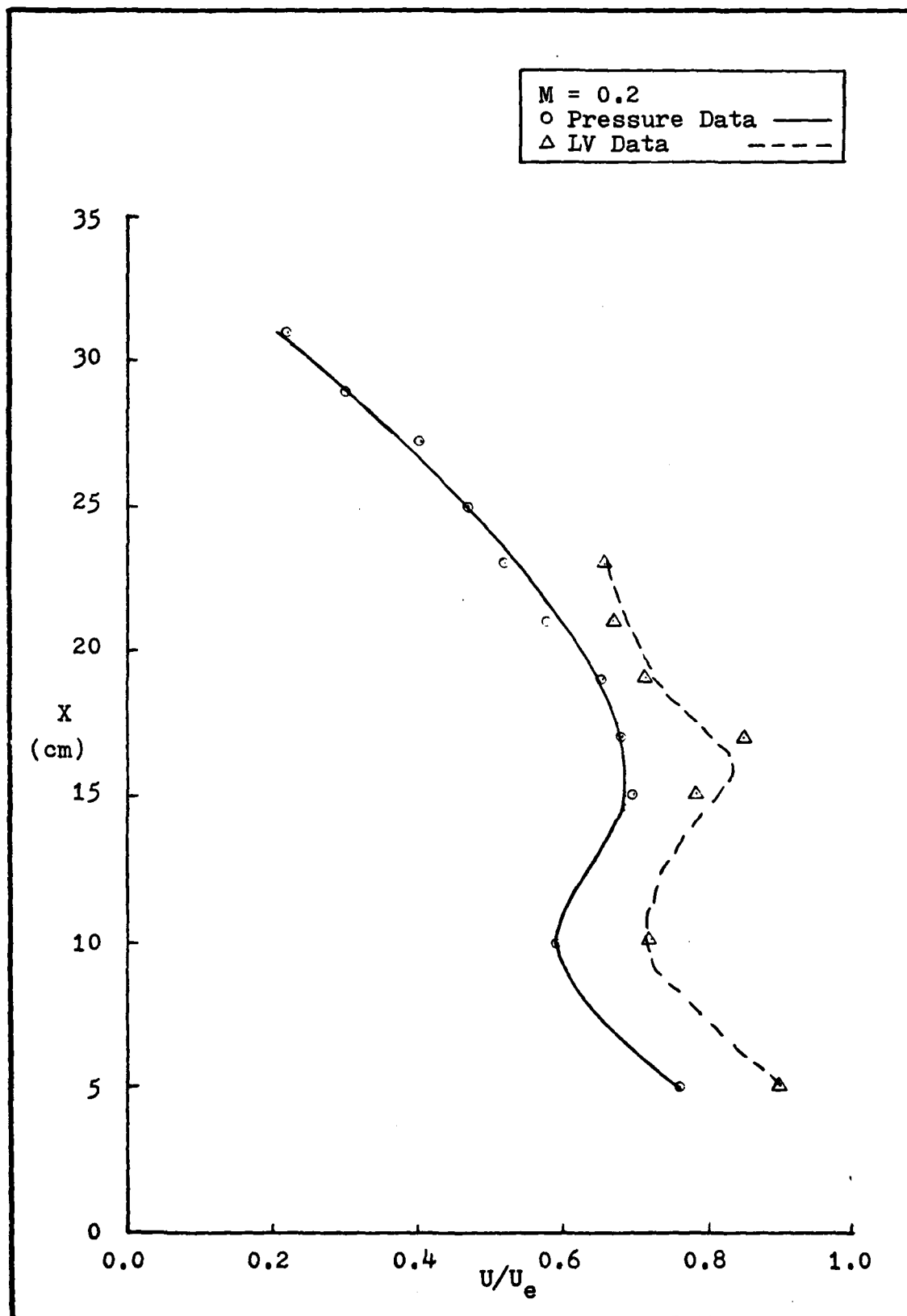


Figure 22. Pressure and LV Velocity Profiles Along the x Axis Centerline for $M=0.2$

Table IV

Top Plate Pressure Data									
x (cm)	Tap no.	M = 0.15				M = 0.2			
		Total (in)	Static (in)	Δh (in)	U (m/sec)	Total (in)	Static (in)	Δh (in)	U (m/sec)
5	6	3.50	0.12	3.38	35.00	7.60	0.10	7.5	52.20
10	18	3.10	0.10	3.00	33.10	4.75	0.27	4.48	40.30
15	31	3.30	0.35	3.65	36.40	5.55	-0.70	6.25	47.70
17	38	2.40	0.50	2.90	32.50	4.77	-0.88	5.60	45.20
19	39	2.05	0.42	2.47	30.00	4.50	-0.82	5.32	44.00
21	40	1.80	0.25	2.05	27.30	3.80	-0.55	4.35	39.80
23	41	1.50	0.11	1.61	24.20	3.20	-0.25	3.45	35.40
25	42	1.25	0.05	1.30	21.80	2.40	-0.10	2.50	30.20
27	43	0.80	0.04	0.84	17.50	2.00	-0.09	2.09	27.60
29	44	0.45	0.05	0.50	13.50	1.10	-0.09	1.19	20.80
31	45	0.30	0.05	0.35	11.30	0.55	-0.09	0.64	15.30

APPENDIX C

LV Experimental Results at $M = 0.15$
and $M = 0.2$ for z Axis Profiles

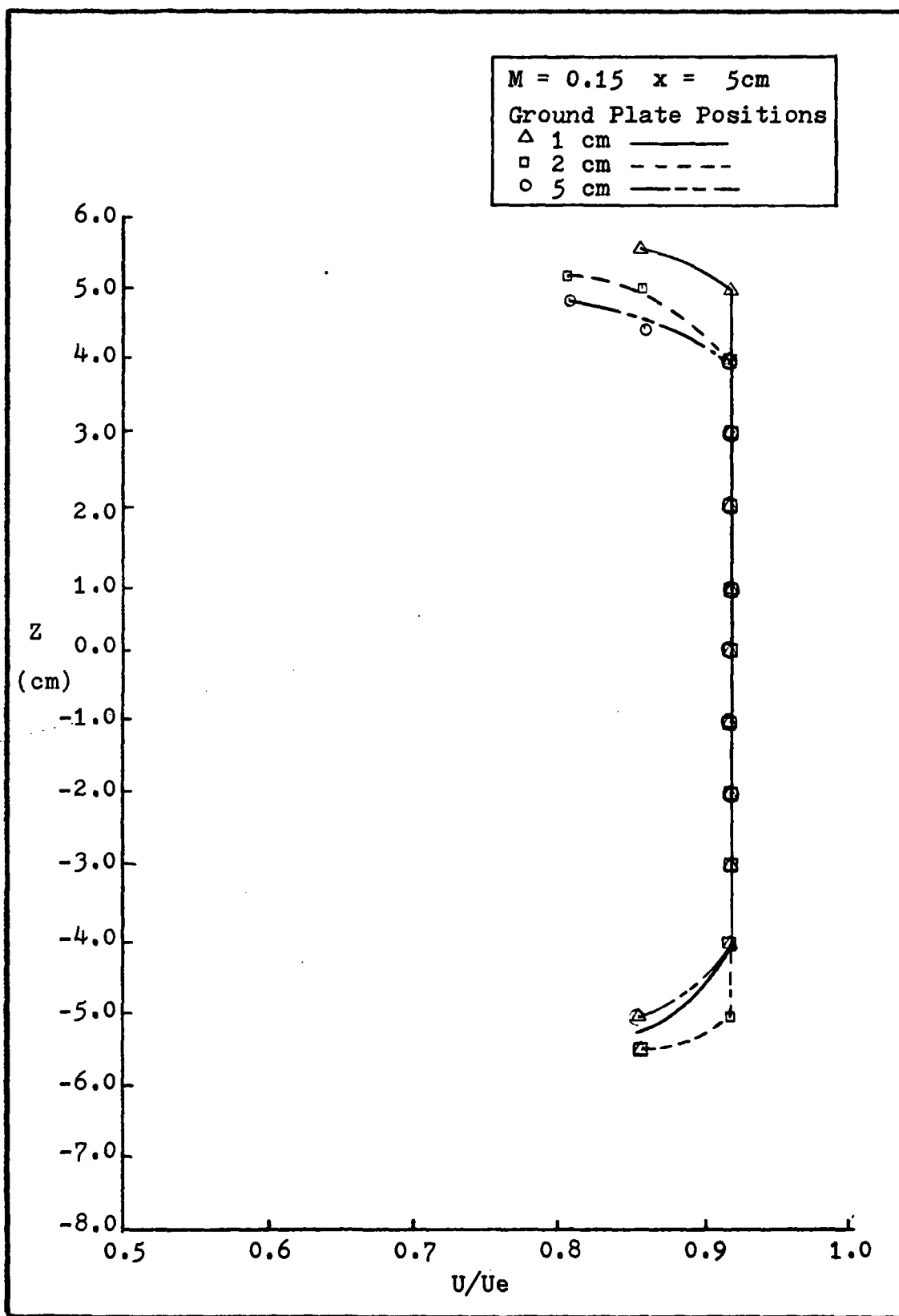


Figure 23. Velocity Profiles for $M=0.15$ at $x=5 \text{ cm}$

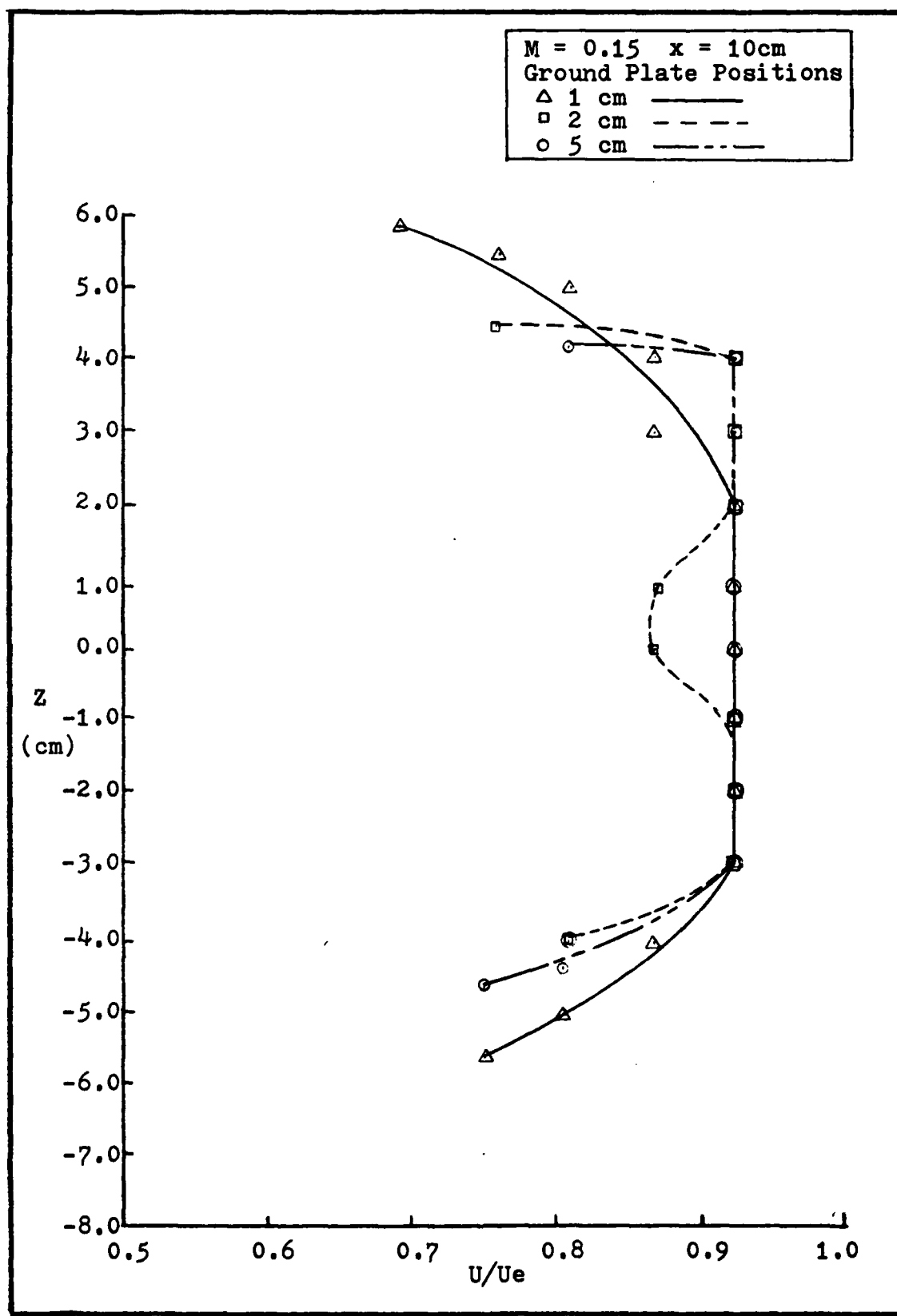


Figure 24. Velocity Profiles for $M=0.15$ at $x=10$ cm

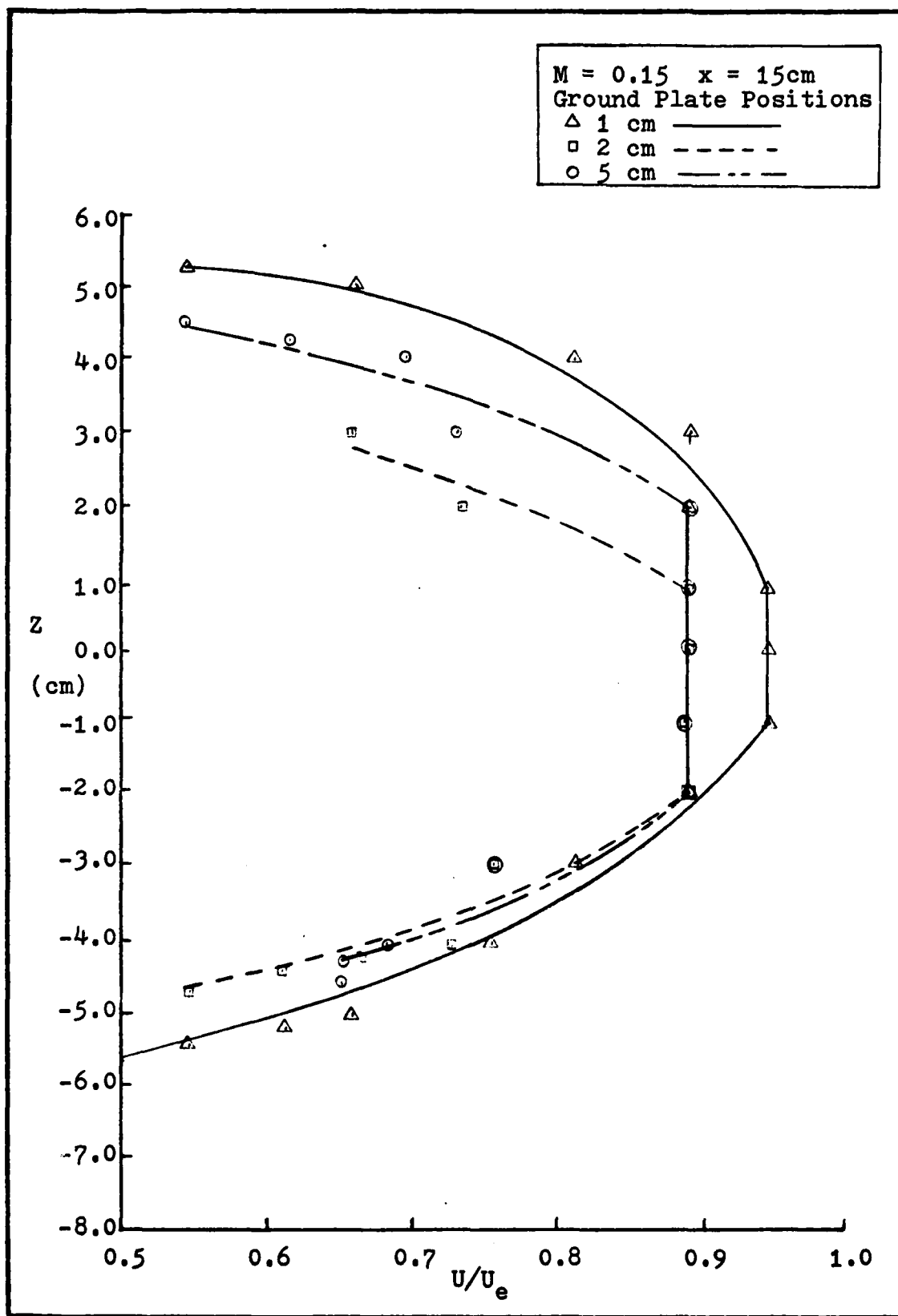


Figure 25. Velocity Profiles for $M=0.15$ at $x=15$ cm

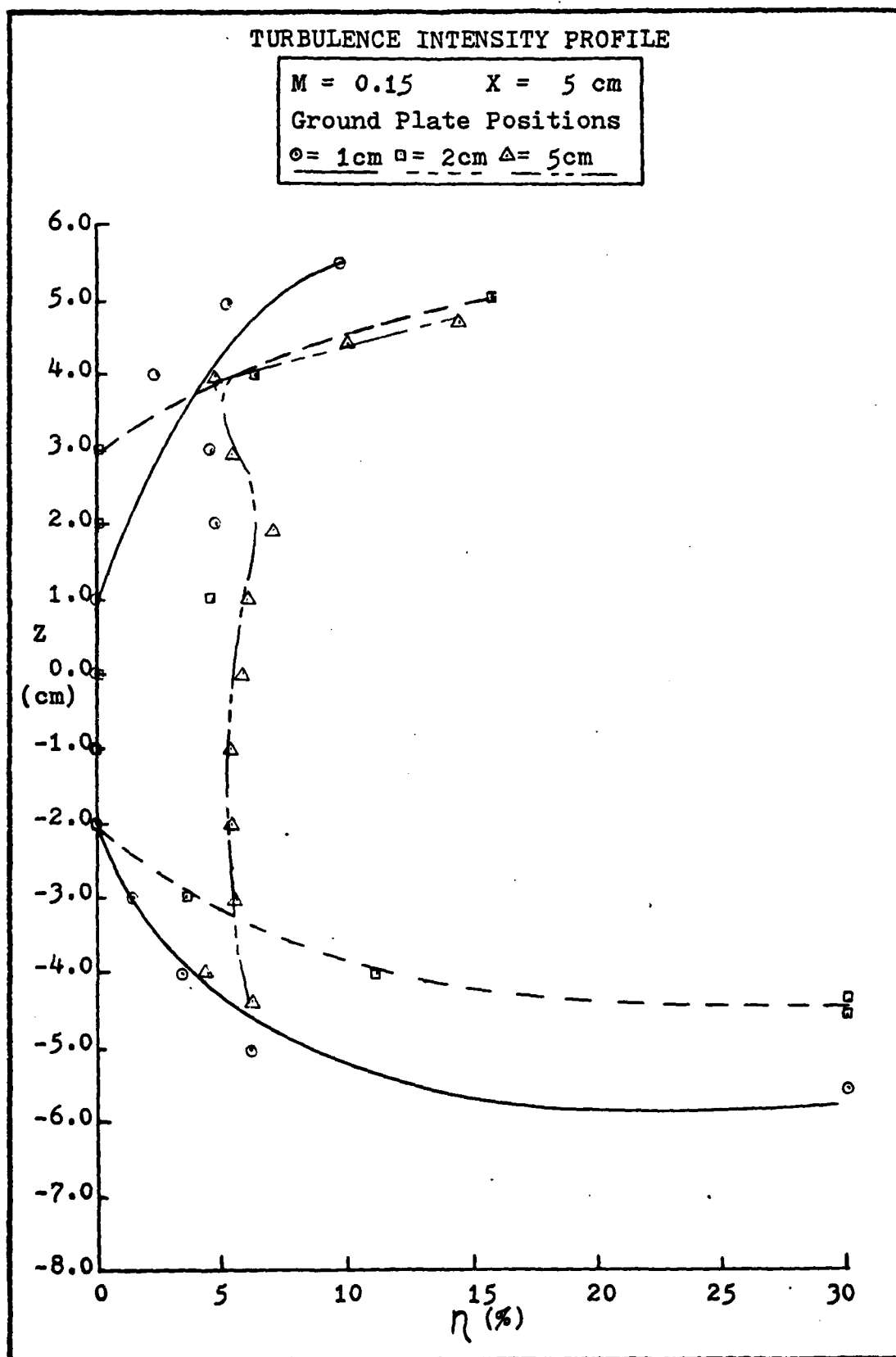


Figure 26. Turbulence Intensity

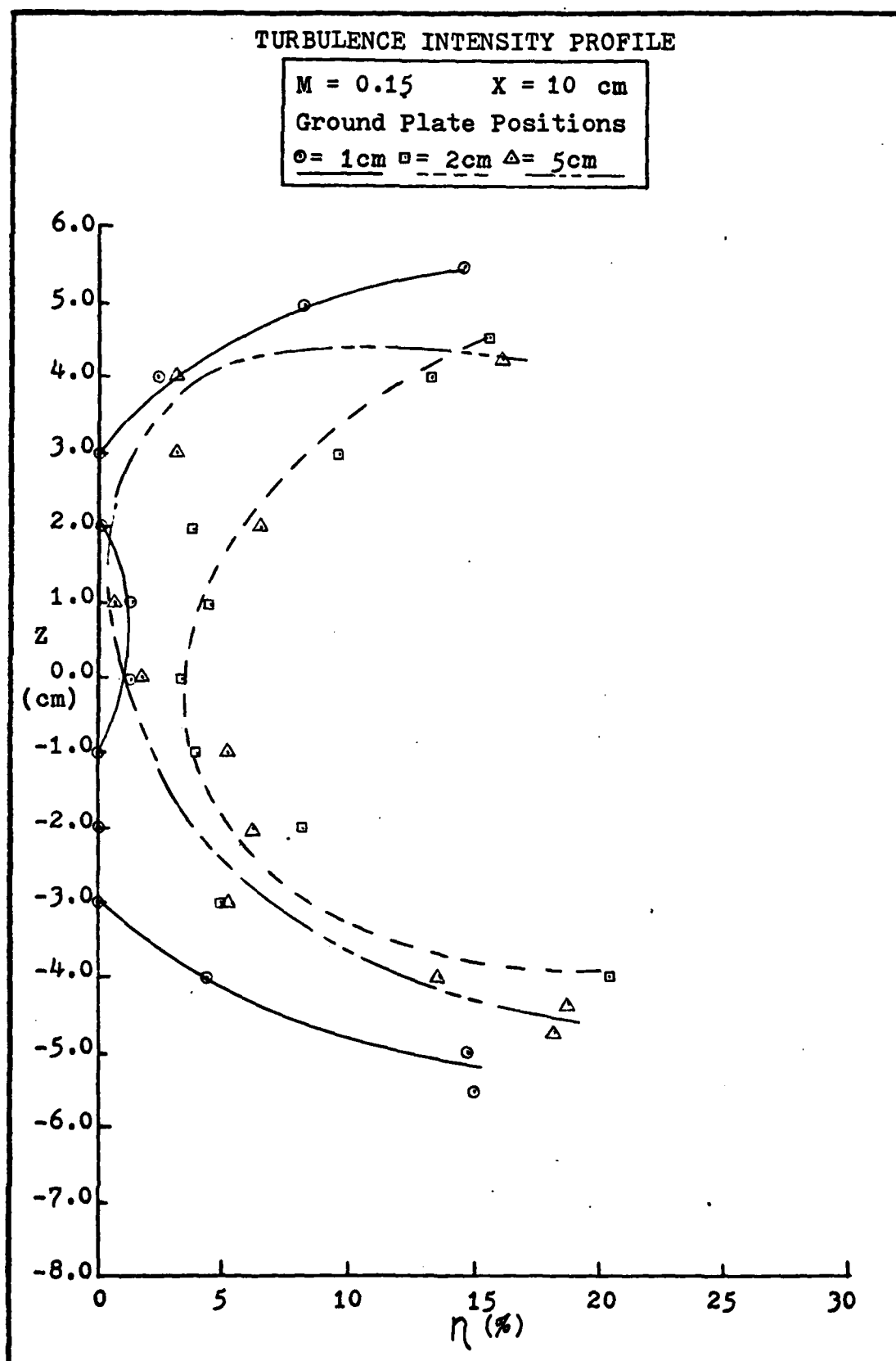


Figure 27. Turbulence Intensity

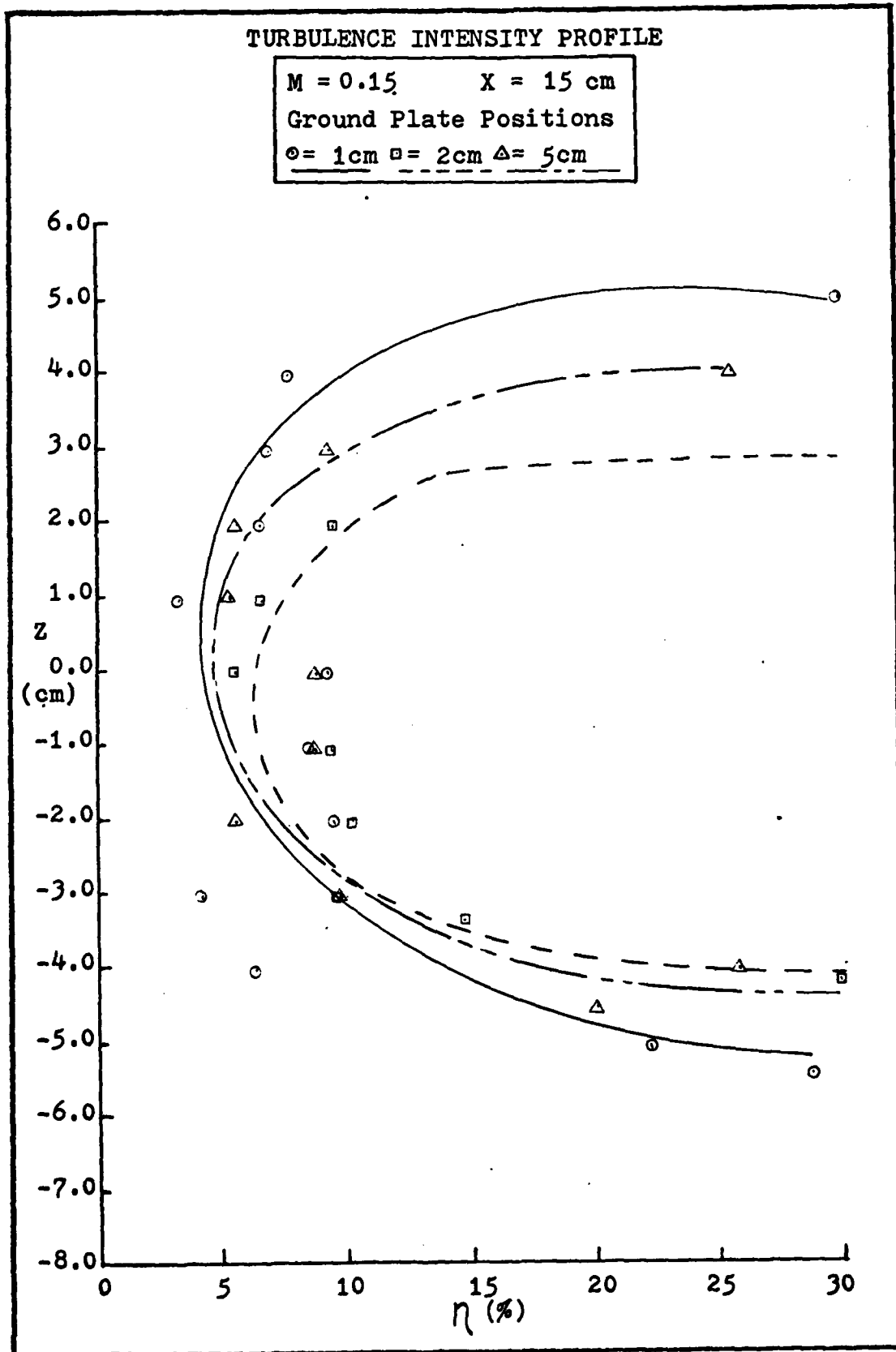


Figure 28. Turbulence Intensity

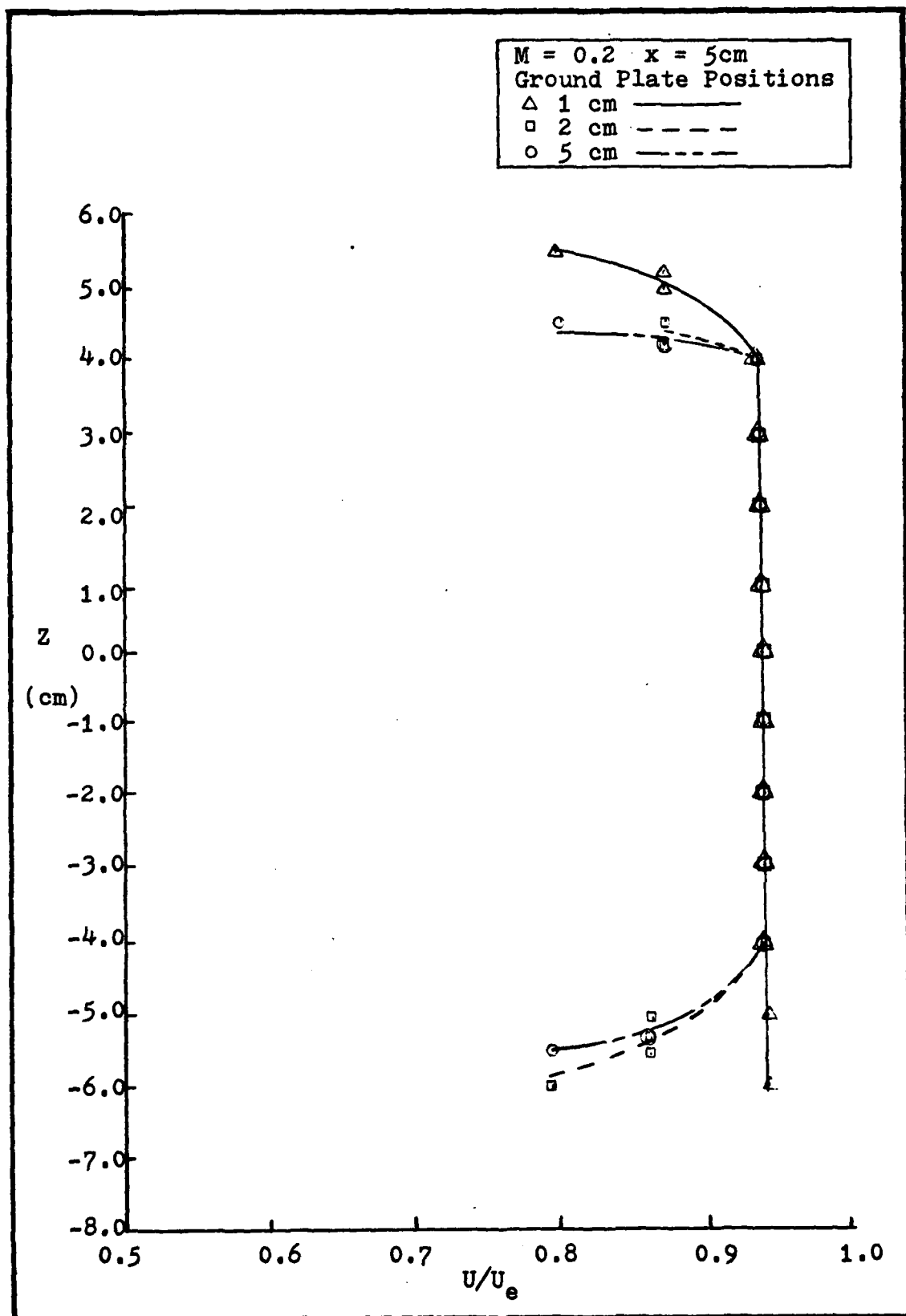


Figure 29. Velocity Profiles for $M=0.2$ at $x=5\text{ cm}$

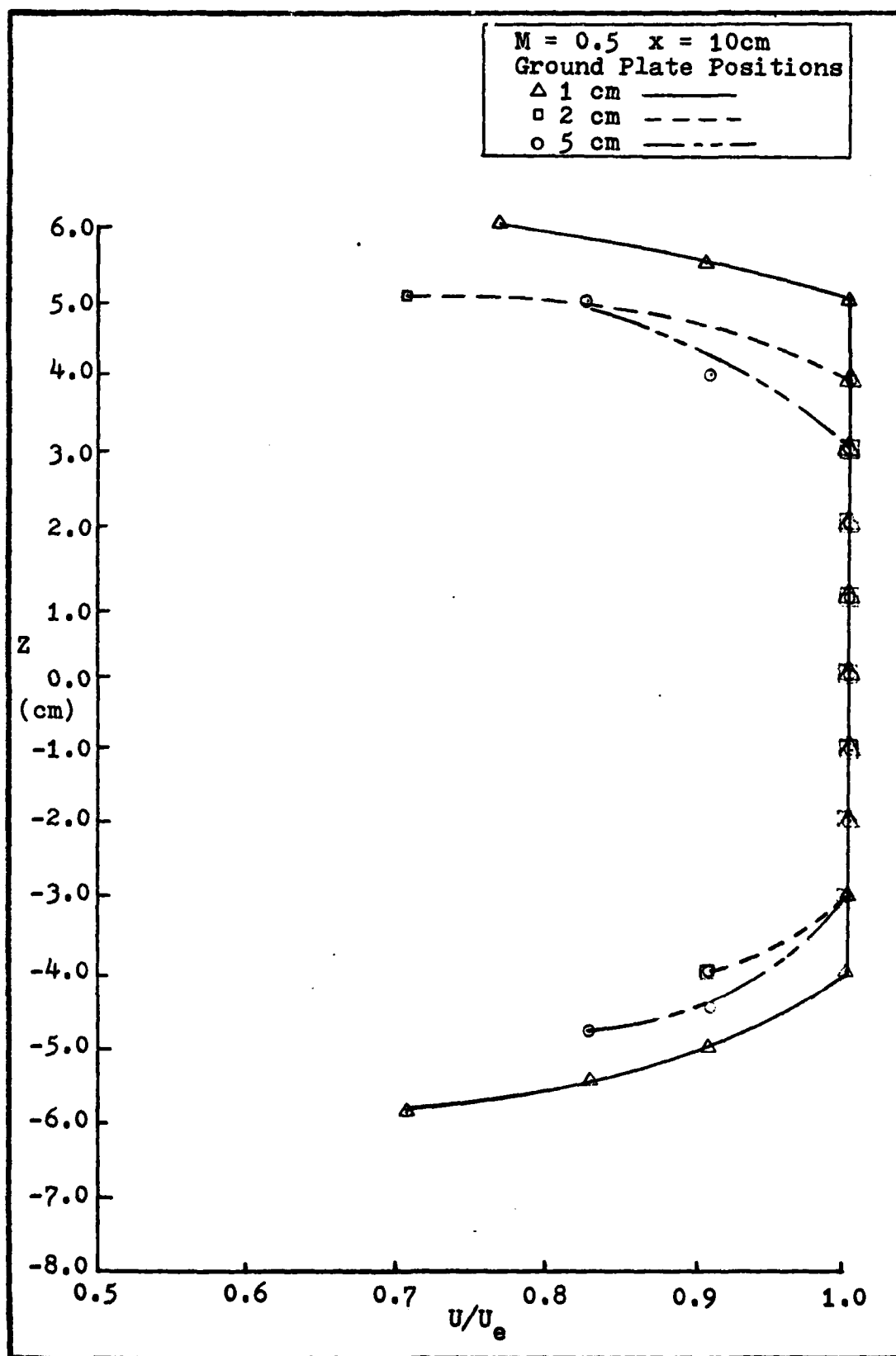


Figure 30. Velocity Profiles for $M=0.2$ at $x=10$ cm

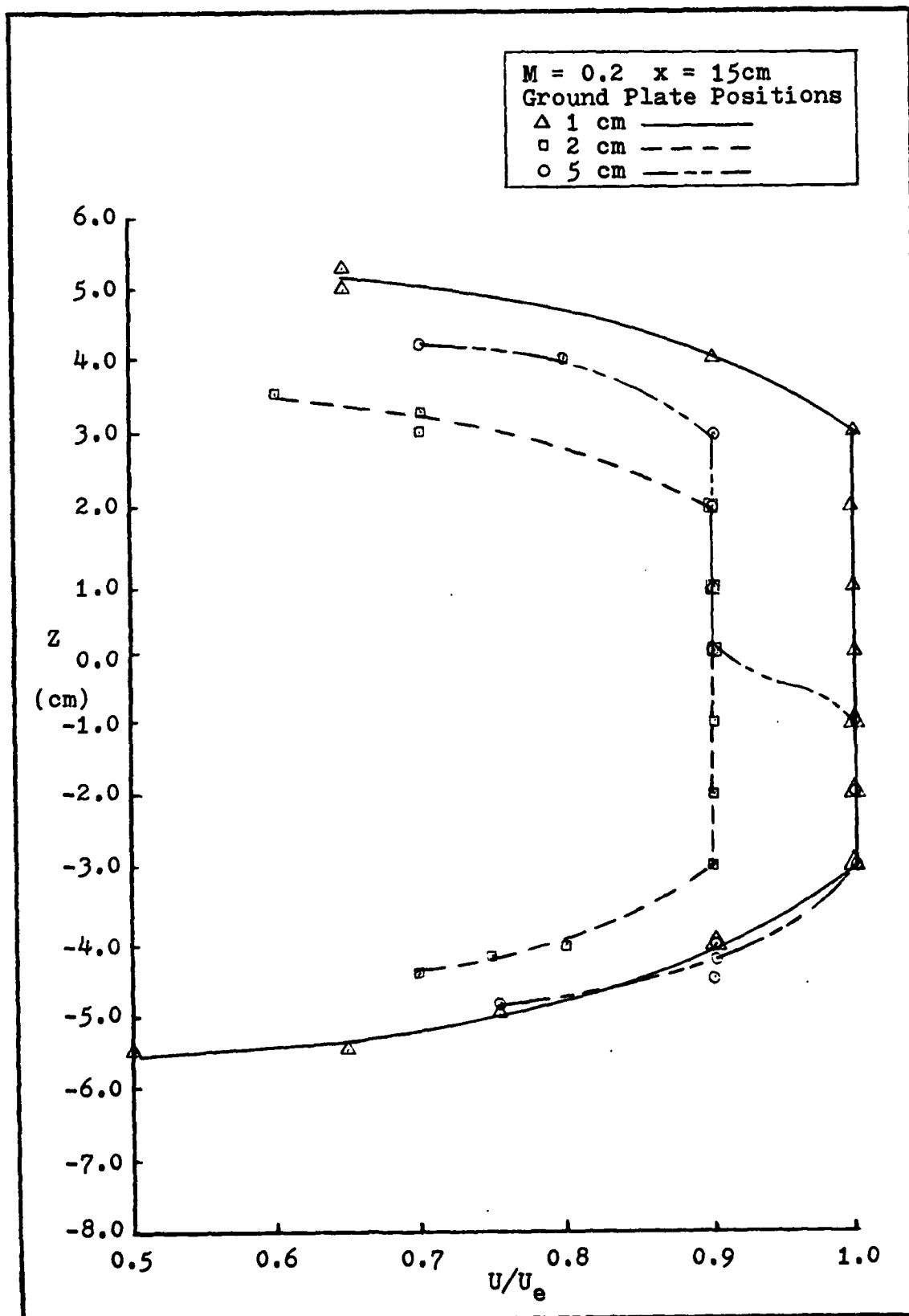


Figure 31. Velocity Profiles for $M=0.2$ at $x=15$ cm

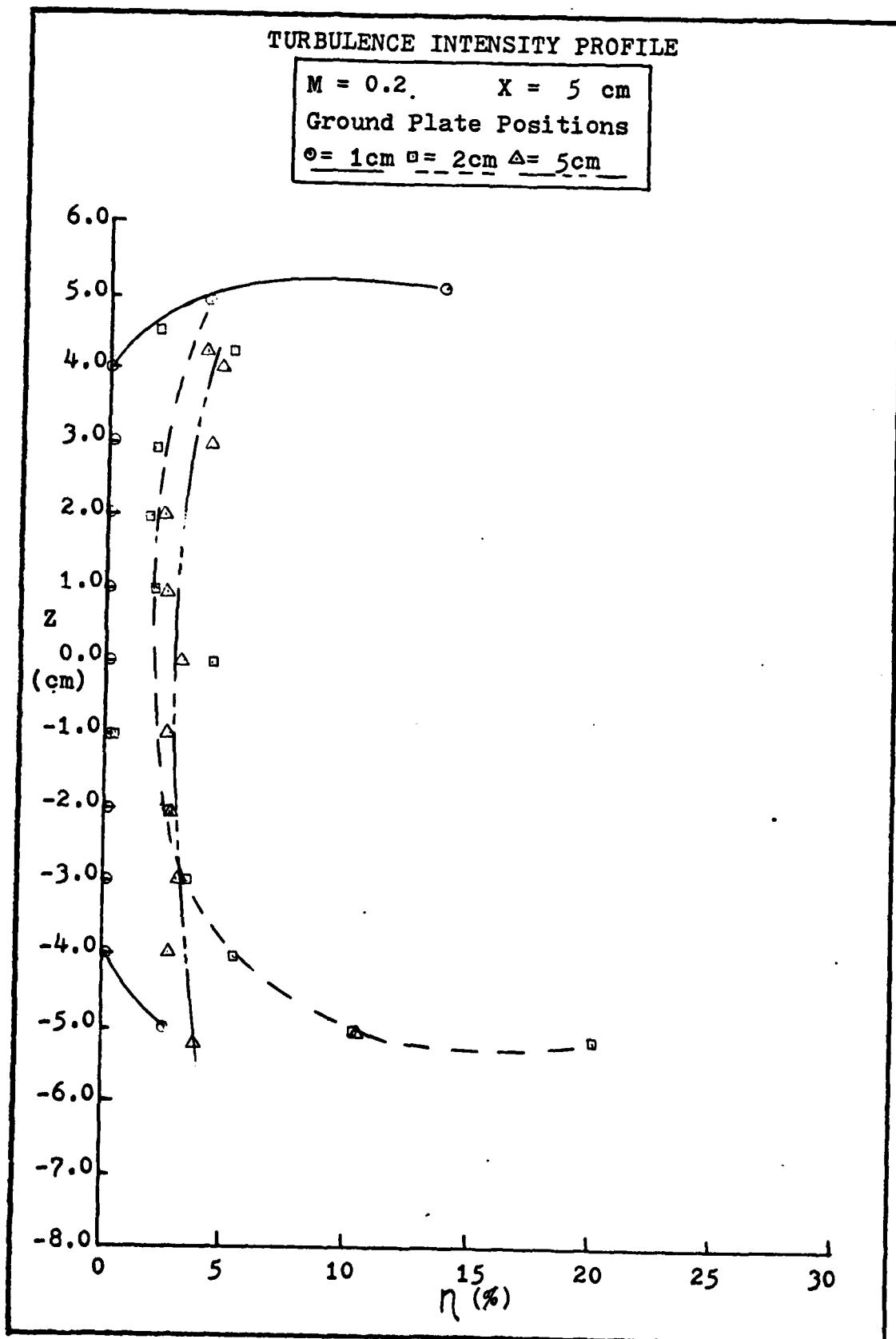


Figure 32. Turbulence Intensity

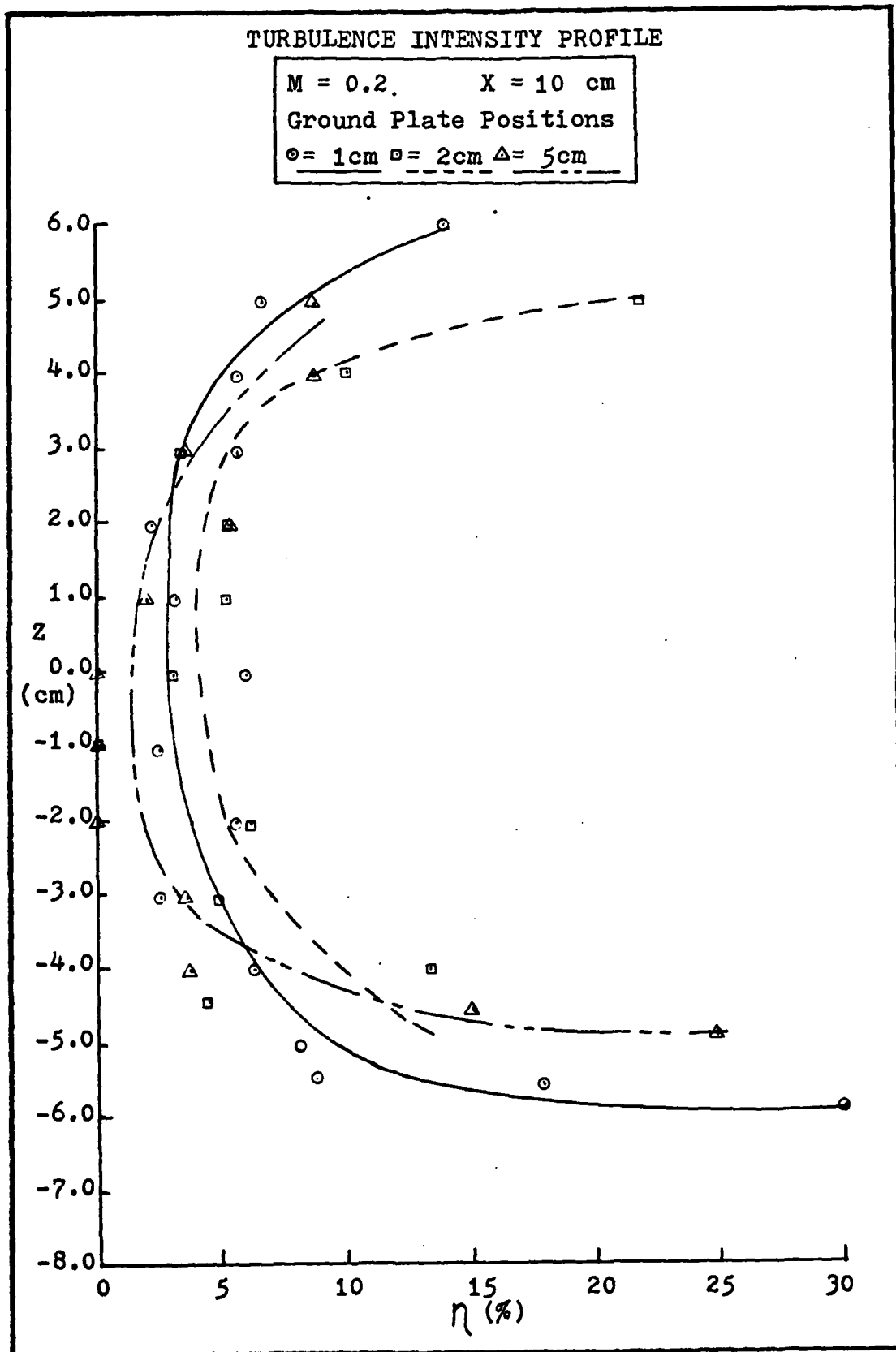


Figure 33 Turbulence Intensity

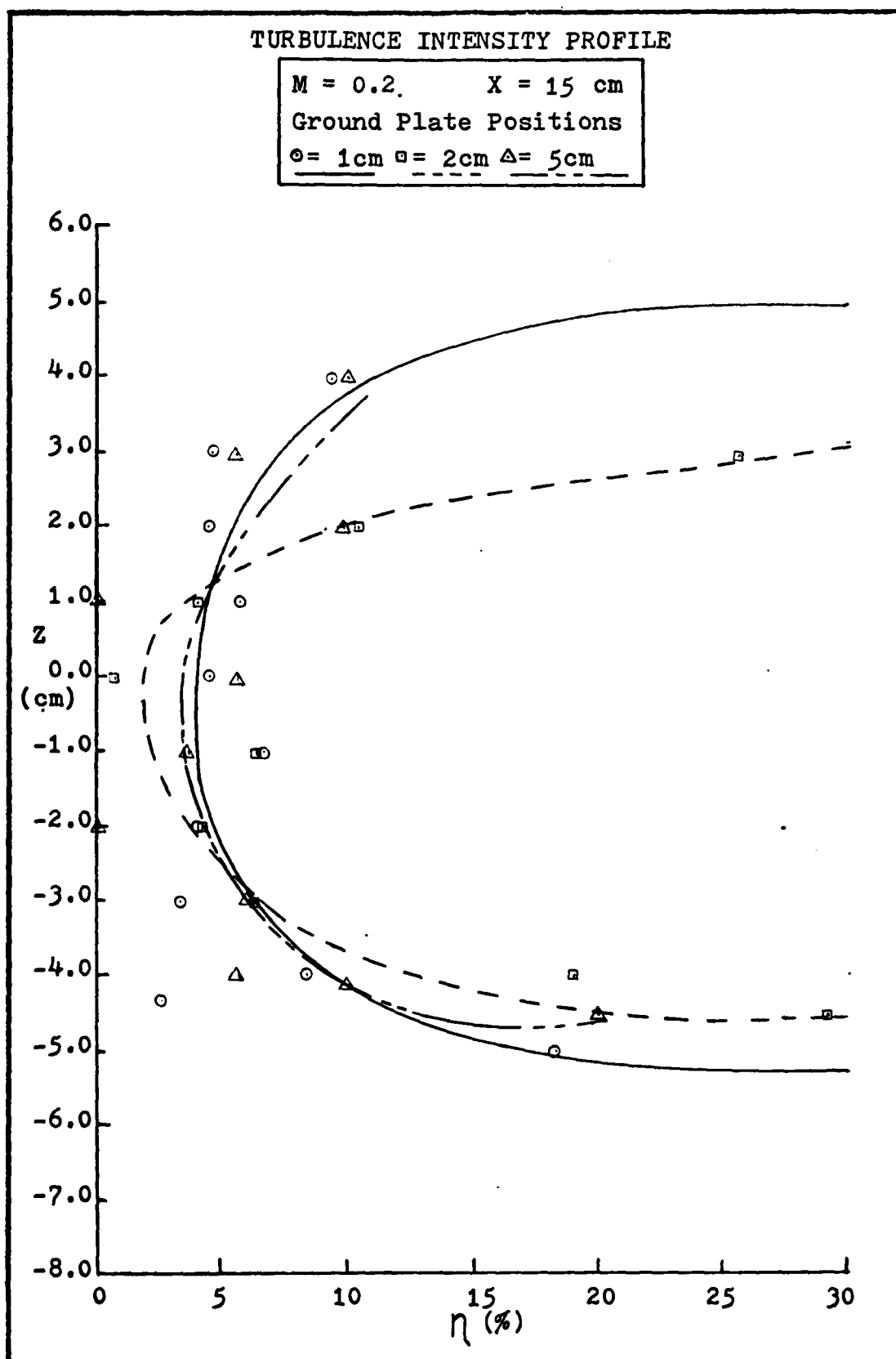


Figure 34 Turbulence Intensity

Table V

VELOCITY PROFILE							
$M = 0.15$ $T_c = 68$ F $U_e = 51.48$ m/sec $L/D = 56.000$ Ground Plate Position = 5 cm $X = 5$ cm $Y = 0$ cm $Z = T$ cm							
Position (cm)	Sample Time (nsec)	Peak (ξ_2)	Channel Content			U	η
			ξ_1	ξ_2	ξ_3	m/sec	%
4.7	50	20	91033	92944	91618	41.69	14.97
4.5	50	19	45501	47343	45816	44.30	10.25
4.0	50	18	15755	17550	15826	47.25	4.63
3.0	50	18	29489	37708	29993	47.25	5.80
2.0	50	18	4821	6126	4968	47.25	8.05
1.0	50	18	29538	37987	30142	47.25	6.29
0.0	50	18	25315	32261	25848	47.25	6.53
-1.0	50	18	9143	11442	9291	47.25	5.95
-2.0	50	18	6292	7555	6357	47.25	5.29
-3.0	50	18	4778	6015	4858	47.25	5.96
-4.0	50	18	9979	12460	10059	47.25	4.17
-5.0	50	19	58808	62310	59196	44.30	7.98

Table VI

VELOCITY PROFILE							
$M = 0.15$ $T_c = 68$ F $U_e = 51.48$ m/sec $L/D = 56.00$ Ground Plate Position = 2 cm $X = 5$ cm $Y = 0$ cm $Z = T$ cm							
Position (cm)	Sample Time (nsec)	Peak (ξ_2)	Channel Content			U	η
			ξ_1	ξ_2	ξ_3	m/sec	%
5.2	50	20				41.69	
5.0	50	19	24817	30100	26654	44.30	16.45
4.0	50	18	994	1609	1049	47.25	7.09
3.0	50	18	6427	10097	6276	47.25	0.00
2.0	50	18	2409	3956	2362	47.25	0.00
1.0	50	18	1704	2887	1750	47.25	4.59
0.0	50	18	1364	2565	1354	47.25	0.00
-1.0	50	18	1295	2153	1267	47.25	0.00
-2.0	50	18	1919	3025	1899	47.25	0.00
-3.0	50	18	12050	21277	12274	47.25	3.62
-4.0	50	18	4878	6113	5152	47.25	12.04
-5.0	50	16	112188	117946	115698	47.25	28.14
-5.2	50	19				44.30	

Table VII

VELOCITY PROFILE							
M = 0.15 $T_c = 68$ F $U_e = 51.48$ m/sec L/D = 56.00 Ground Plate Position = 1 cm X = 5 cm Y = 0 cm Z = T cm							
Position (cm)	Sample Time (nsec)	Peak (ξ_2)	Channel Content			U	η
			ξ_1	ξ_2	ξ_3	m/sec	%
5.5	50	19	23123	24758	24168	44.30	30.01
5.0	50	19	31729	37834	32213	44.30	6.64
4.0	50	18	10944	17879	11105	47.25	3.53
3.0	50	18	14078	23709	14106	47.25	1.41
2.0	50	18	28744	43472	28569	47.25	0.00
1.0	50	18	20983	34492	20635	47.25	0.00
0.0	50	18	9517	14871	9467	47.25	0.00
1.0	50	18	2022	3136	2009	47.25	0.00
2.0	50	18	1550	2664	1599	47.25	4.87
3.0	50	18	19387	30349	19811	47.25	4.56
4.0	50	18	12302	19594	12403	47.25	2.67
5.0	50	18	14807	21308	15125	47.25	5.15
5.5	50	19	67891	85560	70408	44.30	9.21
6.0	50	20	24494	26299	26179	41.69	71.31

Table VIII

VELOCITY PROFILE							
$M = 0.15 T_c = 68 F$ $U_e = 51.48 \text{ m/sec}$ $L/D = 56.00$ Ground Plate Position = 5 cm $X = 10 \text{ cm}$ $Y = 0 \text{ cm}$ $Z = T \text{ cm}$							
Position (cm)	Sample Time (nsec)	Peak (ξ_2)	Channel Content			U	η
			ξ_1	ξ_2	ξ_3	m/sec	%
-4.5	50	21	64619	68888	66237	39.37	17.58
-4.3	50	19	23555	24845	24072	44.30	18.41
-4.0	50	21	14912	16396	15301	39.37	13.42
-3.0	50	18	15198	17271	15892	47.25	5.88
-2.0	50	18	11279	12702	11410	47.25	7.17
-1.0	50	18	18855	21909	19013	47.25	5.26
0.0	50	18	23053	25854	23074	47.25	1.96
1.0	50	18	30964	38560	30934	47.25	1.41
2.0	50	18	22811	28132	23287	47.25	7.05
3.0	50	18	12804	14131	12828	47.25	3.05
4.0	50	18	14038	14954	14059	47.25	3.45
4.2	50	20	27960	29265	28413	41.69	16.41

Table IX

VELOCITY PROFILE							
$M = .15$ $T_c = 68$ F $U_e = 51.48$ m/sec $L/D = 56.00$ Ground Plate Position = 2 cm $X = 10$ cm $Y = 0$ cm $Z = T$ cm							
Position (cm) Sample Time (nsec) Peak (ξ_2)			Channel Content			U	η
			ξ_1	ξ_2	ξ_3	m/sec	%
4.0	50	20	32935	33564	33232	41.69	21.30
3.0	50	18	20016	21630	20090	47.25	4.99
2.0	50	18	16057	18172	15791	47.25	7.90
1.0	50	18	23742	30088	23933	47.25	3.96
0.0	50	19	13385	15705	13435	44.30	3.30
1.0	50	19	9304	10371	9348	44.30	4.66
2.0	50	18	20954	26011	21054	47.25	3.19
3.0	50	18	10196	11185	10353	47.25	9.77
4.0	50	19	25634	29605	26588	44.30	12.66
4.5	50	21	19077	19904	19355	39.37	16.16

Table X

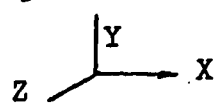
VELOCITY PROFILE							
$M = 0.15$ $T_c = 68$ F $U_e = 51.48$ m/sec $L/D = 56.00$ Ground Plate Position = 1 cm $X = 10$ cm $Y = 0$ cm $Z = T$ cm 							
Position (cm)	Sample Time (nsec)	Peak (ξ_2)	Channel Content			U	η
			ξ_1	ξ_2	ξ_3	m/sec	%
5.5	50	21	30225	31346	30598	39.37	15.89
5.0	50	20	42512	51674	45298	41.69	14.90
4.0	50	19	14629	17039	14723	44.30	4.53
3.0	50	18	16462	21332	16177	47.25	0.00
2.0	50	18	21513	29404	21411	47.25	0.00
1.0	50	18	6975	8562	6966	47.25	0.00
0.0	50	18	5063	7229	5072	47.25	1.63
1.0	50	18	5431	7723	5442	47.25	1.73
2.0	50	18	14546	16373	14443	47.25	0.00
3.0	50	19	5409	6567	5248	44.30	0.00
4.0	50	19	7244	8830	7267	44.30	2.73
5.0	50	20	27553	35063	28561	41.69	8.86
5.5	50	21	16606	17724	16936	39.37	14.57
5.75	50	23	19035	20491	19858	35.44	25.66

Table XI

VELOCITY PROFILE							
$M = 0.15$ $T_c = 68\text{ F}$ $U_e = 51.48\text{ m/sec}$ $L/D = 53.165$ Ground Plate Position = 5 cm $X = 15\text{ cm}$ $Y = 0\text{ cm}$ $Z = T\text{ cm}$							
<div> <div>Position (cm)</div> <div>Sample Time (nsec)</div> <div>Peak (ξ_2)</div> </div>			Channel Content			U	η
			ξ_1	ξ_2	ξ_3	m/sec	%
4.5	50	26				28.04	
4.2	50	24				32.04	
4.0	50	22	110518	116038	113713	35.41	26.40
3.0	50	21	42427	45447	42911	37.38	9.86
2.0	50	19	31261	34052	31418	42.05	5.54
1.0	50	19	103942	113797	104442	42.05	5.26
0.0	50	19	46540	52814	47395	42.05	8.97
-1.0	50	19	47625	50634	48009	42.05	8.64
-2.0	50	19	55332	59904	55606	42.05	5.73
-3.0	50	20	40273	42232	40584	39.58	9.81
-4.0	50	22	56811	57600	57274	35.41	26.48
-4.2	50	23	88857	91421	90024	33.64	20.58
-4.5	50	23				33.64	

Table XII

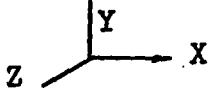
VELOCITY PROFILE							
$M = 0.15$ $T_c = 68$ F $U_e = 51.48$ m/sec $L/D = 53.16$ Ground Plate Position = 2 cm $X = 15$ cm $Y = 0$ cm $Z = T$ cm 							
Position (cm)	Sample Time (nsec)	Peak (ϵ_2)	Channel Content			U	η
			ϵ_1	ϵ_2	ϵ_3	m/sec	%
4.7	50	27	23350	24630	24485	28.04	62.97
4.5	50	24	13772	15116	14784	32.04	39.03
4.2	50	23	6248	7272	6681	33.64	19.58
4.0	50	21	21390	23688	20870	37.38	30.28
3.0	50	20	6986	9062	7271	39.58	9.01
2.0	50	19	14779	16845	15131	42.05	10.22
1.0	50	19	27716	35935	28915	42.05	9.33
0.0	50	19	22179	26841	20967	42.05	5.81
1.0	50	19	20276	28277	21094	42.05	7.64
2.0	50	21	52773	59400	53829	37.38	9.83
3.0	50	23	157295	168838	166403	33.64	43.54

Table XIII

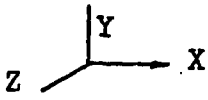
VELOCITY PROFILE							
$M = 0.15$ $T_c = 68$ F $U_e = 51.48$ m/sec $L/D = 53.16$ Ground Plate Position = 1 cm $X = 15$ cm $Y = 0$ cm $Z = T$ cm 							
Position (cm)	Sample Time (nsec)	Peak (ξ_2)	Channel Content			U	η
			ξ_1	ξ_2	ξ_3	m/sec	%
5.2	50	26				28.04	
5.0	50	23	35086	38515	37292	33.64	30.24
4.0	50	19	8931	11341	9283	42.05	9.33
3.0	50	18	14740	16684	14984	44.86	8.56
2.0	50	18	14656	17178	14903	44.86	7.45
1.0	50	17	6849	9133	6900	48.06	3.47
0.0	50	17	22359	25000	22753	48.06	9.56
-1.0	50	17	24014	25642	24215	48.06	8.48
-2.0	50	18	15626	18039	16005	44.86	9.74
-3.0	50	19	8790	10253	8841	42.05	4.33
-4.0	50	20	13066	14450	13183	39.58	6.87
-5.0	50	23	28320	32483	30521	33.64	23.85
-5.2	50	24	16866	18991	18184	32.04	28.78
-5.5	50	26	12886	13862	13629	29.25	40.20
-5.7	50	28				26.91	

Table XIV

VELOCITY PROFILE							
$M = 0.2$ $T_c = 70$ F $U_e = 68.77$ m/sec $L/D = 56.00$ Ground Plate Position = 5 cm $X = 5$ cm $Y = 0$ cm $Z = T$ cm							
Position (cm)	Sample Time (nsec)	Peak (ϵ_2)	Channel Content			U	η
			ϵ_1	ϵ_2	ϵ_3	m/sec	%
4.5	50	16	44791	48406	44921	54.52	4.41
4.2	50	15	32956	34288	33105	59.00	8.02
4.0	50	14	19818	26134	20116	64.43	5.06
3.0	50	14	2645	4135	2708	64.43	4.78
2.0	50	14	5286	8863	5340	64.43	2.88
1.0	50	14	1374	2226	1393	64.43	3.48
0.0	50	14	5052	6862	5200	64.43	6.83
-1.0	50	14	2364	3613	2390	64.43	3.36
-2.0	50	14	15920	26283	16105	64.43	3.12
-3.0	50	14	12491	20629	12703	64.43	3.75
-4.0	50	14	2447	4075	2462	64.43	2.29
-5.0	50	14	5890	7196	6129	64.43	10.68
-5.2	50	15	15903	17513	15961	59.00	4.41
-5.5	50	16				54.52	

Table XV

VELOCITY PROFILE							
M = 0.2 $T_c = 70$ F $U_e = 68.77$ m/sec $L/D = 56.00$ Ground Plate Position = 2 cm X = 5 cm Y = 0 cm Z = T cm							
<div> <div>Position (cm)</div> <div>Sample Time (nsec)</div> <div>Peak (ϵ_2)</div> </div>			Channel Content			U	η
			ϵ_1	ϵ_2	ϵ_3	m/sec	%
4.5	50	15	481523	507408	483004	59.00	5.59
4.2	50	15	2069782	2094886	2069426	59.00	2.78
4.0	50	14	2575875	2732986	2603829	64.43	10.50
3.0	50	14	457671	610094	458780	64.43	2.06
2.0	50	14	432866	580763	434743	64.43	2.65
1.0	50	14	1632756	1749331	1634656	64.43	2.99
0.0	50	14	3466101	3594785	3472016	64.43	4.99
-1.0	50	14	1023271	1304297	1023825	64.43	1.24
-2.0	50	14	1375564	1851518	1387423	64.43	3.69
-3.0	50	14	12147405	12480269	12157648	64.43	4.00
-4.0	50	14	1685799	2284827	1728352	64.43	6.28
-5.0	50	15	15343254	15472917	15374637	59.00	12.74
-5.2	50	15	595105	613539	603824	59.00	21.34
-5.5	50	15	931437	952153	948626	59.00	49.70
-5.7	50	16				54.52	

Table XVI

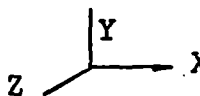
VELOCITY PROFILE							
$M = 0.2$ $T_c = 70^\circ F$ $U_e = 68.77$ m/sec $L/D = 56.00$ Ground Plate Position = 1 cm $X = 5$ cm $Y = 0$ cm $Z = T$ cm 							
Position (cm)	Sample Time (nsec)	Peak (ϵ_2)	Channel Content			U	η
			ϵ_1	ϵ_2	ϵ_3	m/sec	%
5.5	50	16				54.52	
5.0	50	15	1045779	1088523	1047688	59.00	5.17
4.0	50	14	645788	738934	643930	64.43	0.00
3.0	50	14	218549	280130	215617	64.43	0.00
2.0	50	14	864584	988501	859838	64.43	0.00
1.0	50	14	615021	726232	610825	64.43	0.00
0.0	50	14	175128	254073	172765	64.43	0.00
-1.0	50	14	481750	571923	478575	64.43	0.00
-2.0	50	14	499782	586012	497483	64.43	0.00
-3.0	50	14	199079	249331	196709	64.43	0.00
-4.0	50	14	269264	326675	266385	64.43	0.00
-5.0	50	14	887766	1057484	981617	64.43	3.51
-6.0	50	14				64.43	
-6.2	50	14				64.43	

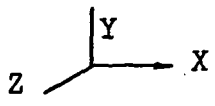
Table XVII

VELOCITY PROFILE							
M = 0.2 $T_c = 63$ F $U_e = 68.64$ m/sec L/D = 56.00 Ground Plate Position = 5 cm X = 10cm Y = 0 cm Z = T cm							
Position (cm)	Sample Time (nsec)	Peak (ξ_2)	Channel Content			U	η
			ξ_1	ξ_2	ξ_3	m/sec	%
-4.7	50	15	28095	29164	28291	59.06	24.91
-4.5	50	14	27684	29590	28281	64.43	15.20
-4.0	50	14	15226	16791	15266	64.43	3.64
-3.0	50	13	42989	49699	43187	70.87	3.92
-2.0	50	13	19618	22431	19466	70.87	0.00
-1.0	50	13	33646	38947	33419	70.87	0.00
0.0	50	13	18666	21920	18544	70.87	0.00
1.0	50	13	23952	28040	23982	70.87	1.93
2.0	50	13	23606	27123	23813	70.87	5.23
3.0	50	13	29166	34098	29297	70.87	3.66
4.0	50	14	18468	20275	18676	64.43	8.12
5.0	50	15	29198	29814	29269	59.06	8.12

Table XVIII

VELOCITY PROFILE							
$M = 0.2$ $T_c = 68^\circ F$ $U_e = 68.64$ m/sec $L/D = 56.00$ Ground Plate Position = 2 cm $X = 10$ cm $Y = 0$ cm $Z = T$ cm							
<div> <div>Position (cm)</div> <div>Sample Time (nsec)</div> <div>Peak (ξ_2)</div> </div>			Channel Content			U	η
			ξ_1	ξ_2	ξ_3	m/sec	%
4.5	50	14	45772	47421	45824	64.43	4.20
4.0	50	14	29301	32226	30045	64.43	13.15
3.0	50	13	18609	23615	18890	70.87	4.87
2.0	50	13	13737	16574	13954	70.87	6.48
1.0	50	13	11520	14782	11488	70.87	0.00
0.0	50	13	18792	23257	18871	70.87	3.02
1.0	50	13	18005	21703	18196	70.87	5.25
2.0	50	13	15258	18614	15460	70.87	5.69
3.0	50	13	45650	55610	45873	70.87	3.41
4.0	50	13	18827	21197	19268	70.87	10.76
5.0	50	17	85372	86290	85852	50.62	23.56

Table XIX

VELOCITY PROFILE							
$M = 0.2$ $T_c = 68 F$ $U_e = 68.64$ m/sec $L/D = 56.00$ Ground Plate Position = 1 cm $X = 10$ cm $Y = 0$ cm $Z = T$ cm 							
Position (cm)	Sample Time (nsec)	Peak (ξ_2)	Channel Content			U	η
			ξ_1	ξ_2	ξ_3	m/sec	%
6.0	50	16	36379	38328	37513	54.52	26.56
5.5	50	14	16433	18751	17143	64.43	14.98
5.0	50	13	17015	20482	17362	70.87	7.54
4.0	50	13	25525	32554	25987	70.87	6.03
3.0	50	13	12757	16323	12997	70.87	6.05
2.0	50	13	17792	23188	17910	70.87	2.22
1.0	50	13	23928	30940	24034	70.87	3.22
0.0	50	13	20724	25770	21118	70.87	6.56
-1.0	50	13	22558	29171	22624	70.87	2.26
-2.0	50	13	17156	21372	17425	70.87	5.92
-3.0	50	13	22258	28646	22351	70.87	2.83
-4.0	50	13	11878	15037	12143	70.87	6.85
-5.0	50	14	21267	25017	21765	64.43	8.84
-5.5	50	15	29341	31282	30059	59.00	17.26
-5.7	50	17	46330	47197	46901	50.62	31.27

AD-A079 877

AIR FORCE INST OF TECH WRIGHT-PATTERSON AFB OH SCHOO--ETC F/G 20/4
GROUND PLANE EFFECTS ON A CONTOURED SURFACE AT LOW SUBSONIC VEL--ETC(U)
DEC 79 J A KRAWTZ

UNCLASSIFIED

AFIT/6A/AA/804-3

NL

2 of 2

AD-A079 877



END

DATE

FORMED

2 - 80

File

Table XX

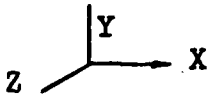
VELOCITY PROFILE							
$M = 0.2$ $T_c = 68$ F $U_e = 68.38$ m/sec $L/D = 53.16$ Ground Plate Position = 5 cm $X = 15$ cm $Y = 0$ cm $Z = T$ cm 							
Position (cm)	Sample Time (nsec)	Peak (ϵ_2)	Channel Content			U	η
			ϵ_1	ϵ_2	ϵ_3	m/sec	%
4.2	50	17				48.06	
4.0	50	15	71673	73281	71954	56.07	10.38
3.0	50	14	46093	48241	46198	61.17	5.15
2.0	50	14	57988	61713	57995	61.17	1.22
1.0	50	14	48256	49464	46300	61.17	0.00
0.0	50	14	34517	36997	34704	61.17	6.47
-1.0	50	13	32836	43767	32883	67.29	3.63
-2.0	50	13	38607	39678	38131	67.29	0.00
-3.0	50	13	89808	93897	90129	67.29	6.61
-4.0	50	14	47585	49096	47678	61.17	5.81
-4.2	50	14	49448	50795	49677	61.17	10.21
-4.5	50	14	49745	51233	50365	61.17	19.04
-4.7	50	16				51.76	

Table XXI

VELOCITY PROFILE							
$M = 0.2$ $T_c = 68 \text{ F}$ $U_e = 68.64 \text{ m/sec}$ $L/D = 53.16$ Ground Plate Position = 2 cm $X = 15 \text{ cm}$ $Y = 0 \text{ cm}$ $Z = T \text{ cm}$							
Position (cm)	Sample Time (nsec)	Peak (ξ_2)	Channel Content			U	η
			ξ_1	ξ_2	ξ_3	m/sec	%
-5.0	50	17				48.06	
-4.7	50	17	49409	54351	52970	48.06	36.06
-4.5	50	16	28047	31615	30229	51.76	28.00
-4.0	50	15	17361	21078	18591	56.07	15.84
-3.0	50	14	9624	11604	9793	61.17	6.92
-2.0	50	14	9515	12765	9625	61.17	4.27
-1.0	50	14	5725	7179	5856	61.17	7.11
0.0	50	14	25875	33415	25878	61.17	0.85
1.0	50	14	19942	24903	20095	61.17	4.01
2.0	50	14	25298	31267	26548	61.17	11.61
3.0	50	17	45198	50619	48298	48.06	26.02
3.2	50	17	75469	86101	82758	48.06	33.23
3.5	50	19	46980	49728	49556	42.05	87.10

Table XXII

VELOCITY PROFILE							
$M = 0.2$ $T_c = 68^\circ F$ $U_e = 68.64$ m/sec $L/D = 53.16$ Ground Plate Position = 1 cm $X = 15$ cm $Y = 0$ cm $Z = T$ cm							
Position (cm) Sample Time (nsec) Peak (ξ_2)			Channel Content			U	η
			ξ_1	ξ_2	ξ_3	m/sec	%
5.5	50	27				28.04	
5.0	50	18	44655	48970	47766	44.86	36.19
4.0	50	14	22909	28556	23676	61.17	8.95
3.0	50	13	29080	35248	29329	67.29	4.67
2.0	50	13	25893	33616	26168	67.29	4.38
1.0	50	13	24863	29499	25165	67.29	5.97
0.0	50	13	18595	24700	18826	67.29	4.52
-1.0	50	13	6169	7712	6331	67.29	7.74
-2.0	50	13	9446	12517	9538	67.29	4.02
-3.0	50	14	17570	21983	17655	61.17	3.23
-4.0	50	14	31397	38744	32197	61.17	7.90
-5.0	50	16	34182	39003	36147	51.76	18.68
-5.5	50	19				42.05	
-5.7	50	20				39.58	

APPENDIX D

LV Experimental Results at $M = 0.15$
and $M = 0.2$ for y Axis Profiles

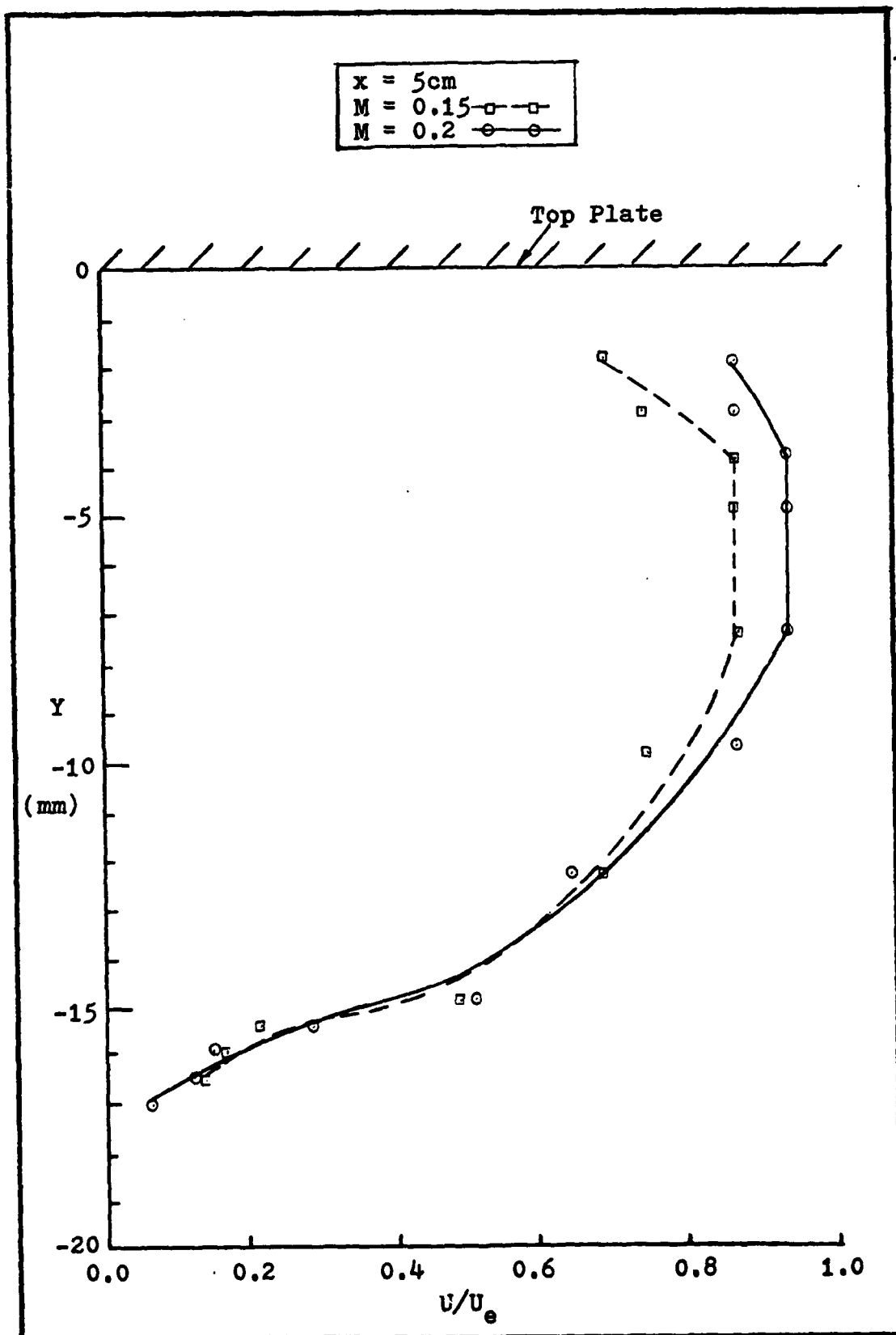


Figure 35. Vertical Velocity Profiles for $M=0.15$ and $M=0.2$ at $x=5\text{cm}$

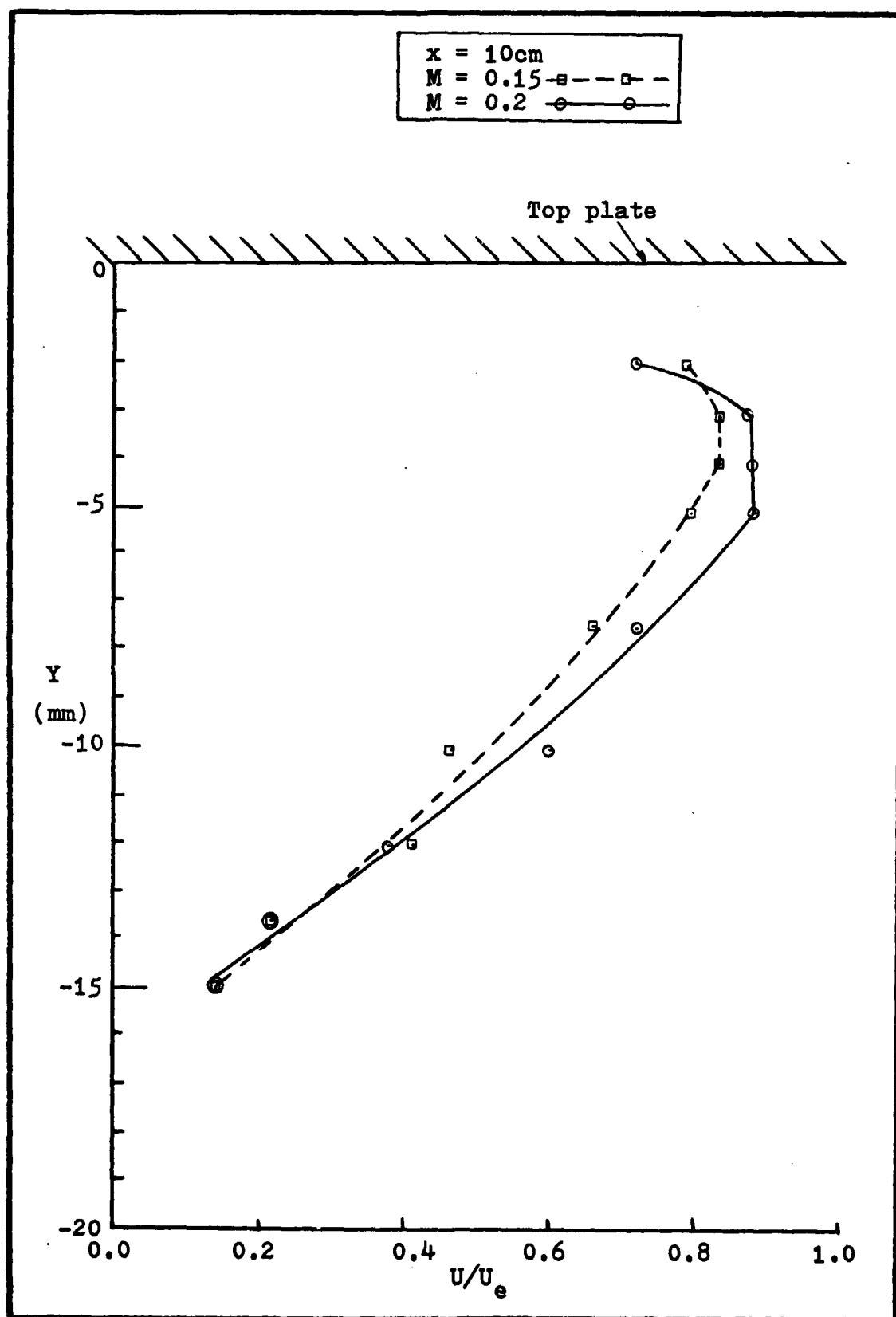


Figure 36. Vertical Velocity Profiles for $M=0.15$ and $M=0.2$ at 10 cm

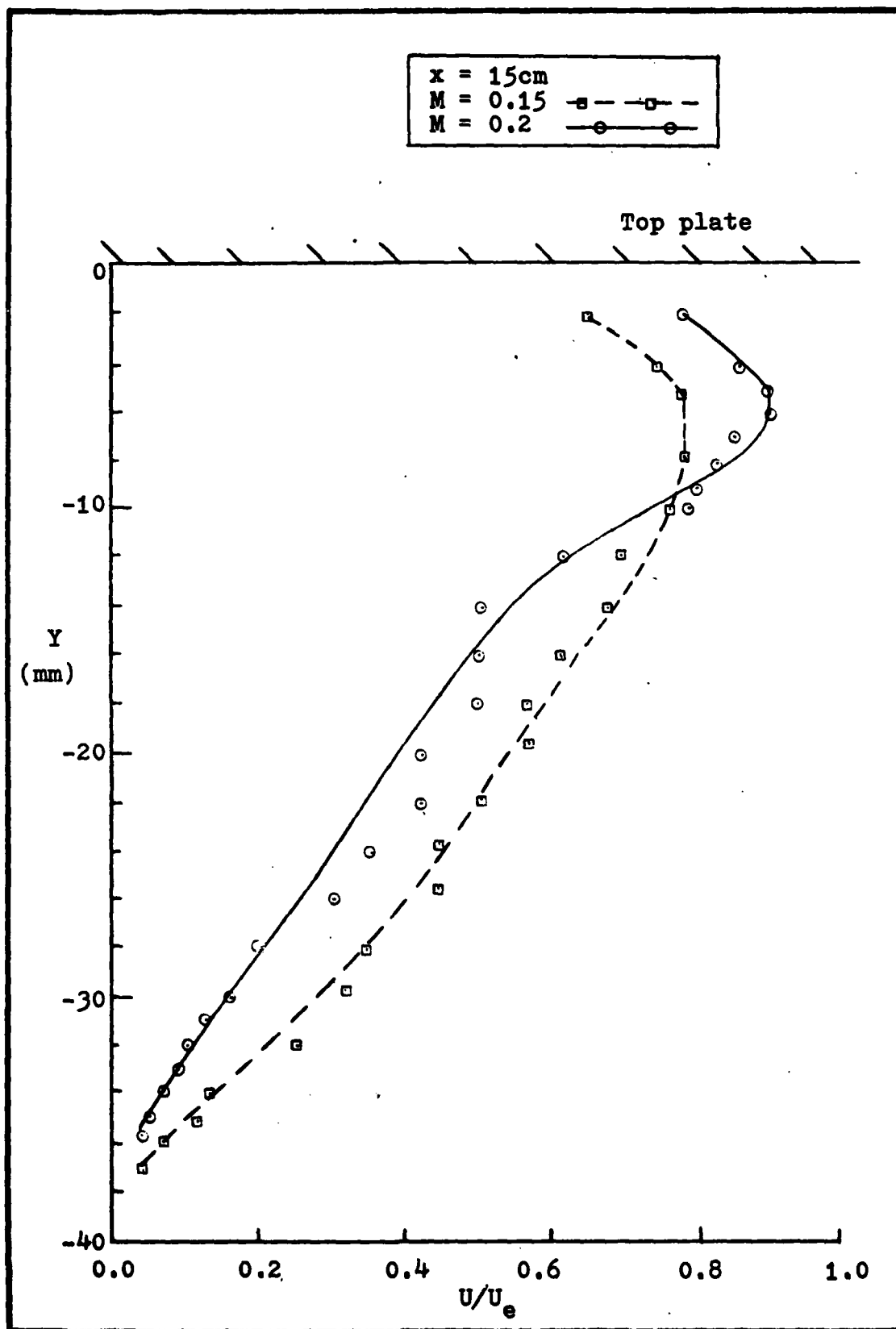


Figure 37. Vertical Velocity Profiles for $M=0.15$ and $M=0.2$ at $x=15$ cm

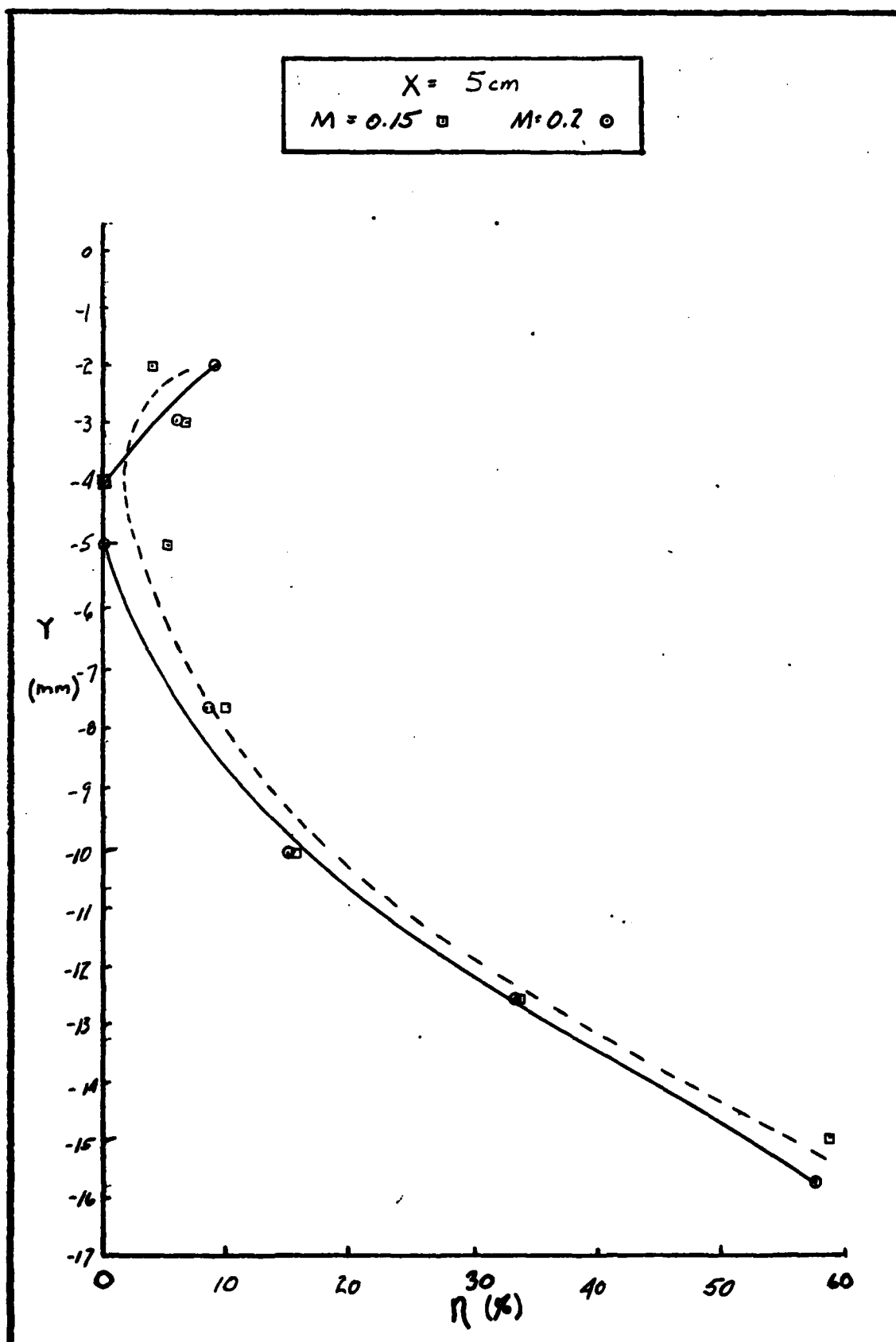


Figure 38 Turbulence Intensity

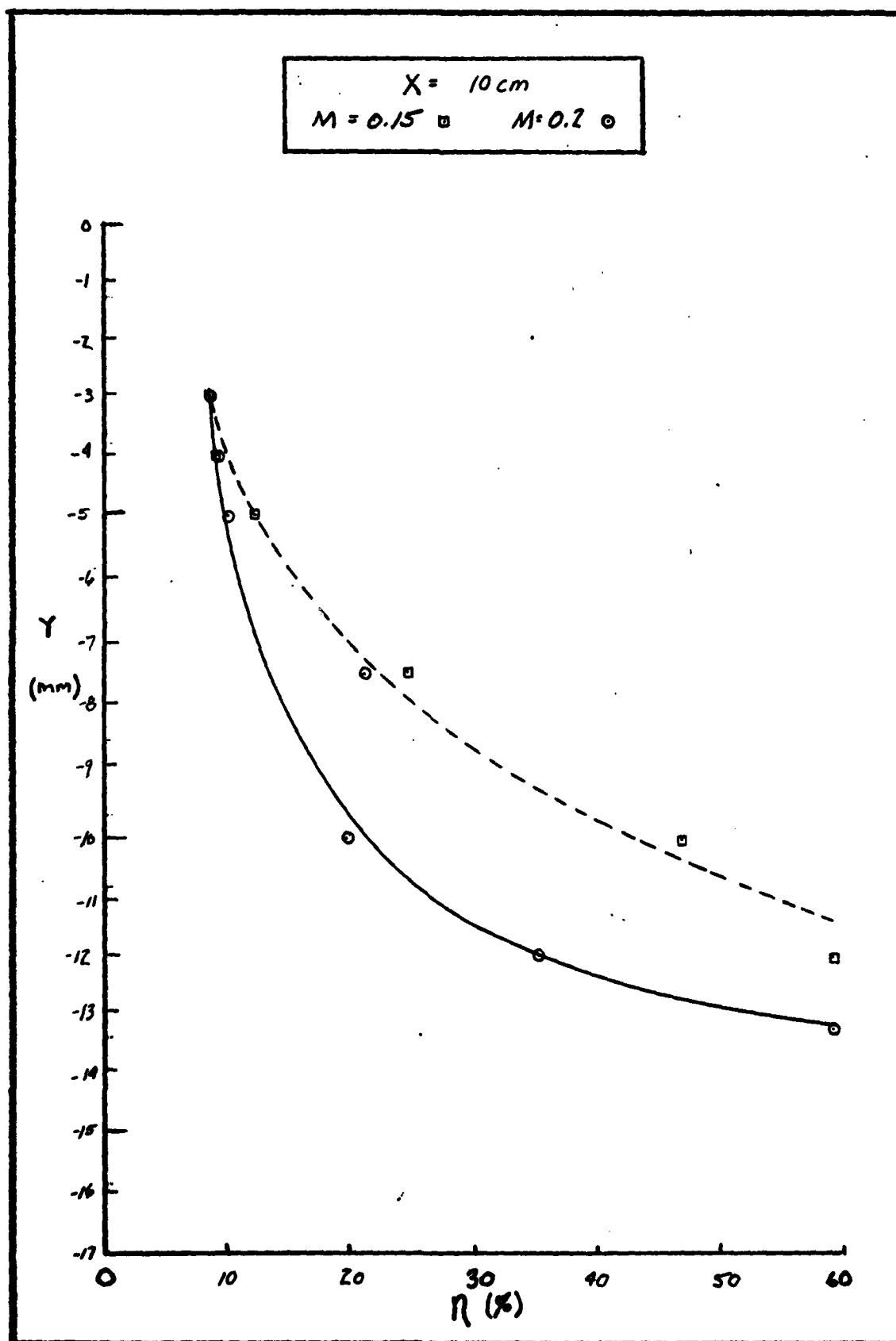


Figure 39 Turbulence Intensity

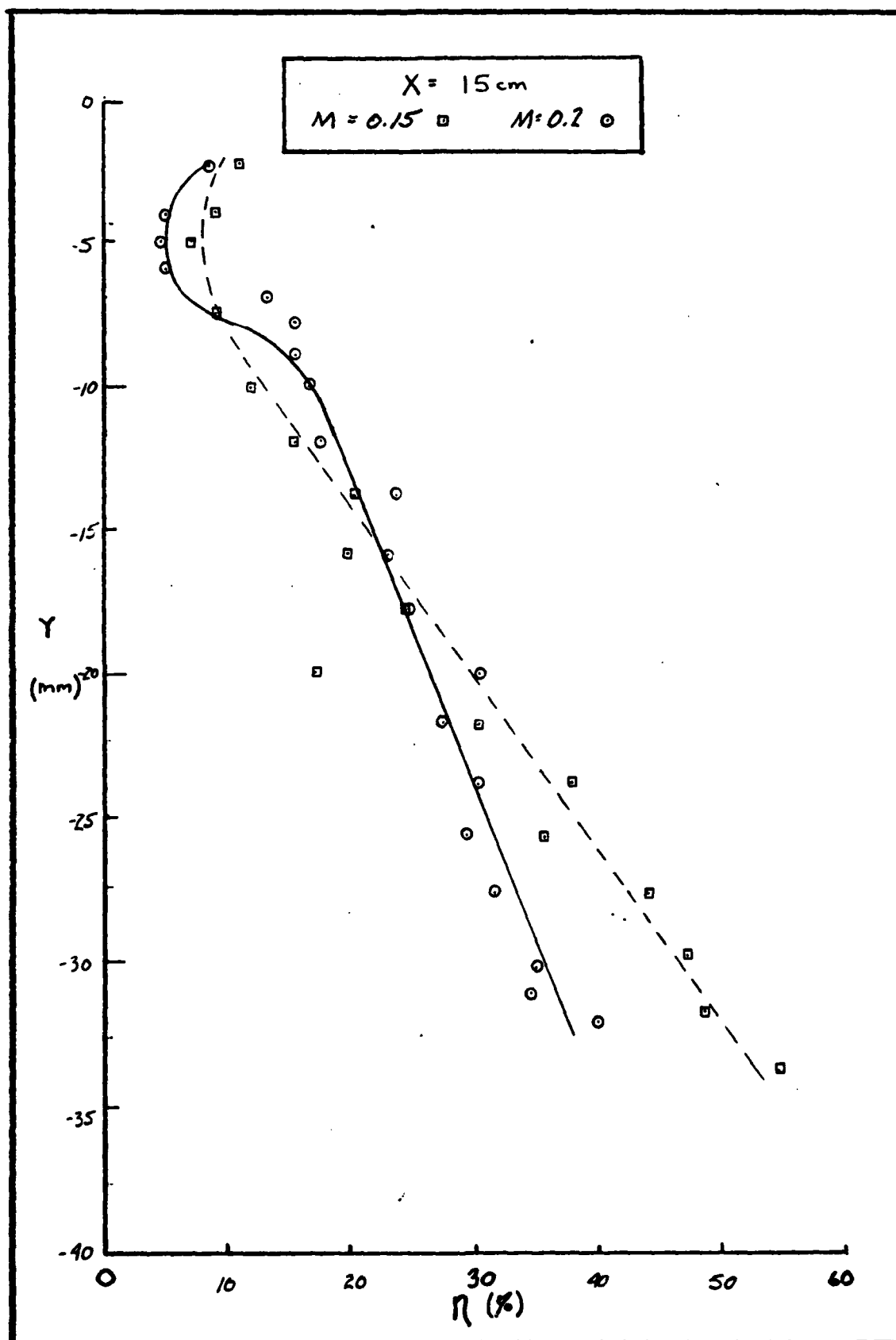


Figure 40 Turbulence Intensity

Table XXIII

VELOCITY PROFILE							
$M = 0.15 T_c = 71 \text{ F}$ $U_e = 51.62 \text{ m/sec}$ $L/D = 60.00$ Ground Plate Position = mm None $X = 5 \text{ cm}$ $Y = T \text{ cm}$ $Z = 0 \text{ cm}$							
Position (mm) Sample Time (nsec) Peak (ϵ_2)			Channel Content			U	η
			ϵ_1	ϵ_2	ϵ_3	m/sec	%
-2.0	50	23	50005	51604	50055	37.97	4.12
-3.0	50	21	22912	35299	24233	42.18	7.82
-4.0	50	19	1619	2740	1535	47.46	0.00
-5.0	50	19	2121	3466	2204	47.46	5.82
-7.5	50	19	2116	3431	2340	47.46	10.23
-10	50	21	4184	6337	4971	42.19	17.10
-12.5	50	26	8834	11003	10345	35.89	34.12
-15.0	100	17	20997	24235	23831	27.12	59.62
-15.5	200	20				11.17	
-16.0	200	22				9.99	
-16.5	200	24				9.04	

Table XXIV

VELOCITY PROFILE							
$M = 0.2$ $T_c = 71$ F $U_e = 68.83$ m/sec $L/D = 60.00$ Ground Plate Position = cm None $X = 5$ cm $Y = T$ cm $Z = 0$ cm							
Position (mm)	Sample Time (nsec)	Peak (ξ_2)	Channel Content			U	η
			ξ_1	ξ_2	ξ_3	m/sec	%
-2.0	50	16	86624	89998	87073	58.41	8.85
-3.0	50	16	2104	3396	2192	58.41	6.10
-4.0	50	15	17349	26935	17324	63.28	0.00
-5.0	50	15	1581	2630	1560	63.28	0.00
-7.5	50	15	2112	3297	2263	63.28	8.64
-10.0	50	16	2137	3084	2457	58.41	16.10
-12.5	50	20	12953	15892	15651	44.67	33.20
-15.0	100	14	31286	35821	35416	34.52	71.89
-15.5	150	16	54491	57439	57034	19.47	56.41
-16.0	200	20				11.17	
-16.5	200	24				9.04	
-17.0	200	37				5.58	

Table XXV

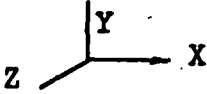
VELOCITY PROFILE							
$M = 0.15$ $T_c = 70$ F $U_e = 51.58$ m/sec $L/D = 50.33$ Ground Plate Position = mm None $X = 10$ cm $Y = T$ cm $Z = 0$ cm 							
Position (mm)	Sample Time (nsec)	Peak (ϵ_2)	Channel Content			U	η
			ϵ_1	ϵ_2	ϵ_3	m/sec	%
-2.0	50	21				41.01	
-3.0	50	20	278700	347255	287001	43.43	8.39
-4.0	50	20	130037	182928	137730	43.43	9.32
-5.0	50	21	45247	57540	48661	41.01	13.98
-7.5	50	24	46129	55802	51526	35.16	25.31
-10.0	150	13	105345	115824	113976	24.61	48.65
-12.0	150	14	92911	97265	96729	22.37	60.08
-12.5	200	19				11.54	
-15.0	200	28				7.38	

Table XXVI

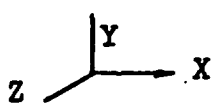
VELOCITY PROFILE							
$M = 0.2$ $T_c = 70$ F $U_e = 68.77$ m/sec $L/D = 58.33$ Ground Plate Position = xx None $X = 10$ cm $Y = T$ cm $Z = 0$ cm 							
Position (mm)	Sample Time (nsec)	Peak (ϵ_2)	Channel Content			U	η
			ϵ_1	ϵ_2	ϵ_3	m/sec	%
-2.0	50	18				49.22	
-3.0	50	15	231595	338828	243614	61.52	8.06
-4.0	50	15	20458	29652	21883	61.52	9.62
-5.0	50	15	28104	35749	29480	61.52	10.61
-7.5	50	18	45734	55607	50845	49.22	23.33
-10.0	50	21	45054	46217	45576	41.01	20.36
-12.0	100	17	111567	123542	120339	26.37	36.91
-13.5	200	15	153955	162472	161452	15.38	60.81
-15.0	200	21				10.25	

Table XXVII

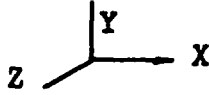
VELOCITY PROFILE							
$M = 0.15$ $T_c = 70$ F $U_e = 51.58$ m/sec $L/D = 60.00$ Ground Plate Position = mm None $X = 15$ cm $Y = T$ cm $Z = 0$ cm 							
Position (mm)	Sample Time (nsec)	Peak (ξ_2)	Channel Content			U	η
			ξ_1	ξ_2	ξ_3	m/sec	%
-2.0	50	25	7594	9454	7962	34.52	11.21
-4.0	50	23	12027	15687	12551	37.97	9.23
-5.0	50	22	3530	4429	3619	39.96	7.50
-7.5	50	22	13555	16537	14000	39.96	9.46
-10	50	23	17421	26153	19621	37.97	13.09
-12	50	24	6832	9773	7882	36.16	16.79
-14	50	25	7476	10164	8784	34.51	21.93
-16	50	27	5076	5857	5423	31.64	20.14
-18	100	16	7429	8702	8132	29.21	25.01
-20	100	16	12211	12989	12499	29.21	17.27
-22	100	18	10810	13927	12849	25.31	30.97
-24	100	19	14069	16345	15759	23.73	38.23
-26	100	19	21976	26920	25478	23.73	35.09
-28	150	17	9144	9949	9780	18.08	43.67
-30	100	25	24514	27253	26734	17.26	46.56
-32	150	23	18426	21990	21366	12.65	48.87
-34	350	19	35757	36907	36746	6.78	55.80
-35	350	21				6.03	
-36	500	32				4.22	
-37	500	35				2.37	

Table XXVIII

VELOCITY PROFILE							
$M = 0.2$ $T_c = 70$ F $U_e = 68.77$ m/sec $L/D = 60.00$ Ground Plate Position = MM None $X = 15$ cm $Y = T$ cm $Z = 0$ cm							
Position (mm)	Sample Time (nsec)	Peak (ϵ_2)	Channel Content			U	η
			ϵ_1	ϵ_2	ϵ_3	m/sec	%
-2.0	50	17	8959	10633	9177	54.24	8.74
-4.0	50	16	2300	2970	2337	58.41	5.50
-5.0	50	15	5171	6056	5210	63.28	4.90
-6.0	50	15	8580	10247	8669	63.28	5.40
-7.0	50	16	1790	2725	2027	58.41	13.14
-8.0	50	17	1997	2800	2274	54.24	16.35
-9.0	50	17	6766	7287	6964	54.24	16.73
-10.0	50	19	5610	5837	5695	47.46	17.43
-12.0	100	12	2482	3336	2813	42.19	17.92
-14.0	100	13	25651	26211	25014	37.97	24.01
-16.0	100	14	6765	7196	6988	34.52	23.32
-18.0	100	14	41023	42284	41723	34.52	25.16
-20.0	100	16	3418	3617	3551	29.21	31.96
-22.0	100	16	4594	5921	5385	29.21	27.36
-24.0	150	13	4971	5909	5584	25.31	30.92
-26.0	150	15	9321	10502	10070	21.09	29.65
-28.0	100	30	5288	6206	5904	14.06	32.16
-30.0	200	19	12658	15292	14563	11.86	36.40
-31.0	300	16	19480	22872	21898	9.74	35.48
-32.0	350	17	8628	10423	10007	7.75	40.99
-33.0	250	19				6.78	
-34.0	350	23				5.42	
-35.0	350	27				4.52	
-35.5	350	34				3.50	

Vita

Lieutenant Joseph A. Krawtz was born in Latrobe, Pennsylvania in 1956. He graduated from high school in Derry, Pennsylvania in 1974 and enrolled in the Aerospace Engineering School at The Pennsylvania State University. He graduated in 1978 with a Bachelor of Science and received a commission in the USAF through the ROTC program. In that same year he was chosen to attend the Air Force Institute of Technology in the Graduate Astronautical Engineering program.

Permanent address : P. O. Box 238

Bradenville, PA 75620

UNCLASSIFIED

SECURITY CLASSIFICATION OF THIS PAGE (When Data Entered)

REPORT DOCUMENTATION PAGE		READ INSTRUCTIONS BEFORE COMPLETING FORM
1. REPORT NUMBER AFIT/GA/AA/80M-3 ✓	2. GOVT ACCESSION NO.	3. RECIPIENT'S CATALOG NUMBER
4. TITLE (and Subtitle) GROUND PLANE EFFECTS ON A CONTOURED SURFACE AT LOW SUBSONIC VELOCITIES		5. TYPE OF REPORT & PERIOD COVERED M.S. Thesis
7. AUTHOR(s) Joseph A. Krawtz 2nd Lt USAF		6. PERFORMING ORG. REPORT NUMBER
9. PERFORMING ORGANIZATION NAME AND ADDRESS Air Force Institute of Technology (AFIT-EN) Wright-Patterson AFB, OH 45433		8. CONTRACT OR GRANT NUMBER(s)
11. CONTROLLING OFFICE NAME AND ADDRESS		10. PROGRAM ELEMENT, PROJECT, TASK AREA & WORK UNIT NUMBERS
14. MONITORING AGENCY NAME & ADDRESS (if different from Controlling Office)		12. REPORT DATE December 1979
		13. NUMBER OF PAGES 112
		15. SECURITY CLASS. (of this report) Unclassified
		15a. DECLASSIFICATION/DOWNGRADING SCHEDULE
16. DISTRIBUTION STATEMENT (of this Report) Approved for public release; distribution unlimited.		
17. DISTRIBUTION STATEMENT (of the abstract entered in Block 20, if different from Report)		
18. SUPPLEMENTARY NOTES Joseph P. Hipps, Major, USAF Director of Public Affairs AFIT		
19. KEY WORDS (Continue on reverse side if necessary and identify by block number) Low subsonic velocities Wing-in-ground effect Laser Velocimeter Turbulence Ground Plane Effects		
20. ABSTRACT (Continue on reverse side if necessary and identify by block number) The wing-in-ground effect phenomenon was examined by investigating the flow between a flat ground plate and a contoured upper plate. Velocity and turbulence intensity measurements were taken at various points in the flow with a Laser Doppler Velocimeter. Mach numbers studied were Mach 0.15 and Mach 0.2 at the exit plane of a 1 cm by 10 cm two-dimensional nozzle.		

UNCLASSIFIED

SECURITY CLASSIFICATION OF THIS PAGE (When Data Entered)

UNCLASSIFIED

SECURITY CLASSIFICATION OF THIS PAGE(When Data Entered)

↓
Measurements were taken across the width of the jet, 5, 10, and 15 cm downstream with plate separations of 1, 2, and 5 cm and vertically without the ground plate. In addition measurements were taken near the top plate with conventional pressure measuring techniques and the results compared.

The proximity of the ground plate had the effect of spreading the flow outward across the 10 cm width of the jet by 20%. The laser velocimeter showed the turbulence intensity to be constant across the potential core of the jet. Turbulence intensity increased beyond 10% in the boundary layers of the jet and in the plate boundary layer. The pressure measurement data correlated well with the laser velocimeter results. ↘

UNCLASSIFIED

SECURITY CLASSIFICATION OF THIS PAGE(When Data Entered)